

Title	ホウ素 / ケイ素バイメタル型共重合体の合成とその特性
Author(s)	Puneet , Puhup
Citation	
Issue Date	2016-09
Type	Thesis or Dissertation
Text version	ETD
URL	http://hdl.handle.net/10119/13813
Rights	
Description	Supervisor: 松見 紀佳, マテリアルサイエンス研究科, 博士

Preface

The present dissertation is the consolidation of results of the works on the topic “Synthesis and Properties of Boron/Silicon Bimetallic Copolymers” under the guidance of *Prof. Noriyoshi Matsumi* at the School of Materials Sciences, Japan Advanced Institute of Science and Technology during 2013-2016.

With the constant evolution of science and engineering, demand of comparatively cost effective and more accessible materials is growing parallelly. Although there are a number of organic materials available, most of which suffer some or other limitation in design and source. There are several examples available in the literature, of inorganic polymers possessing exotic elements in the main chain. However, as a scope of improvement, study of bimetallic copolymer may be an interesting approach. It may provide numerous other possibilities of material design in order to achieve required properties. The author’s main focus is to address the above mentioned approach by 1) The synthesis and of various types of silicon/boron bimetallic copolymers and 2) Study their applications.

The work presented in this thesis covers the synthesis, characterization and applications of various novel silicon/boron bimetallic copolymers. To the best of my knowledge the presented work is original and no part of the thesis has been plagiarized.

Puhup Puneet

School of Materials Science

Japan Advanced Institute of Science and Technology

June 2016

Acknowledgement

The present study in thesis have been carried out under the guidance of *Prof. Noriyoshi Matsumi* at the School of Materials Science, Japan Advanced Institute of Science and Technology during 2013-2016. The studies are concerned with the design and synthesis of novel boron/silicon bimetallic copolymers with their applications.

The author express his deep gratitude to his supervisor *Prof. Noriyoshi Matsumi* for his kind guidance, valuable suggestions and heartfelt encouragements throughout this work.

I would also like to thank the members of my Review committee *Prof. Toshiaki Taniike, Prof. Yuzuru Takamura, Prof. Tatsuo Kaneko, Prof. Kazuaki Matsumura* and *Prof. Tomokazu Umeyama* who have spent their valuable time to read my manuscript and gave valuable comments and remarks to enhance the quality of my thesis.

The author is thankful to *Dr. Frieder Jackle*, for giving him an opportunity to carry out experiments at his laboratory at Department of Chemistry, Rutgers University, Newark, New Jersey, USA. Furthermore, the author wishes to express his special thanks to *Dr. Frieder Jackle* and members at his laboratory for their active collaboration, warm support and valuable suggestion's during the author's stay in USA.

The author also takes an opportunity to thank *Assistant Prof. Raman Vedarajan* for his guidance and encouragement at a professional and personal level. I am also grateful to other laboratory members, for their valuable inputs, cooperation and active discussions throughout my time at JAIST.

The author expresses his heartfelt gratitude to his parents and dear ones, for their relentless encouragement at difficult times. Finally, the author expresses his humble gratitude to the Almighty for everything.

School of Materials Science

Puhup Puneet

Japan Advanced Institute of Science and Technology

March 2016

Contents

Chapter 1: General Introduction	1
1. Introduction:	1
1.1 Boron Containing Polymers:	2
1.1.1 Boron Containing Main Chain Polymers	3
1.1.2 Hydroboration Polymerization:	3
1.1.3 Haloboration Polymerization	9
1.1.4 Phenylboration Polymerization	9
1.1.5 Alkoxyboration Polymerization	10
1.1.6 Grignard and Organolithium Reagents	10
1.1.7 Poly(pyrazabole)s via Cross-Coupling Reactions: Sonagashira Coupling	11
1.1.8 Dehydrocoupling Polymerisation:	13
1.2 Applications of Organoboron Polymers:	14
1.2.1 Anion Sensing	14
1.2.2 Emitting Materials for Organic Light Emitting Diode (OLED)	17
1.2.3 Electrolyte in Energy Devices	18
1.3 Silicon Containing Polymers	19
1.3.1 Polysilanes	19
1.3.2 Electronic Properties of Polysilanes	19
1.3.3 Synthetic Aspects of Polysilanes	21
1.3.4 Organic Polysilanes: Poly(organosilane)s	22
1.3.5 Applications of Polysilanes	23
1.3.6 σ - π Conjugated Organosilicon Polymers	24
1.3.7 σ - π Conjugated Organosilicon Polymers	25
1.3.8 Polycarbosilanes (SiC)	27
1.3.9 Polysiloxanes:	27
1.3.10 Poly(silylene-phenylene-siloxane): Dehydrocoupling Polymerization	27
1.3.11 Polysilsequioxane:	28
1.4 Boron-Silicon Containing Polymers	29
1.5 Survey of this Thesis	33
1.6 References	34
Chapter 2: σ -p Conjugated Copolymers via Dehydrocoupling Polymerization of Phenylsilane and Mesitylborane	38
2.1 Introduction	38
2.2 Experiment	40
2.2.1 Materials and Methods	40
2.2.3 Synthetic Procedure	40
2.2.4 Characterisation	40
2.3 Results and Discussion	41
2.4 Conclusions	47

Chapter 3: Synthesis and Applications of Poly(borosiloxane)	49
3.1 Introduction	49
3.1.1 Solid State Ultra-sensitivity Towards Fluoride Ions in Aqueous Media	51
3.1.2 Self-Healing Properties of Poly(borosiloxane)	52
3.1.3 Ion Conductive Properties of Ion-Gels with Poly(borosiloxane) Polymer Support	54
3.2 Experiment	55
3.2.1 Synthesis and Characterization	55
3.3 Application of Poly(borosiloxane)	63
3.3.1 Solid State Ultra-sensitivity Towards Fluoride Ions in Aqueous Media	63
3.3.1.1 Conclusion	68
3.3.2 Self-Healing Properties of Poly(borosiloxane)	69
3.3.2.1 Conclusion:	77
3.3.3 Ion Conductive Properties of Ion-Gels with Poly(borosiloxane) Polymer Support	78
3.3.3.1 Conclusion:	83
3.4 References	83
Abbreviations	86
Chapter 4: Poly(silylene/phenylene/borane) as Ultraviolet Emitter via Thermally Activated Delayed Fluorescence	87
4.1 Introduction	87
A) Incorporation of Heavy Metals	87
B) Triplet-Triplet Annihilation (TTA)	88
C) Hybridized Local and Charge-Transfer (HLCT)	89
D) Thermally Activated Delayed Fluorescence (TADF)	90
4.2 Experiment	94
4.3 Results and Discussion	98
4.4 Conclusion	107
4.5 References	107
Chapter 5: General Conclusion	109
5.1 General Conclusion	109

Chapter 1: General Introduction

1. Introduction:

Polymers:

A polymer is a long molecule made up of chains or rings of linked monomer units. They possess remarkable properties such as high thermal stability, high mechanical strength and so on¹. Generally, polymers can be classified as follows:

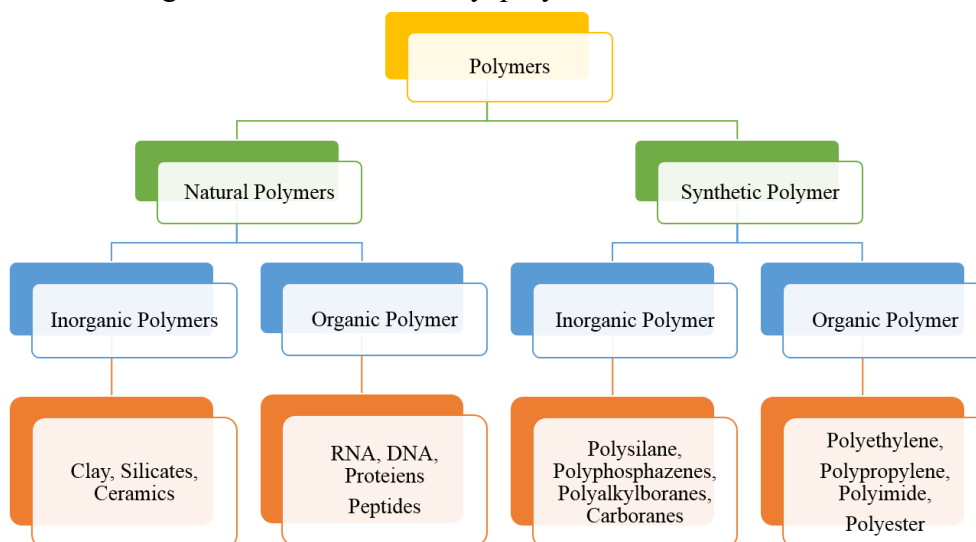


Figure.1: Classification of polymers.

Inorganic Polymers:

Polymer chemistry and technology cover molecular and materials science which involve nearly every aspect of modern life^{2,3}, technology, medicine, fibers, films, elastomers and so on. Most of these polymers are organic polymers i. e., the polymer chain mainly composed of carbon atoms and may have heteroatom such as oxygen and nitrogen. A major set of organic polymers are mainly derived from petroleum products or from plants, animals, or microorganisms which makes it easily available and are cost effective^{4,5}. In spite of the widespread importance of organic polymers, increasing interest has been developed towards inorganic polymers alongside organic polymers. This can be explained in two ways⁶. First, many organic polymers react with atmospheric oxygen or ozone over time and tend to lose their beneficial assets. Most organic polymers when burnt release toxic gases. Many organic polymers degrade easily and suffer from lack of durability. Also, it is very well in the chart of thought that the availability of many organic polymers may one day cease due to the availability of limited from petroleum fractions. Hence, it is believed that polymers with inorganic elements such as boron, silicon or phosphorus in main chain may solve a few or all of

these problems.

Secondly, inorganic elements may form dissimilar combinations of properties than do organic counterpart. These polymers more often than not are longer, stronger, and highly environment resistant. In addition, inorganic elements possess different valencies as compared to carbon and therefore allow enormous number of possibilities to design functional materials.

Among the numerous types of inorganic polymers we are focusing on **boron** and **silicon** containing polymers which covers a major range and types of polymers with interesting applications.

1.1 Boron Containing Polymers:

Fifth element in the periodic table, boron, has a vacant p-orbital which makes it interesting element. The sp^2 hybridized orbitals of boron sits at the vertices of an equilateral triangle whereas the vacant p-orbital points perpendicular to the plane of the equilateral triangle⁷. Therefore, boron compounds facilely react with electron rich species in order to overcome its electron deficiency. These properties together make boron very interesting in the field of material design and opens a wide window of functional materials. In spite of interesting properties of the small molecules of organoboron compounds, they still possess the problem of stability and are limited only to certain applications.

In early 1920's, Alfred Stock has reported the formation of boron polymers by the incorporation of boron hydride⁸. After this report various research groups started publishing number of papers and explored various kinds of polymers containing boron atom either in the main chain or in the pendant group. These polymers were found to have excellent properties and were employed in high performance composites, fibers, catalyst support, non-linear optics, chemo-sensors and so on. Although, the organoboron polymers itself cover a wide range of polymeric materials, herein, we will be focusing specifically on the polymers containing boron atom in the main chain.

Also, detailed description on different ways of synthetic roots and applications will be provided here. Before we classify these polymers it will be helpful to have a look into the interesting characteristics of the boron containing polymers.

1) Electrochemical characteristics: extension of π -conjugation via the vacant p-orbital was firstly studied theoretically by Good et al., based on Hückle MO theory⁹. Later overlap of π -orbitals to vacant p-orbitals was explored for the design of various p- π conjugated polymers¹⁰.

2) Nuclear characteristics: boron atom naturally exist in two isotopes (B^{10} , B^{11}). Therefore, B^{10} has ability to capture neutrons. This unique property of boron containing polymers were exploited in the therapeutic effect and cancer treatment¹¹. Also, it is used as control rods in nuclear reactor.

3) It can react with oxygen at higher temperatures to form B_2O_3 char which can act as protecting layer for high-performance materials.

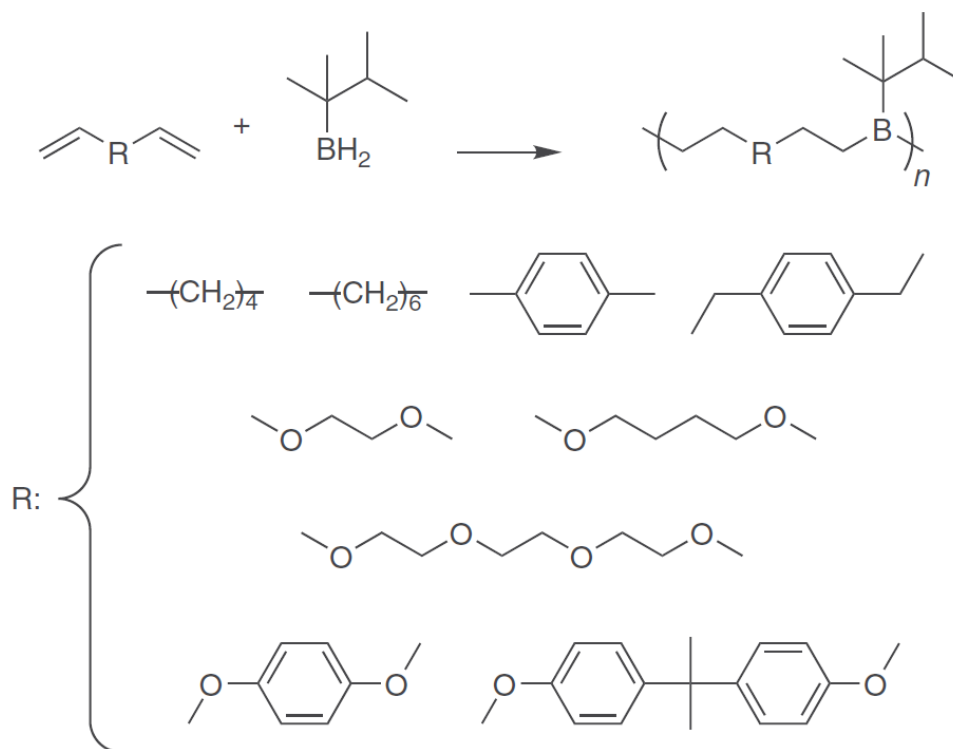
1.1.1 Boron Containing Main Chain Polymers

A variety of organoboron polymers has been studied by Chujo et al.,¹² and their properties were reported. Most of them were prepared by the hydroboration reaction which was developed by H. C. Brown et al.,¹³ in his pioneering work.

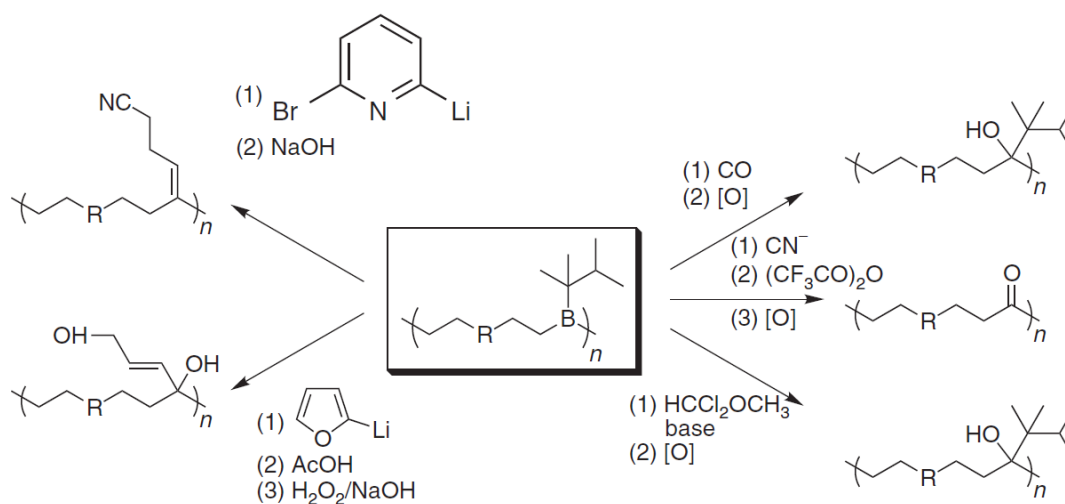
1.1.2 Hydroboration Polymerization:

Hydroboration of Diene Monomers:

The quantitative addition of diene and hexylborane yielded poly(alkylborane)s (**Scheme 1**)¹⁴. These reactions were carried out at lower temperatures and under nitrogen atmosphere. Prepared polymers were subjected to thermal and oxidative stability examination and were found to be more stable in air compared to trialkylboranes. Later, in the modification, the hexylborane was replaced by mesitylborane and trisopropylphenylborane. Also, these polymers act as Lewis acidic polymers and therefore are termed as reactive polymers which were proved to be useful in the transformation into functional polymers as poly(alcohol)s, poly(ketone)s etc. (**Scheme 2**)^{15,16}.



Scheme 1: Hydroboration Polymerisation of Various Diene Monomers With Thexylborane.



Scheme 2: Various Reaction of Organoboron Polymers.

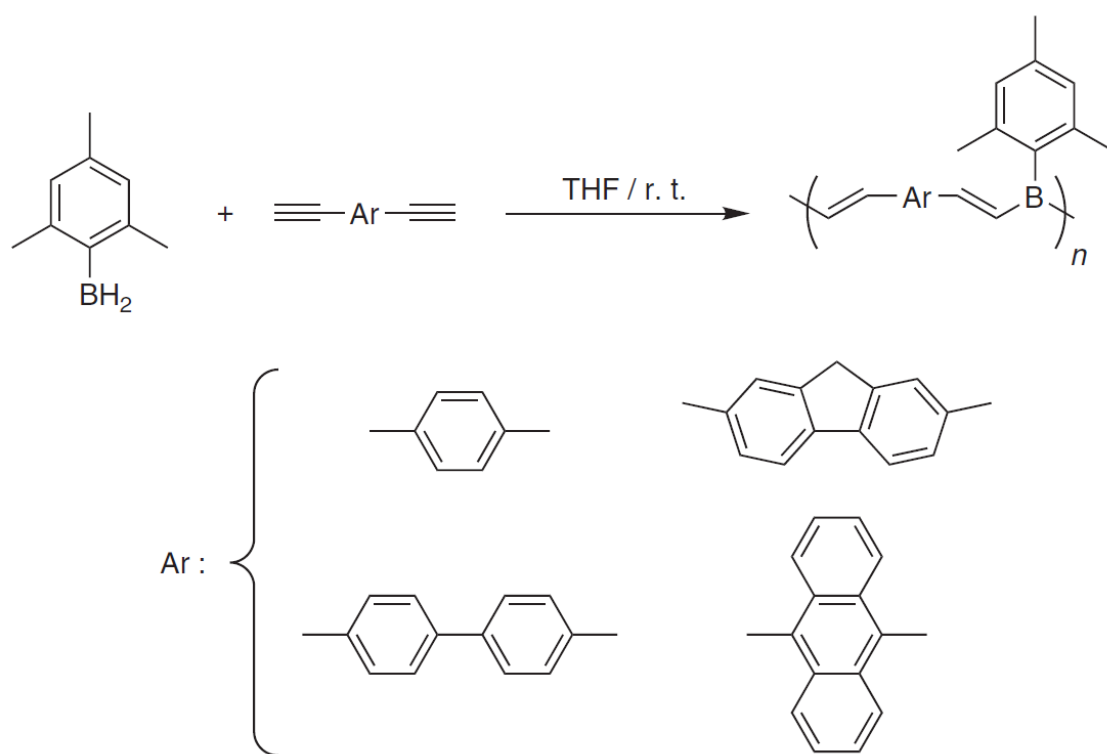
π -Conjugated Organoboron Polymers:

Hydroboration of Diyne monomers:

π -conjugated polymers¹² have been in the lime light after the discovery of

electrically conductive polyacetylenes for their contribution in the design of functional materials in the field of light emitting polymers, third order non-linear optical fibers and electronic conductors. The conjugation of π -electron of vinyl group and boron moiety has been previously studied and investigated by ^{11}B -NMR spectroscopy and UV-vis absorption spectra¹⁷. These analysis were in clear agreement to the results from theoretical calculation results of molecular orbital theory.

Aromatic organoboron polymers were expected to behave like π -conjugated polymers with unknown electronic states having holes built through the polymer system. In order to explore these interesting properties of π -conjugated organoboron systems, hydroboration polymerization of diynes monomers with mesitylborane and triisopropylphenylborane were performed to yield various kinds of π -conjugated organoboron polymer (**Scheme 3**)¹⁰.



Scheme 3: Synthesis of Conjugated Organoboron Polymers From The Hydroboration Reaction Between Mesitylborane and Diynes.

These polymers showed intense visible blue light fluorescence emission when a dilute solution in chloroform was irradiated at 350 nm at ambient temperature. Similarly, hydroboration polymerization of heteroatomic diyne (2,5-diethynyl thiophene, 2,5-diethynyl furan and 2,5-diethynyl pyridine) with mesitylborane was done. Thus, the donor-acceptor unit pair was inserted into the conjugated system (**Chart**

1)¹⁸. These polymers also showed large Stokes shift because of energy transfer in the excited state.

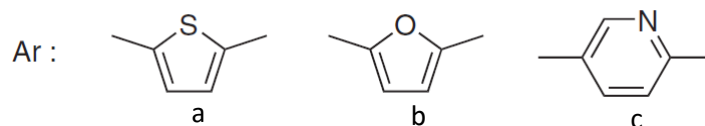


Chart 1: Donor-Acceptor Type Conjugated Organoboron Polymer Having (a) Thiophene, (b) Furan and (c) Pyridine In The Main Chain.

$d\pi\text{-}p\pi^*$ Transition In The π -Conjugated Organoboron Polymer By the Incorporation of Ruthenium Complex:

Hydroboration polymerization between mesitylborane and tetrayne type monomer having ruthenium phosphine complex was carried out¹⁹. Resulted polymer exhibited two maxima in UV-vis absorbance spectrum due to $\pi\text{-}\pi^*$ transition and $p\pi\text{-}d\pi$ transition at 359 nm and 524 nm respectively. A large red shift of 114 nm than that of monomer can be attributed to the push-pull effect between electron rich ruthenium complex and electron deficient organoboron moiety. Also, increased length of π -conjugation in the polymer backbone can explain such red shift of the maxima in absorbance spectra (**Chart 2**).

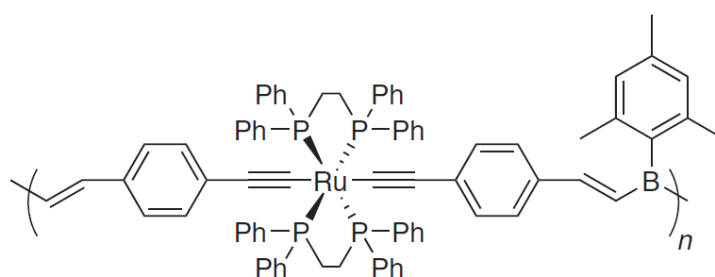


Chart 2: Example of Ruthenium Incorporated Conjugated Organoboron Polymer.

Platinum or palladium containing π -Conjugated boron polymers were prepared by hydroboration polymerization between tetrayne/metal complex monomers and triphenylborane²⁰ (**Chart 3**). Number-average molecular weights of the polymers reached more than 9000 g/mol. The absorption peaks due to $\pi\text{-}\pi^*$ transition were observed around 390 nm in the UV-vis spectra and fluorescence emission peak observed at 490 nm.

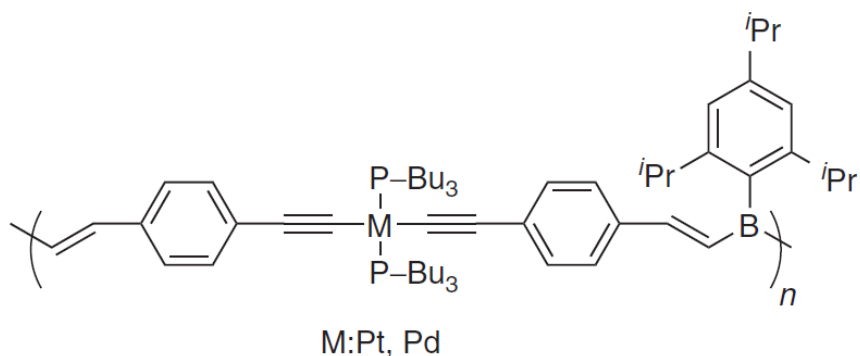
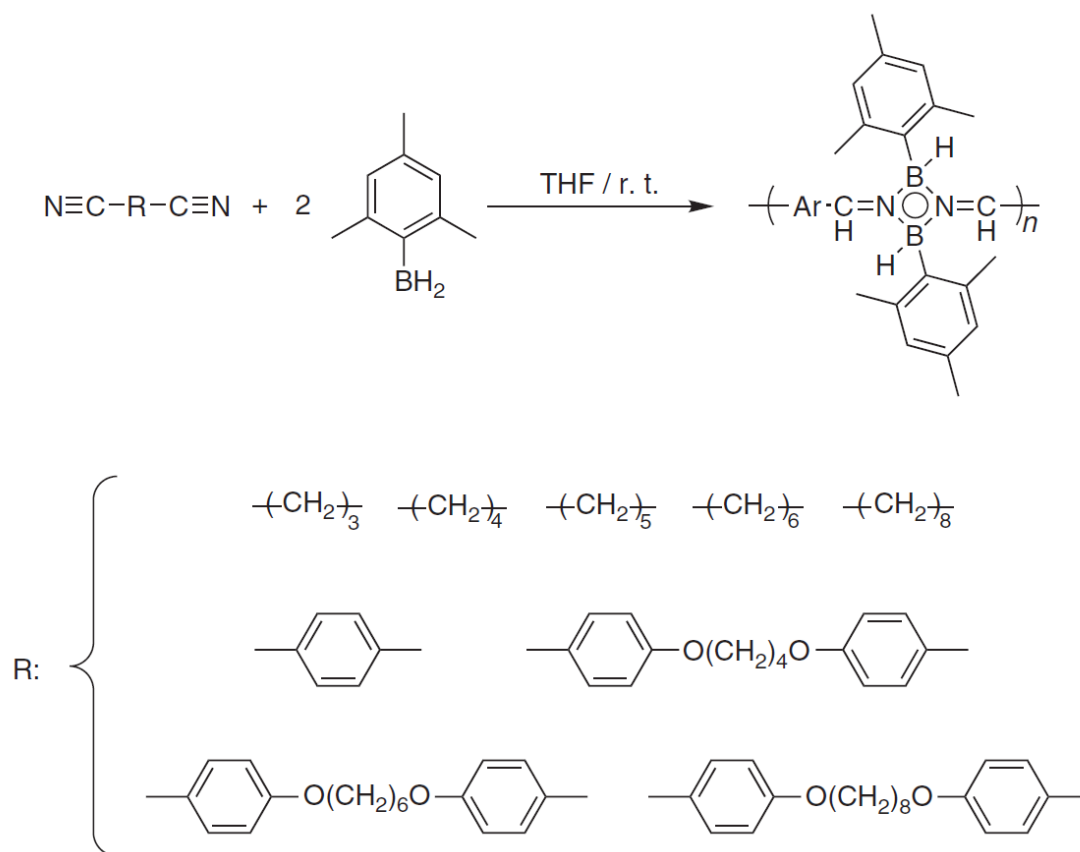


Chart 3: Example of Platinum and Palladium Incorporated Conjugated Organoboron Polymer.

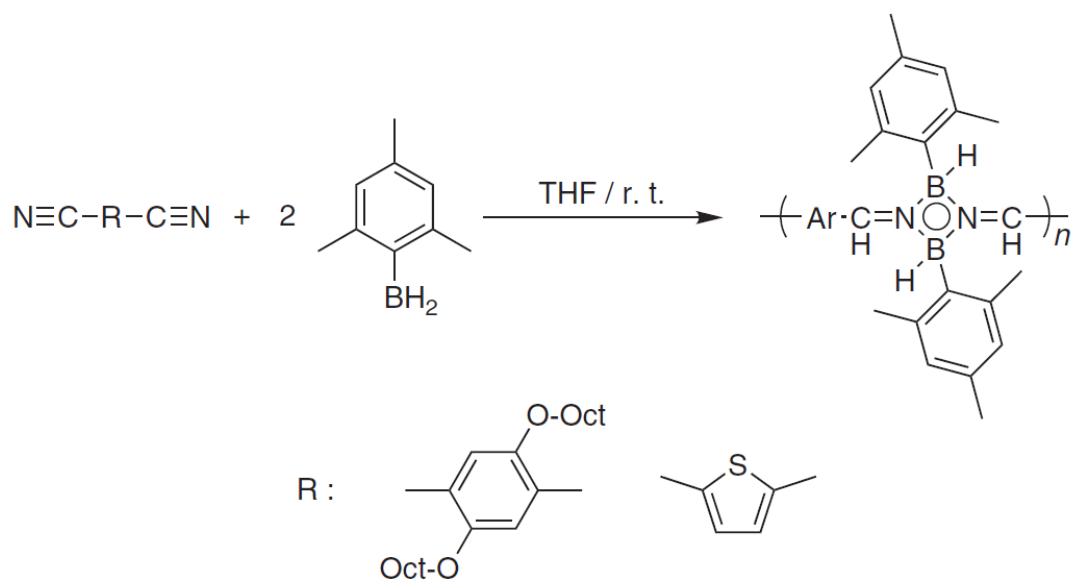
Poly(cyclodiborazane)s via Hydroboration Polymerization of Dicyano monomers:

Synthesis of poly(cyclodiborazane)s via hydroboration polymerization of dicyano compounds were examined²¹. Cyclodiborazane structures possessing four-membered boron nitrogen rings were formed by dimerization of iminoborane. Further, in order to prepare soluble, high molecular weight and stable polymer, more bulky and electron rich borane monomers were incorporated (**scheme 4**). Due to the presence of bulky mesityl groups, formation of borazine as a side product were almost negligible.



Scheme 4: Synthesis of organoboron polymers with cyclodiborazane units in the main chain.

π -Conjugated organoboron with fully aromatic poly(cyclodiborazane)s were synthesized. It is important to mention here that no significant extension of conjugation length was observed when 1,4-dicyanobenzene was used as a dicyano monomer. Later on, incorporation of the electron donating structure in the poly(cyclodiborazane)s backbone (**Scheme 5**) led to a dramatic bathochromic-shift in absorption, indicating the occurrence of intramolecular charge-transfer (ICT) interaction due to interunit conjugation along the chain²². Also, it gives an idea about the extreme sensitivity of electronic state of poly(cyclodiborazane) around the cyclodiborazane unit. In these polymer systems, the emission wavelength was found to be fine-tunable.



Scheme 5: Synthesis of Conjugated Organoboron Polymers with Cyclodiborazane Units in The Main Chain.

Apart from hydroboration polymerization there are few more methods of boration polymerization:

1.1.3 Haloboration Polymerization

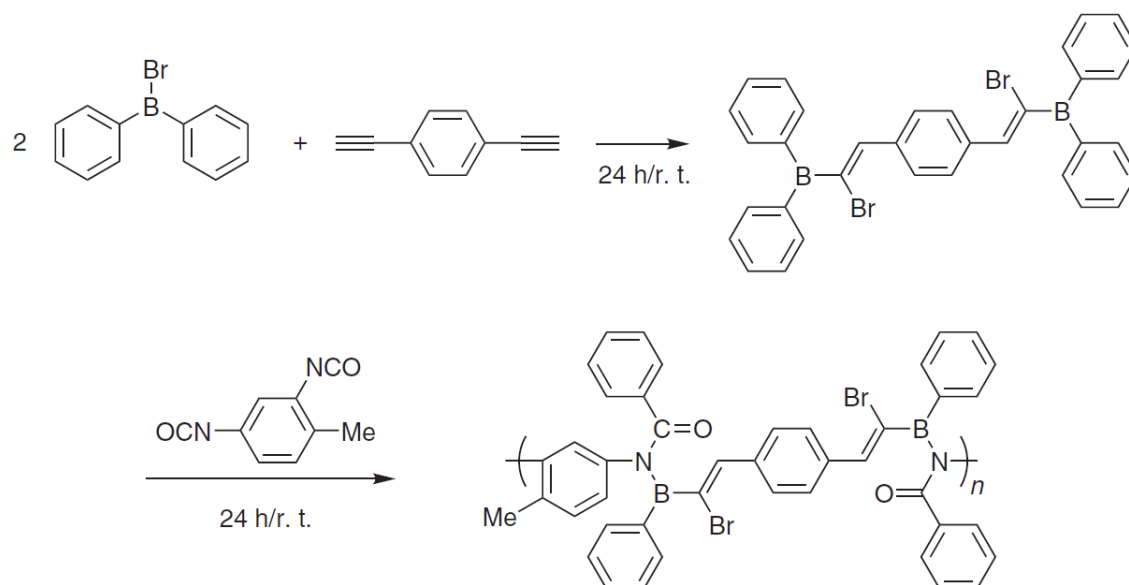
Dialkenylboron bromide prepared by haloboration²³ of a diyne with BBr, has a low Lewis acidity due to the two alkenyl groups on the boron atom. Therefore, differently reactive B-Br and dialkenylboron bromide creates a possibility of gelation with efficient crosslinking but after treatment with alcohol dialkenylalkoxyborane is formed (**Scheme 6**).



Scheme 6: Schematic of Haloboration Polymerization.

1.1.4 Phenylboration Polymerization

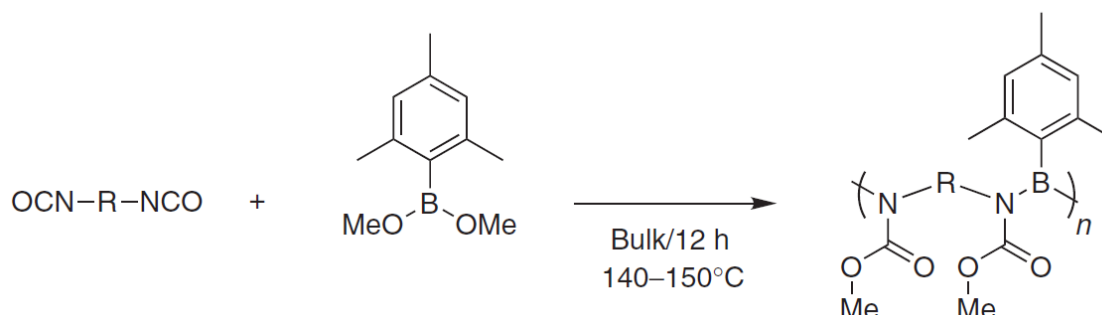
The polymers prepared by phenylboration polymerization of diynes showed relatively high durability and could withstand against air and thermal oxidation. Making use of different boration reactivities between diynes and diisocyanates²⁴ (**Scheme 7**), alternating boration copolymers were prepared.



Scheme 7: Schematic of Phenylboration Polymerization.

1.1.5 Alkoxyboration Polymerization

Alkoxyboration polymerization were performed with diisocyanates and mesityldimethoxyborane to yield poly(boronic carbamate)s²⁵ (**Scheme 8**).

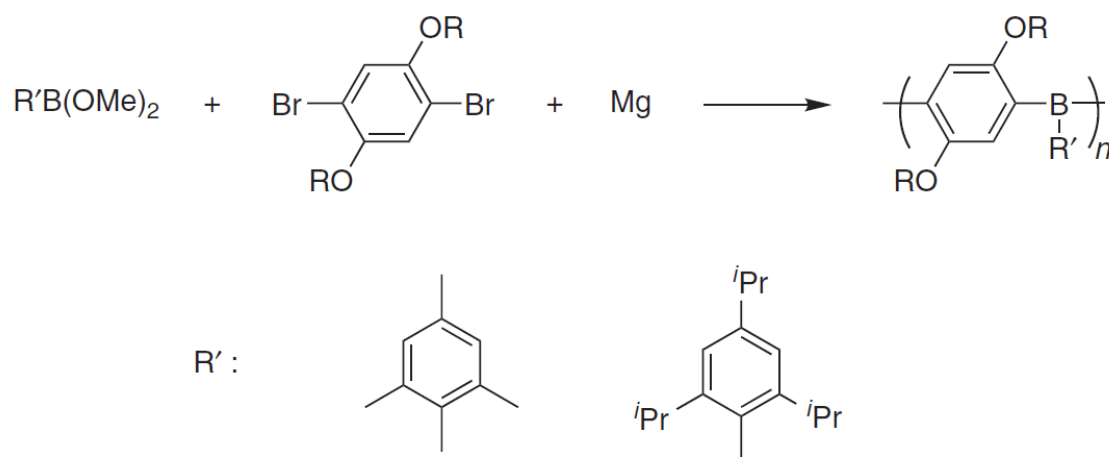


Scheme 8: Schematic of Alkoxyboration Polymerization.

1.1.6 Grignard and Organolithium Reagents

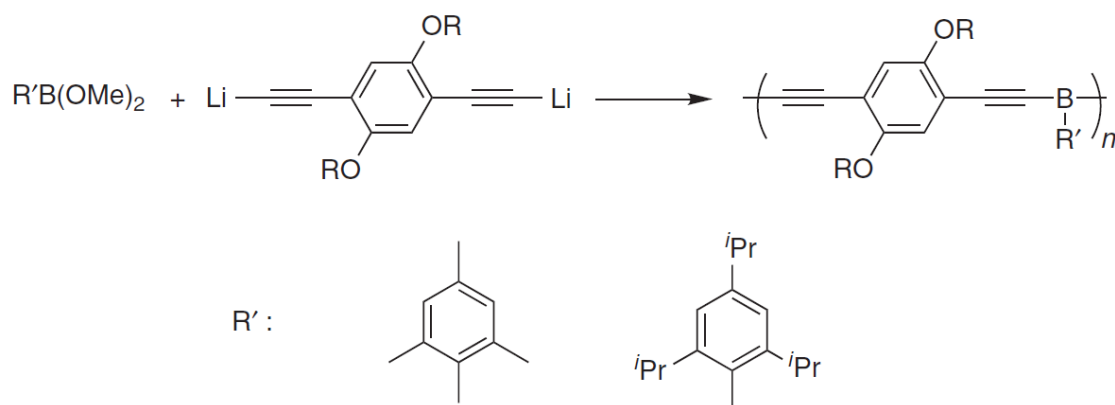
The preparation of organoboron polymerization was not limited only by hydroboration polymerization but also different approaches were adopted by various researchers. Organometallic approaches involving Grignard reagent and organolithium were examined. Poly(*p*-phenylene-borane)s were prepared by polycondensation of aryl dimethoxyboranes and *in situ* generated bifunctional Grignard reagents²⁶ (**Scheme 9**). This provided a novel methodology for the preparation of organoboron conjugated polymers, which then proved to be promising alternative to hydroboration polymerization. These polymers can be considered as a novel n-type conjugated

polymers with good stability in air and moisture. Better thermal stability is also expected because of absence of a retrohydroboration (β -elimination) process via thermal degradation.



Scheme 9: Synthesis of Conjugated Organoboron Polymer By In Situ Generated Grignard Reagent.

Also, Poly(ethynylene-*p*-phenylene-ethynylene-borane)s were synthesised by polycondensation of bifunctional lithium acetylides and aryldimethoxyborane²⁷ (**Scheme10**). These polymers showed intense fluorescence emission spectra, wavelength maximum at 456 nm in the visible blue region.



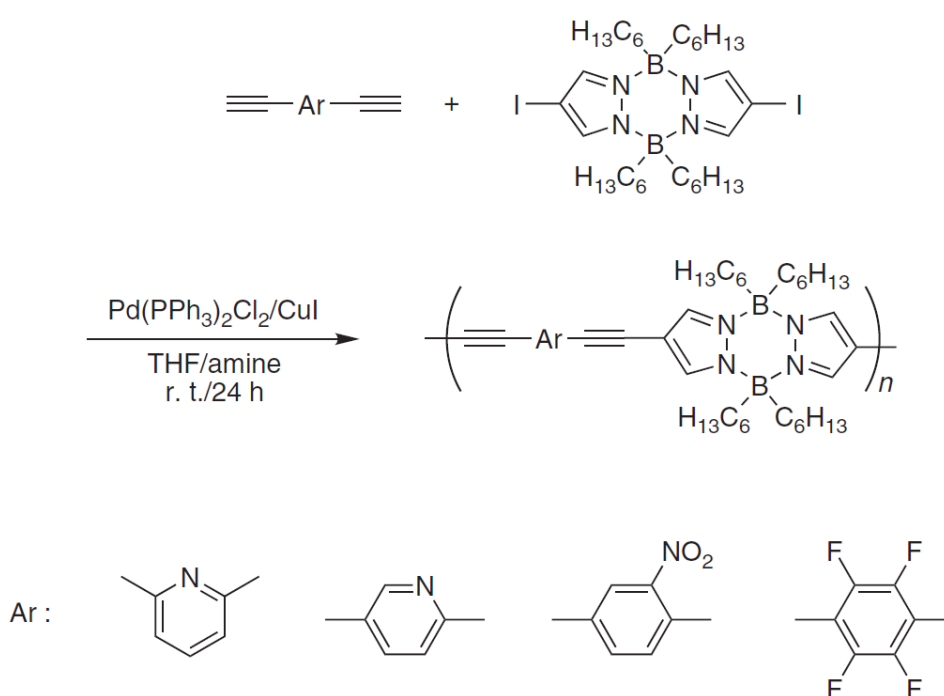
Scheme10: Synthesis of Conjugated Organoboron Polymer by In Situ Generated Organolithium Reagent.

1.1.7 Poly(pyrazabole)s via Cross-Coupling Reactions: Sonagashira Coupling

After the first report of pyrazaboles synthesis²⁸ in 1967, a number of pyrazaboles have been designed and their properties were investigated. Structures and properties have not been fully understood of this novel class of boron heterocycles.

Pyrazaboles were found to be appreciably stable, thus a number of derivatives having various functional groups were also prepared by simple organic reaction. Several recent applications of pyrazaboles have been reported²⁹, one of them is to use it as building blocks for discotic liquid crystals or good bridges for *ansa*-ferrocenes to form active container molecules for supramolecular assembly.

Sonogashira–Hagihara coupling was employed as a facile method for the preparation of organoboron polymers containing pyrazaboles in the main chain. Reaction between diyne and pyrazabole derivatives gave the corresponding polymers³⁰ (Scheme11).

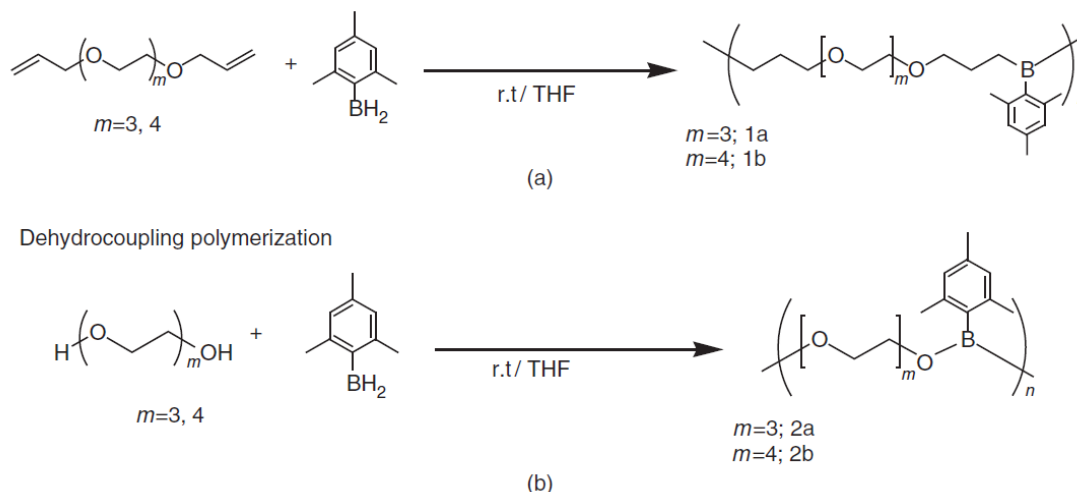


Scheme 11: Synthesis of Conjugated Pyrazabole Containing Polymers Using Sonogashira Coupling.

Neutron scintillator materials require a high detection efficiency and a large n/g ratio. Poly(pyrazabole)s were investigated as a neutron scintillator material³¹. The poly(pyrazabole)s consisting only of light elements such as C, N, B, and H. As a thumb rule, high detection efficiency and a large n/g ratio, the materials should contain light elements (^3He , ^6Li , and ^{10}B).

1.1.8 Dehydrocoupling Polymerisation: Anion-Trapping-Type Organoboron Polymer Electrolytes

Synthesis of organoboron polymer electrolytes³² was examined by hydroboration polymerization between mesitylborane and triethyleneglycol diallyl ether³³. Further, dehydrocoupling polymerization³⁴ method was used to prepare poly(alkoxyborane) type of electrolytes (**Scheme 12, below**).



Scheme 12: Poly(alkoxyborane)s Prepared by Hydroboration Polymerization and Dehydrocoupling Polymerization.

Ionic conductivity of these polymers was observed to be 3.05×10^{-5} – $5.22 \times 10^{-6} \text{ Scm}^{-1}$ at 50 °C. It was inferred that ionic conductivity of these polymers was not restricted by bulky substituents on the boron atom. Alkylborane-type polymers showed a larger temperature dependence of ionic conductivity in comparison with boric-ester-type polymers. This is due to lower segmental mobility of alkylborane polymers, as implied from their higher glass-transition temperature.

The lithium ion transference number³⁵ (t_{Li^+}) at 30 °C was 0.50–0.35 which is significantly higher than polyethyleneoxide type of electrolytes and it is evident that anions were significantly trapped in these systems giving rise to a better transport of lithium ion selectively. Few more organoboron polymers prepared by dehydrocoupling polymerization are shown below^{33,34} (**Chart 4**)

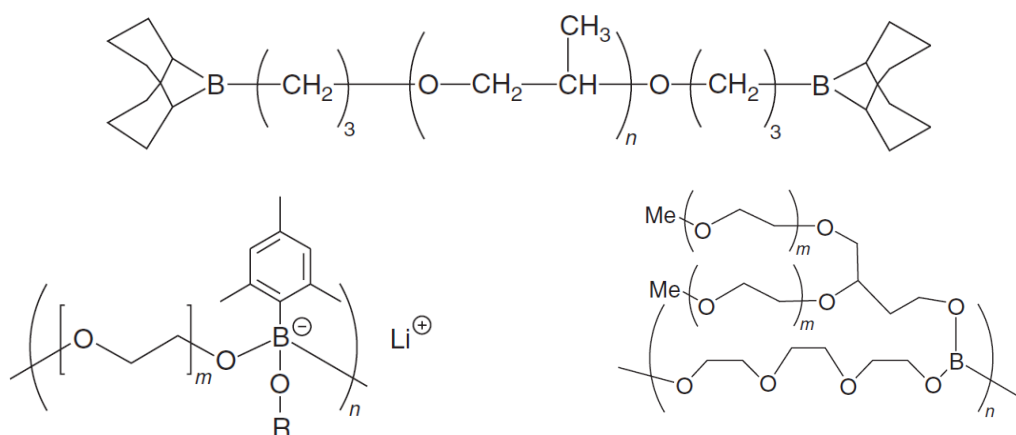


Chart 4: Examples of poly(alkoxyborane)s.

1.2 Applications of Organoboron Polymers:

The organoboron polymers are special class of materials which covers variety of different type of polymers having electronic, mechanical and functional properties. A wide expanse of applications are possible with these material, to name a few:

1.2.1 Anion Sensing

Lewis acidic triarylboranes react facilely with small and strong Lewis basic anions including fluoride to yield fluoroborates. This reaction is customarily known as an addition reaction, which occurs via donation of an electron pair of the fluoride anion into the p-orbital of the boron center³⁶. A number of low molecular weight as well as polymeric organoboron compounds are already reported in the literature³⁷. The sensing of fluoride ions can be seen visually and also analyzed spectroscopically. Quenching of absorbance and/or fluorescence emission of organoboron polymers have been evident by the reaction of fluoride anions. For instance, π -Conjugated polycarbazole boron complex exhibit colorimetric as well as spectroscopic changes on fluoride anions³⁸ (Chart 5, Figure 2, Figure 3).

Recently, electrochemical measurements turned out to be a powerful tool to specifically analyze the fluoride ion sensing. Here, in this case, cyclic voltammetry technique was employed to monitor the redox behavior of the polycarbazole- BF_3 complex in tetrahydrofuran (THF)/ tetrabutyl ammonium perchlorate (TBAP) solution with subsequent addition of various concentrations of TBAF. The complex exhibited a significant shift in reduction peak 1 (near 0V) as shown in **Figure 4**.

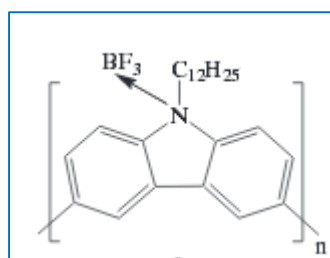


Chart 5

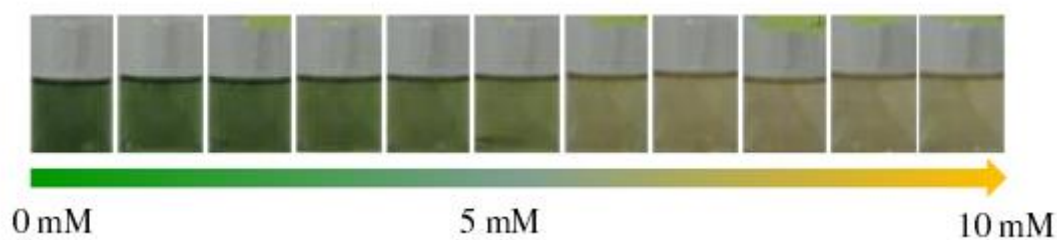


Figure 2: Colorimetric Changes During the F^- Titration of 10 Mm In THF. [TBAF] = 0, 1, 2, 3, 4, 5, 6, 7, 8, 9, 10 Mm (Left To Right).

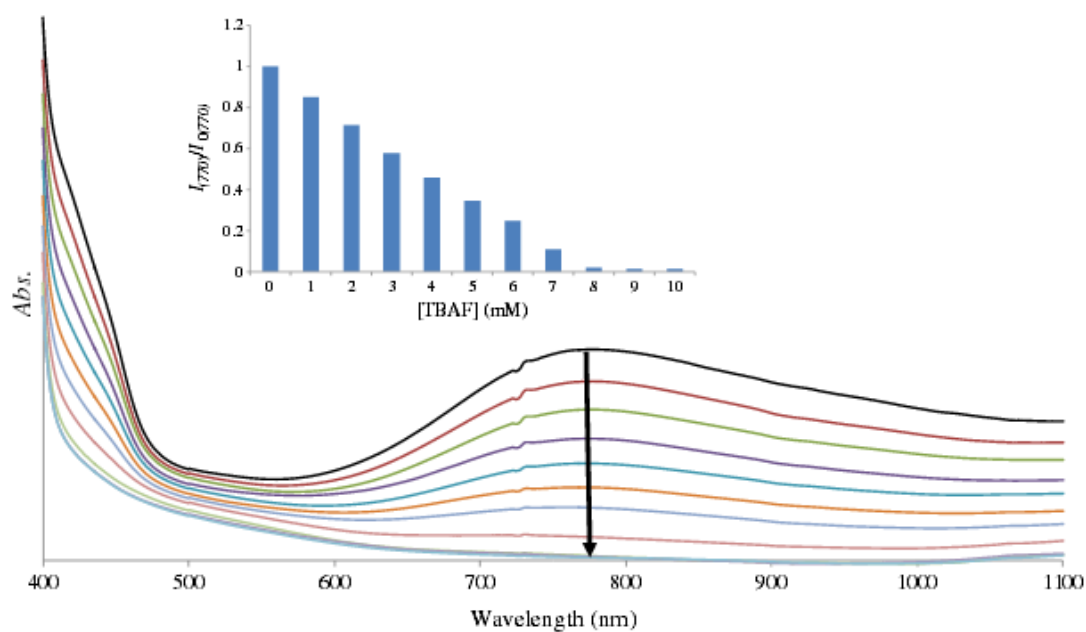


Figure 3: Changes in The UV–Vis Spectra (10mm) in THF Solution With Addition Of F^- . [TBAF]=0, 1, 2, 3, 4, 5, 6, 7, 8, 9, 10 mM (Top To Bottom). (Inset): Absorption Change At 790 Nm, $I_{790}/I_0(790)$.

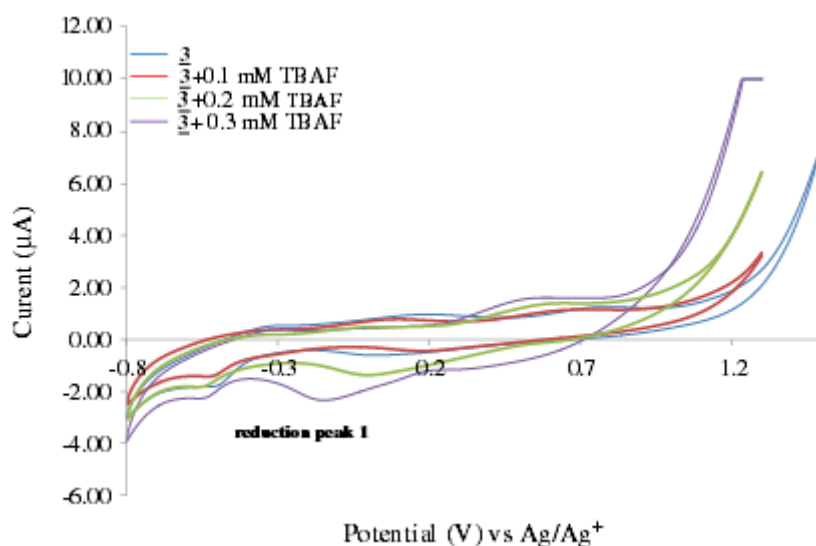


Figure 4: CVs of 1 mM Polymer During Addition of TBAF 0.1–0.3 mM Measured in THF/TBAP at a Sweep Rate of 75 mV/S.

Moreover, the solid state sensing ability of polycarbazole–BF₃ complex was evaluated. The open circuit voltage (OCV) measurement of casted film on glassy carbon (GC) electrode was carried out and it showed a step-wise decrease in potential with the addition of tetrabutyl ammonium fluoride (TBAF) in a 100% aqueous media (**Figure 5**).

These electrochemical methods, interestingly does not require chromophoric group in the sensing materials, thus could be an extraordinarily useful technique.

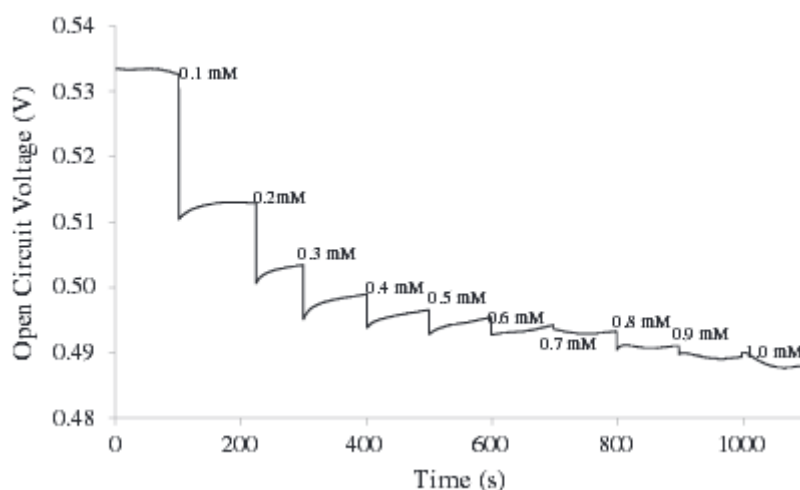


Figure 5: Open Circuit Voltage Responses of Film on GC to 0.1mM–1.0 mM TBAF in H₂O.

1.2.2 Emitting Materials for Organic Light Emitting Diode (OLED)

Boron has one less electron than carbon. Because of the vacant-p orbital present in tricordinate boron unique properties can be induced other than that of introduction of atoms having lone pair of electrons³⁹. Also, by boron incorporation, lower levels of LUMO can be achieved in a conjugated system¹². To explore it further, a number of organoboron polymers having various types of boron complexes have been studied (**Chart 6**)³⁹. Most of the polymeric structure showed intense fluorescence emission in comparison to the monomeric structure. This can be because of extension of conjugation in polymers.

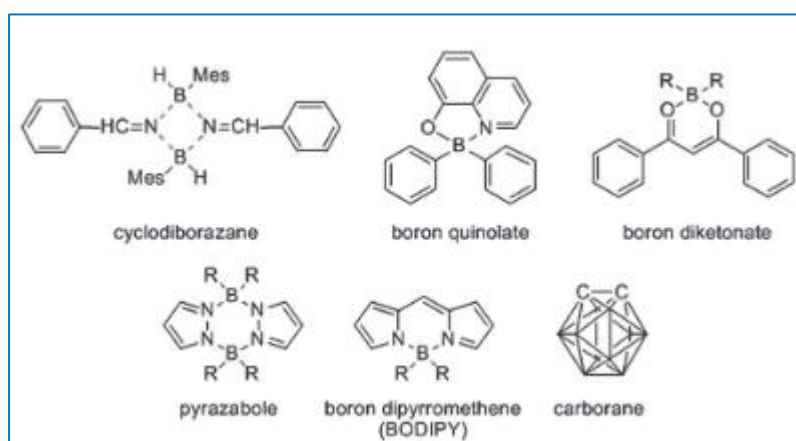


Chart 6: Various Types of Boron Complexes.

The above mentioned properties of organoboron conjugated polymers make them strong candidate to be used as emitting material in OLED. In addition, specifically in the case of organoboron quinolate polymers where conjugated system from the quinolate ligand can be separated by boron atom, there is a possibility to tune the electronic structure at both the sides^{40,41} (**Chart 7**).

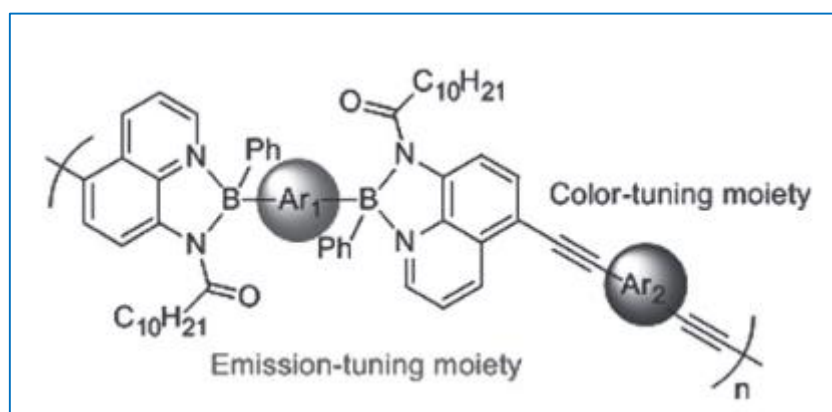


Chart 7: Example of Organoboron Quinolate Polymers with the possibility of color-tuning with change in aromatic units.

1.2.3 Electrolyte in Energy Devices

In majority of polymer electrolytes, both anions and cations migrate under a potential gradient. Efficient transport of target cation is also inhibited by the binding of lithium cations by polar ether oxygens (**Figure 6**)⁷. Generally, the lithium transference number of polyether-type electrolytes are nearly 0.1-0.2 at room temperature which are very low.

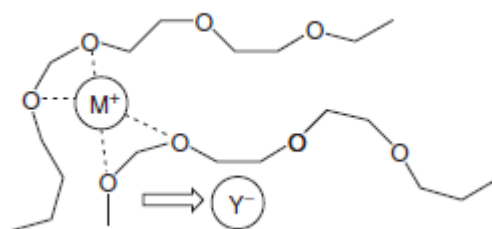


Figure 6: A Schematic Illustration of Ether Oxygens Binding to Lithium Ions.

By hydroboration polymerization and dehydrocoupling polymerization methods, several lewis acidic organoboron polymers have been studied by various groups^{32,42}. These, polymer show relatively high cation transport because of the anion trapping effect of boron atoms. This, in turn, also help in lithium salt dissociation for the betterment of ion conduction.

1.3 Silicon Containing Polymers

Organosilicon polymers chemistry is currently in the stage of its importance where development⁴³ and design of advanced materials without organosilicon polymers is difficult to imagine. Several reviews and reports validate the above mentioned fact for good number of years now and it is valid to date and it has imitated the reality without any failure. The new synthetic approaches are in use these days⁴⁴, contemporary techniques and new methods of analysis of the synthesized polymers are also in process of development. Because of exceptional properties of organosilicon polymers, they are in lime light in almost every field of materials design and act as an impelling cause for further expansion and improvement of their syntheses. Further modification of polymers having useful practical applicability are strongly required in this field.

In the introduction of silicon containing polymers, it is mandatory to mention the fact that because of silicon, 14th element of the periodic table is very similar to carbon in terms of catenation unlike boron. Having loosely bound sigma electrons, it can enjoy delocalization of sigma electrons through the chain in the case of polysilanes⁴⁵. Also, having a vacant d-orbital it can accept the lone pair of electrons when bound with electronegative atoms⁴⁶ showing very high stability and usefulness in a variety of applications. In order to understand it in detail, it will be useful to categorize it as following and also to brief note on the synthetic and application aspects of these polymeric materials.

1.3.1 Polysilanes

Polysilanes with silicon backbone, are known for a long time but there are limited methods available in the literature for controlled synthesis. The formation of Si-Si bonds to yield polysilanes are still under investigation by many researchers. Polysilanes possess unique electro- and photochemical properties which comes from σ -conjugation in the Si-Si-chain. These properties make polysilanes a promising material to be used in devices.

1.3.2 Electronic Properties of Polysilanes

Linear permethylpolysilanes, $\text{Me}(\text{SiMe}_2)_n\text{Me}$, exhibited absorption in ultraviolet region. The absorption intensity kept on increasing with increasing number of Si units along with a bathochromic shift⁴⁷. This was very similar to that of conjugated polyenes and appeared to be one of the first indications of electron delocalization in silicon-silicon bonds of polysilanes which was later diagnosed as σ -conjugation.

Further, the cyclic peralkylsilane oligomers, $(R_2Si)_n$ with $n = 4-6$, revealed strong delocalization of electron⁴⁸. These rings structurally looked to be similar to aromatic hydrocarbons. For example, formation of anion radicals via reduction electronically, for instance naphthalene. In the case of naphthalene, unpaired electron occupies the lowest unoccupied molecular orbital (LUMO) (**Chart 8**). Similarly, the cyclosilanes $(RR'Si)_n$, where $n = 4-6$, yield strongly colored anion radicals. Further, electron spin resonance spectra clearly signifies complete delocalization of unpaired electron over the ring⁶ (**Chart 9**).

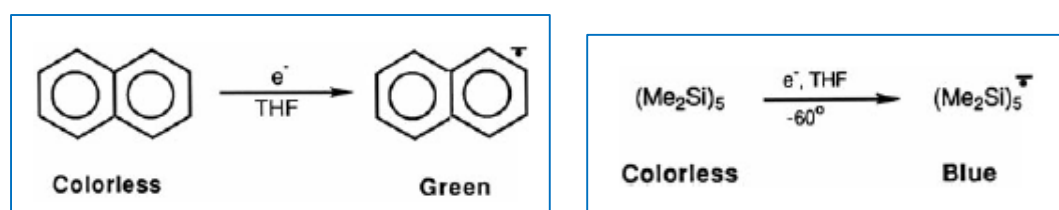


Chart 8: Naphthalene Changes Color on Reduction. **Chart 9: Cyclosilanes Changes Color on Reduction.**

In polysilanes, owing to the delocalization of electron through the polymer chain, additional physical properties such as strong electronic absorption, electronic conductivity, photoconductivity are achieved. These polymers are very much different from other conjugated polymers such as polyacetylene, as in these systems delocalization happens via π -electrons.

For better understanding, the absence of delocalization of σ -electrons in other systems like polyethylenes can be explained with help of ionization energies for the sigma-electrons. In most of the covalent bonds (C-C, C-H, C-O, Si-O, etc.), the ionization energies of the σ -electrons are much larger. The fact that the σ -electrons are strongly bound make them unconsiderable for the delocalization. Whereas, the ionization energies of electrons in Si-Si sigma bonds are appreciably lesser and in a few cases they have been found to be even lesser than that of π -electrons in olefins. For comparison, the first ionization energy for each compound are listed below⁴⁹:

$CH_3CH_2CH_2CH_3$: 10.6 eV; $H_2C=CH-CH=CH_2$: 9.1 eV; and $Me(SiMe_2)_4Me$: 8.0 eV.

Further, the interaction with neighboring Si-Si bonds can be visualized as a split up of energy. Splitting results in filled Si-Si σ -bonding orbitals as well as σ^* antibonding orbitals, which are also split by σ -resonance. The band gap between the σ

HOMO and σ^* LUMO becomes smaller as the number of Si atom increases. Finally, the filled orbitals combine to form a valence band whereas the unfilled orbitals combine to generate an empty conduction band⁴⁸ (**Figure 7**).

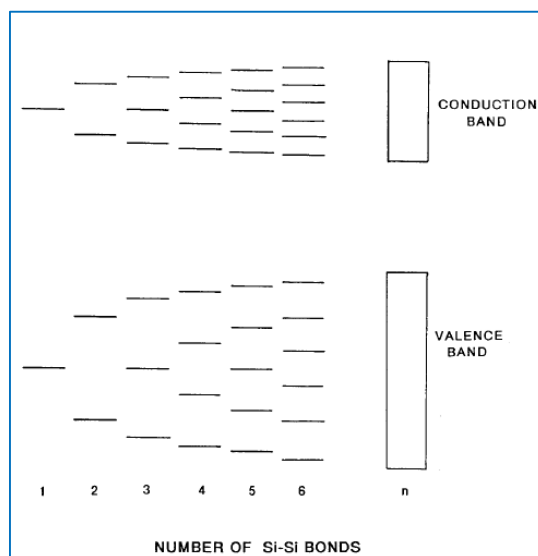


Figure 7: Schematic Diagram Showing Splitting of Filled and Unfilled Energy Levels in Polysilanes.

The aforementioned phenomenon can be experimentally determined by UV-Vis spectra of some of the polysilanes are given in **Figure 8**⁵⁰. Here, increase in absorption intensity along with red shift in the maximum wavelength is clearly observed with increase in the chain length of polysilanes.

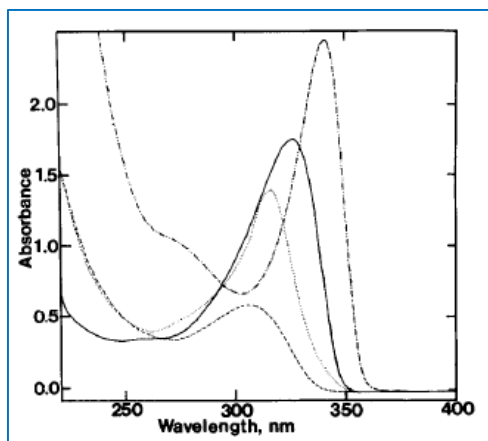


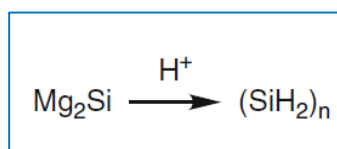
Figure 8: Absorption Spectra of Various Polysilanes. -.-.-. (PhSiMe)*n*, _____ (cycloHexSiMe)*n*, (*n*-exSiMe)*n*, (*n*-DodecylSiMe)*n*.

1.3.3 Synthetic Aspects of Polysilanes Polyhydrosilanes

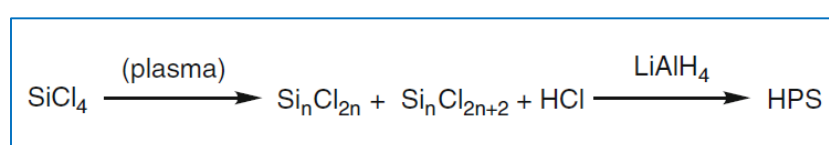
Fehér and co-workers designed a synthetic procedure for making oligomeric

silanes on a large scale from magnesia silicide⁵¹ (**Scheme 13 b**), also in 2008, a novel approach was employed for the production of polysilanes. SiCl₄ and H₂ are reacted in a plasma process to yield perhalogenated polysilanes, further by hydrogenation via LiAlH₄ results in high molecular weight polyhydrosilane (HPS)⁵² (**Scheme 13 b**).

(a)



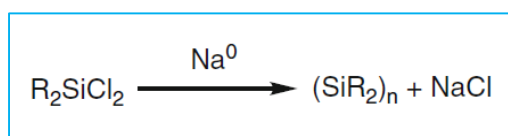
(b)



Scheme 13: Synthesis of Polyhydrosilanes.

1.3.4 Organic Polysilanes: Poly(organosilane)s Wurtz-Type Coupling of Chlorosilanes

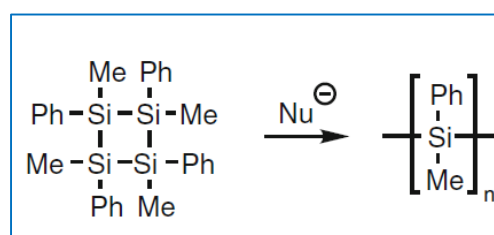
A well known Wurtz-type dehalogenative coupling reaction was first examined by Kipping et al⁵³., and it is widely known method for the synthesis of polysilanes. A dichlorodiorganosilane is reacted with a slight excess of sodium in an inert condition and refluxed to yield the polysilane as shown in **Scheme 14**.



Scheme 14: Synthesis of Poly(organosilane)s via Wurtz coupling.

Ring Opening Polymerization of Silacycles:

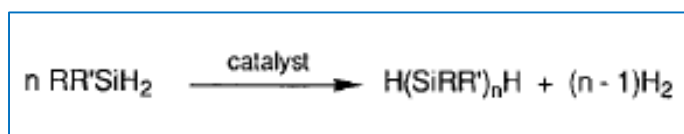
Matyjaszewski et al., found that (PhMeSi)₄ readily undergoes polymerization by nucleophilic initiators such as organolithium compounds⁵⁴ (**Scheme 15**).



Scheme 15: Synthesis of Poly(Organosilane)s Via Ring Opening Polymerization.

Dehydrogenative Coupling Polymerization:

Catalytic reactions of silanes to give polysilanes and hydrogen is called dehydrocoupling reactions^{55,56} (**Scheme 16**). This is a promising route for the preparation of functionalized polymers but low molecular weight of polymers are achieved. The required monomers for this type of polymerization need to possess at least two Si–H groups. Therefore, some of the suitable silanes are primary (RSiH₃) and secondary silanes (R₂SiH₂). PhSiH₃ is readily available and liquid at room temperature that is why it is used mostly in the preparation of polysilane (**Table 1**).



Scheme 16: Synthesis of Poly(Organosilane)S Via Dehydrocoupling Polymerization.

Table 1: Silane Units Employed for Dehydrocoupling Polymerization.

Arylsilanes	<i>M_n</i> ; PDI
<i>m</i> -MeC ₆ H ₄ -SiH ₃	900; 2.1
<i>p</i> -MeC ₆ H ₄ -SiH ₃	530; 1.9
	1,530; 1.5
<i>p</i> -MeOC ₆ H ₄ -SiH ₃	2,330; 1.5
	800; 3.5
<i>p</i> -FC ₆ H ₄ -SiH ₃	3,780; 1.9
<i>p</i> -Me ₂ NC ₆ H ₄ -SiH ₃	400; 1.5
	590; 1.7
<i>p</i> -(<i>i</i> -Pr)OC ₆ H ₄ -SiH ₃	2,150; 1.3
<i>m</i> -CF ₃ C ₆ H ₄ -SiH ₃	1,680; 1.5
<i>p</i> -CF ₃ C ₆ H ₄ -SiH ₃	630; 2.4
	6,400; 1.4
<i>p</i> -MeSC ₆ H ₄ -SiH ₃	4,450; 2.2
3, 5-Me ₂ C ₆ H ₃ -SiH ₃	1,460; 1.5
3, 5-(CF ₃) ₂ C ₆ H ₃ -SiH ₃	830; 1.2
C ₆ F ₅ -SiH ₃	730; 1.5

1.3.5 Applications of Polysilanes

(i) Polysilanes in OLEDs

Polysilanes are used as hole transporting materials or emitters in OLED devices in polymer OLEDs. Polymer OLEDs are manufactured by solution processing techniques to coat on transparent substrates glass pre-coated by indium-tin-oxide (ITO). The fundamental design of a polymer OLED⁴⁵ is given in **Figure 9**. The emitting layer

mainly composed of $p-n$ junction formed by a mixture of an emitting material, electron transporting polymer and hole transporting polymer. The applied voltage injects electrons and holes to the electrodes which emit light on their recombination in emitting layer. Polysilanes can serve as hole transporting materials as well as emitting materials in OLEDs. More specifically, polysilanes can serve as triplet harvesting materials in OLEDs containing phosphorescent emitting materials such as transition metal complexes⁵⁷.

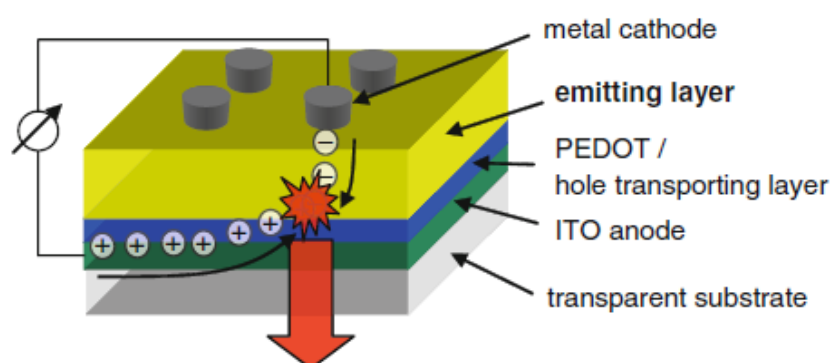


Figure 9: Image of OLED Device.

(ii) Polysilanes as UV Emitters

Among the variety of emitting materials, UV emitting materials are scarce. Polysilane mostly emit light in UV region and were employed as UV emitters in OLEDs⁵⁸. In a polysilane based UV OLEDs with a layered design, the polysilane acts as semiconducting and emitting layer. For example; polymethylphenylsilane and poly(bis(4-butylphenyl)silane⁵⁹.

1.3.6 σ - π Conjugated Organosilicon Polymers

σ - π Conjugation:

σ - π Conjugation is a well-known phenomenon and has been confirmed successfully by the help of electronic absorption spectroscopy⁶⁰. σ - π Conjugated systems are acknowledged because of its potential utility^{61,62} in electronically conducting, emitting and semiconducting properties. Another distinct property of silyl substituted aromatic polymers is that there exist a charge transfer in the excited state among disilyl (or polysilyl) unit and aromatic units resulting in emission.

Similar to σ -conjugation, σ - π conjugation also exhibits enhancement of delocalization with longer silyl units, in other words the extent of conjugation was

observed increases with increase in the number of silyl units (m) in the polymer backbone which can be seen in emission spectra⁶³ (**Chart 10, Figure 10**). This can be explained as, on excitation of π -electrons vacant π -orbitals are generated and invite the free sigma electrons for the delocalization.

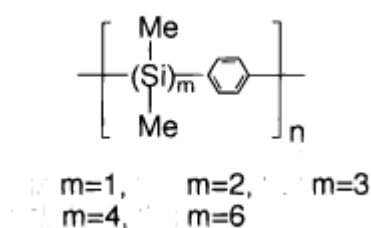


Chart 10: Polysilanes with Various Numbers of Silicon Atoms in Unit Structure.

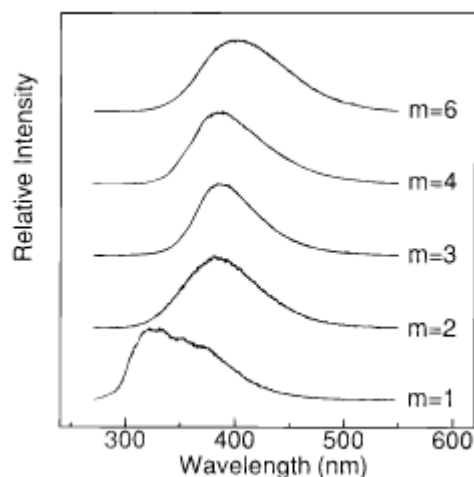


Figure 10: Emission Spectra of Silylen-Phenylene Polymers; Excitation Wavelength 250nm.

1.1.1.1 σ - π Conjugated Organosilicon Polymers

Thiophene does not show photo-luminescence, but biithiophene show luminescence. In oligothiophenes, the quantum efficiency increases with increasing length of conjugation. Ohshita et al., have studied various oligothiophenesilane dimers bridged by mono-, bi-, or trisilanylene units^{64,65}. In these materials it has been possible to involve the σ - π conjugation amongst the oligothiophene units and the silanylene unit which results in the semiconducting properties of oligomers or polymers. With these properties these materials may find applications in organic photonics and electronics.

Further, because of their unique electronic structure, σ - π conjugated materials gained a lot of interest, as a result various polymers constituting of alternating organosilicon and σ -electron in the polymer sequence were designed⁶⁶ (**Chart 10**).

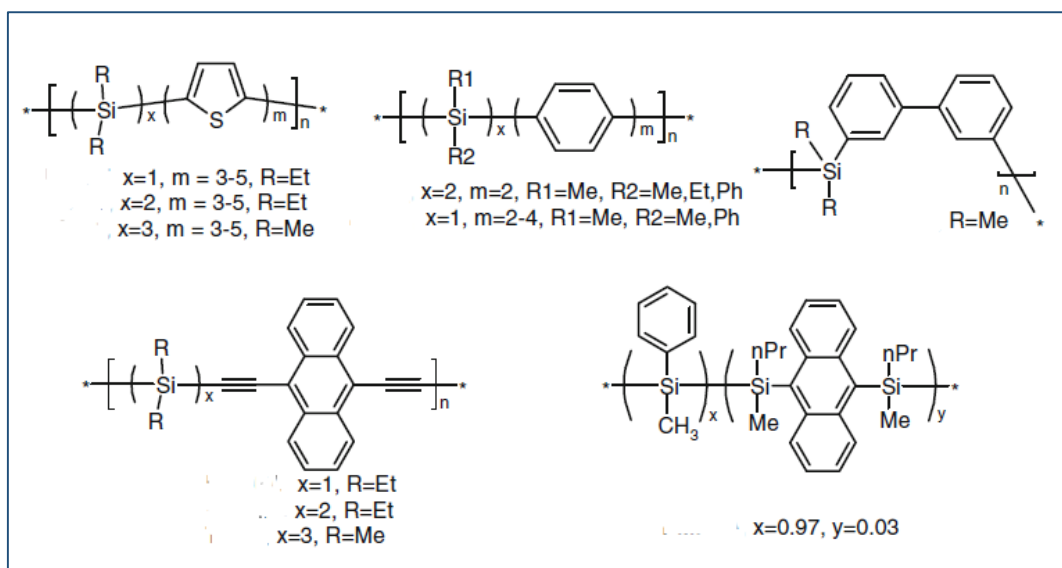
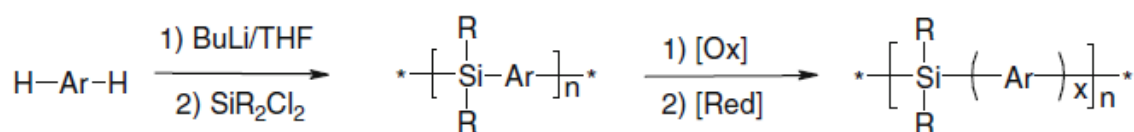


Chart 10: σ - π Conjugated Organosilicon Polymers.

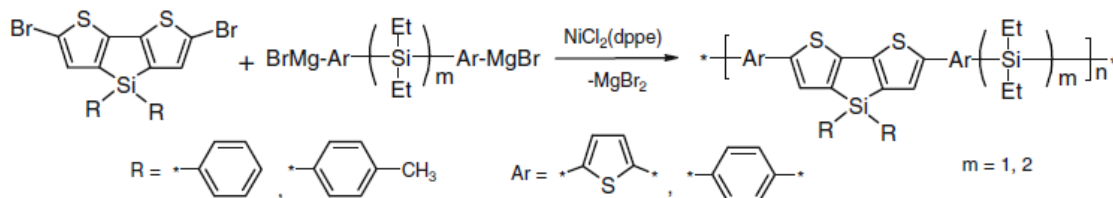
Among the numerous types of synthetic methods, a few important methods are given below:

- (1) Wurtz-type coupling of bis(chlorosilyl) units
- (2) Polycondensation of dichlorosilanes with organolithium derivatives
- (3) transition metal-catalyzed polycondensation of magnesium, zinc or tin-derivatives of diarylsilanes.
- (4) Condensation polymerization of alkoxy silanes with Grignard reagents derived from dibromoaromatic compounds.

A few synthetic methods are demonstrated⁶⁷ in **Scheme 16** and **Scheme 17**.



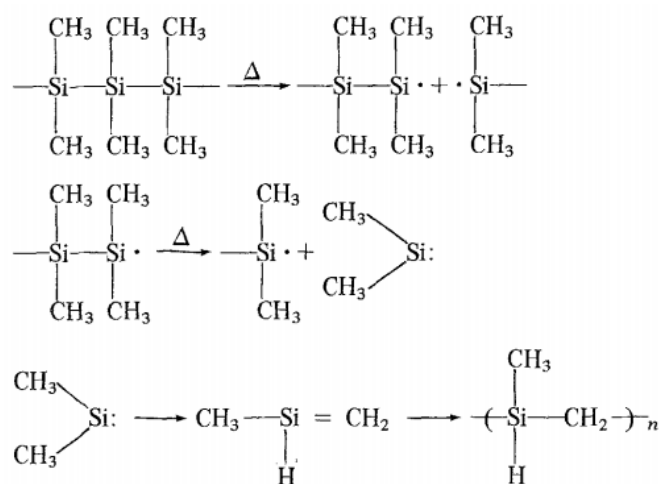
Scheme 16: Synthesis of σ - π Conjugated Organosilicon Polymers Via Polycondensation of Organolithium Derivatives.



Scheme 17: Synthesis of σ - π Conjugated Organosilicon Polymers Via Polycondensation of Grignard Reagent.

1.3.8 Polycarbosilanes (SiC)

The SiC fibres are industrially useful material because of its very high tensile strength and Young's modulus. The precursor, SiC fibres must have properties such as high spinnability, easy handling, minimal oxygen content, high atom efficiency in the conversion, and less production of carbon. The above mentioned properties are closely related to the polycarbosilanes, therefore, in order to obtain SiC, polycarbosilanes are extensively employed as a precursor. A number of methods were practiced for the synthesis of polycarbosilanes by researchers, one of them is by thermal decomposition of polydimethylsilane⁶⁸ (**Scheme 18**).



Scheme 18: Synthetic Scheme of Polycarbosilane.

1.3.9 Polysiloxanes:

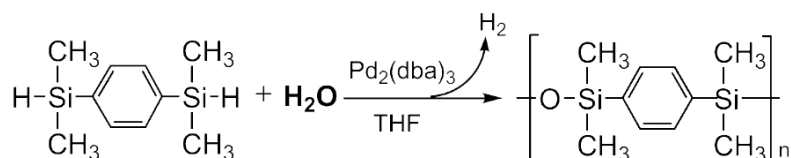
There has been continuous and increasing requirement on the development of high temperature heat resistant or flame retardant materials. For elastomers for electronic application the thermal stability must be up to several hundred degree and at same time should exhibit flexibility at ambient temperatures. Previously, halogen, nitrogen, or phosphorous containing polymers, such as fluorocarbon polymers, polyimide, polyphosphazenes are widely used as heat resistant. Major disadvantage of these materials is that on combustion it releases toxic and corrosive gasses.

Polysiloxane⁶⁹ is a good alternative for such functional materials because of flexible and heat resistant Si-O-Si backbone, which also leads to good dielectric and surface properties,

1.3.10 Poly(silylene-phenylene-siloxane): Dehydrocoupling Polymerization

Silylene-phenylene-siloxane polymers have been generally synthesized by homocondensation reaction of phenylene disilanol or heterocondensation of disilanol

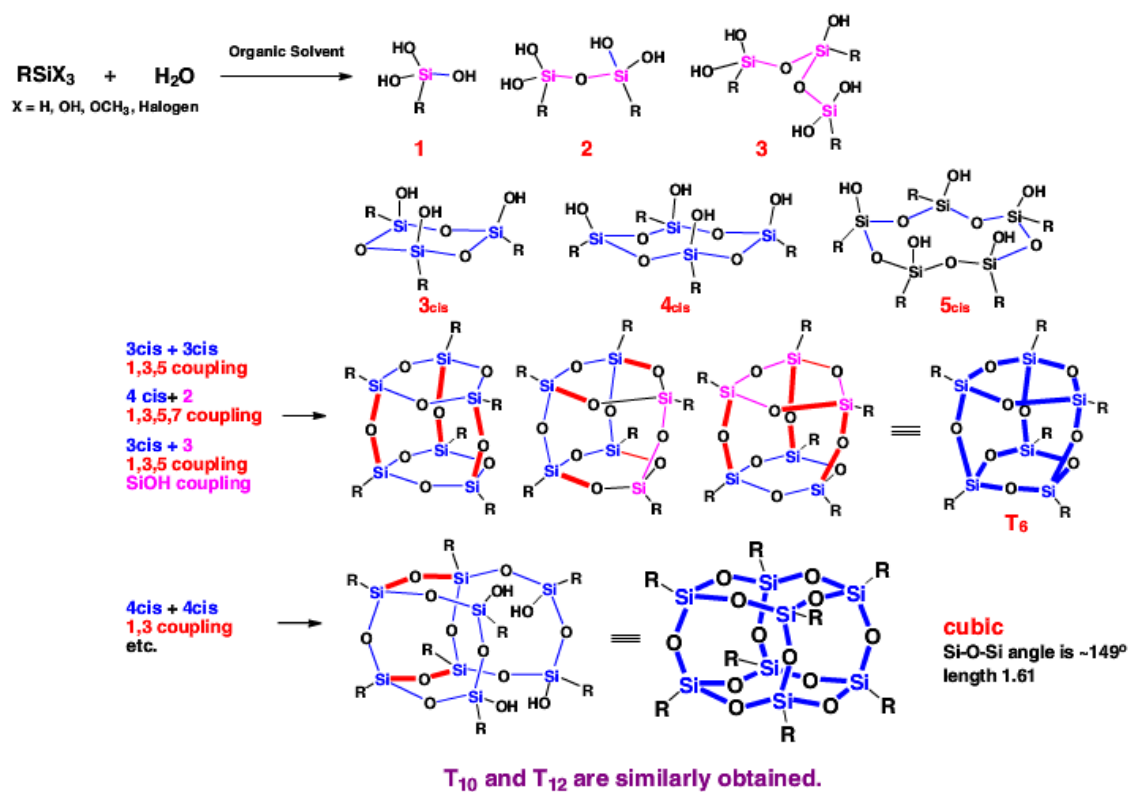
with suitable difunctional silane or siloxane. In the presence of transition metal catalyst in water, polysiloxane were prepared by dehydrocoupling polymerization⁷⁰ (**Scheme 19**).



Scheme 19: Synthesis of Polysiloxane Via Dehydrocoupling Polymerization.

1.3.11 Polysilsequioxane:

Synthesis of polysilsequioxane were done by polycondensation of silane in the presence of water. Formation of various structures of siloxanes and polysiloxanes are possible which may further lead to polysilsequioxane. Thus prepared cyclic siloxanes are proved to be useful in functional design of the polymers⁷¹ (**Scheme 20**).

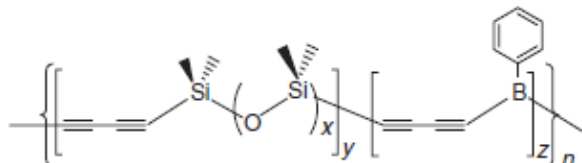


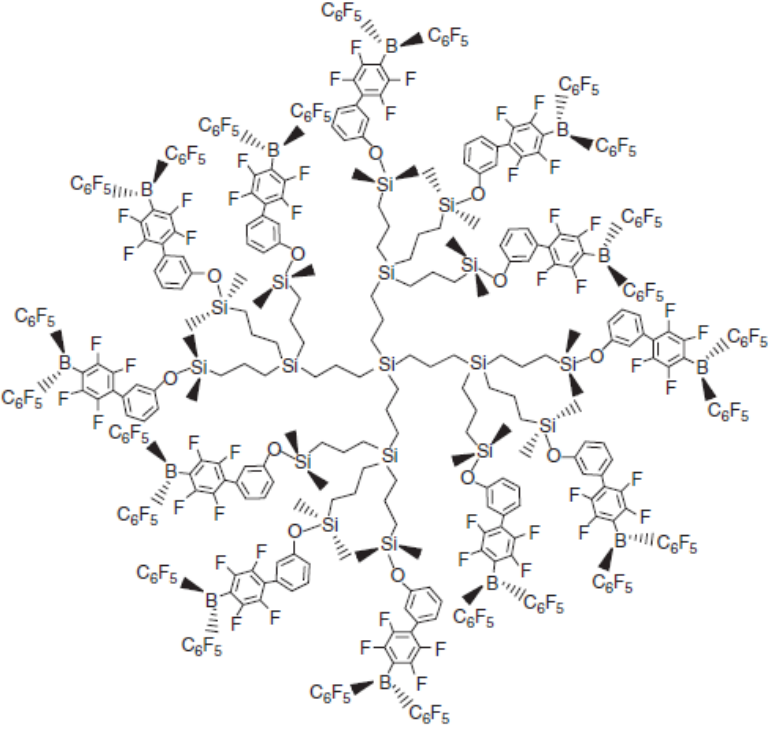
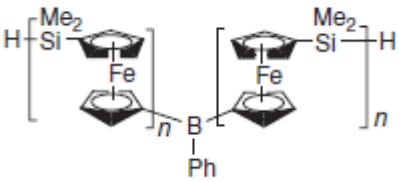
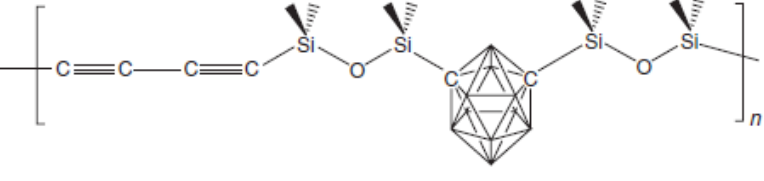
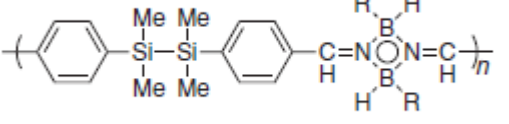
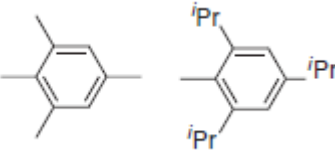
Scheme 20: Schematic of Polysilsequioxane Synthesis.

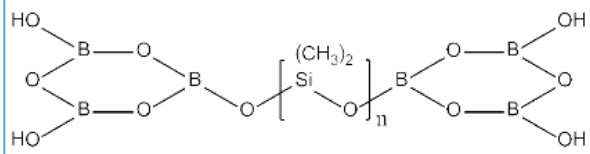
1.4 Boron-Silicon Containing Polymers

After the detailed overview of organosilicon and organoboron polymers separately, it is possible to think of designing polymeric materials possessing both boron and silicon atom in the main chain and exploit their properties to good effect. Some of the examples are summarized in **Table 2**. Certainly this field of boron and silicon bimetallic polymers can enjoy the synergistic contributions of both atoms and preparing these polymers makes it a promising and interesting branch of material design.

Table 2: Examples of Silicon/Boron bimetallic polymers, their properties and applications.

Boron-Silicon Polymers	Properties and Applications																				
<div><table><thead><tr><th></th><th>x</th><th>y</th><th>z</th></tr></thead><tbody><tr><td>a</td><td>0</td><td>0.8</td><td>0.2</td></tr><tr><td>b</td><td>1</td><td>0.8</td><td>0.2</td></tr><tr><td>c</td><td>1</td><td>0.9</td><td>0.1</td></tr><tr><td>d</td><td>2</td><td>0.9</td><td>0.1</td></tr></tbody></table><p>a-d</p></div>		x	y	z	a	0	0.8	0.2	b	1	0.8	0.2	c	1	0.9	0.1	d	2	0.9	0.1	<p>Sundar and Keller have reported number of boron-silicon-diacetylene copolymers⁷² a-d. These polymers were observed to possess exceptional thermooxidative stabilities.</p>
	x	y	z																		
a	0	0.8	0.2																		
b	1	0.8	0.2																		
c	1	0.9	0.1																		
d	2	0.9	0.1																		

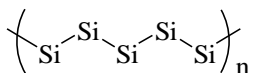
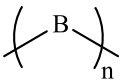
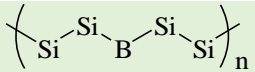
	<p>The synthesis of a variety of lithium ion conducting three dimensional borosiloxane polymers were done⁷³ having the Lewis acidic boron and silicon in the main chain of the polymer. Their strong affinity with anions increased the selective cation transport.</p>
	<p>Boron and silicon containing electroactive polyferrocene⁷⁴.</p>
	<p>The oligomer of polysiloxane with carborane unit in the main behaved like a plastic polymer⁷⁵. Also, it was extremely stable towards thermooxidation with very high char yields (~90 %).</p>
<div data-bbox="384 1529 916 1720" style="border: 1px solid blue; padding: 10px; margin-bottom: 10px;">  </div> <div data-bbox="424 1742 871 1933" style="border: 1px solid blue; padding: 10px;"> <p>R :</p>  </div>	<p>The presence of $\sigma-\pi$ was designed utilizing the property of disilane unit for the donation of loosely bound sigma electron and electron withdrawing ability of boron containing cyclodiborazane unit⁷⁶. Thus prepared poly(cyclodiborazane)s exhibited novel optical behavior for $\sigma-\pi$ conjugated polymers. It showed intense emission because of the intramolecular charge transfer.</p>

	By the incorporation of boron unit in polydimethylsiloxane chain, the dramatic increase in the dynamic moduli was observed ⁷⁷ .
---	--

Taking inspiration from above mentioned examples, we explored three different ways of boron/silicon bimetallic copolymer in which boron and silicon moieties can be present in the main chain. The detail of material design is explained below:

- 1) Polysilanes are well known for σ -conjugation and their utility as photoluminescence and photoresist materials. On the other hand polyboranes are not known to date but boron atom itself has vacant p-orbital. By the incorporation of boron moiety in the main chain of polysilane may facilitate the σ -electron flow via vacant p-orbital, resulting in σ -p conjugated copolymer which will be first of its kind (**Table 3**), whose properties are unknown. Therefore, to explore this new class of material is quite interesting from academic point of view.

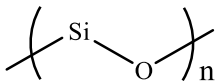
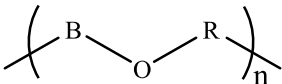
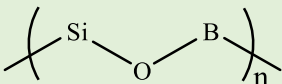
Table 3: Design of Polysilylborane.

Polymer	Advantages	Disadvantages
 Polysilane	σ -conjugation, photoluminescence, photoresist material	
 Polyborane	Not known (Boron atom has vacant p-orbital)	
 Polysilylborane	σ -p conjugation, fluoride anion sensing	

- 2) As a flexible, non-flammable and heat resistant material, polysiloxanes were vastly studied. Apart from their advantages, there are few limitations also associated with polysiloxanes such as low viscosity, inability of film formation and low functionality. Whereas, polyalkoxyboranes are also flexible polymeric material extensively studied as anion trapping polymeric electrolyte for enhanced cation transport. By combining both, design of well-defined

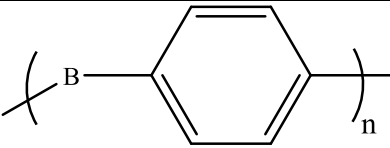
polyborosiloxane may possess properties like flexibility, anion trapping, anion sensing, non-flammability and so forth (**Table 4**).

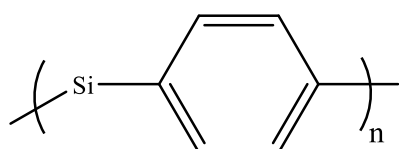
Table 4: Design of Poly(borosiloxane).

Polymer	Advantages	Disadvantages
 Polysiloxane	Flexible, Thermal Stability, Non-flammability	Low viscosity, Low Functionality
 Polyalkoxyborane	Flexible, Anion Trapping, Polymer Electrolyte	Low Stability Towards Air and Moisture
 Poly(borosiloxane)	Flexible, Non-flammable, Anion Trapping, Anion Sensing, Polymer Electrolyte	

- 3) p- π Conjugated poly(phenylene/borane)s exhibit intense emission and can show third order non-linear optical properties. But these polymer suffer from low molecular weight in the range of several thousands and therefore processing such material is challenging. On the same token, poly(phenylene/silane)s are well known for semiconducting and heat resistant properties. By the design of poly(silylene/phenylene/borane) it is possible to achieve heat resistant polymer which may show intense emission (**Table 5**). Also, there is a possibility to achieve UV-emission because of the widening of band gap.

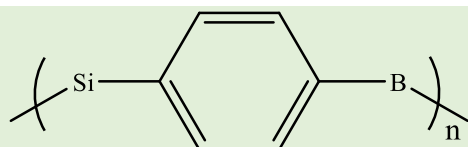
Table 5: Design of Poly(silylene/phenylene/borane).

Polymer	Advantages	Disadvantages
 Poly(phenylene/borane)	p- π Conjugation, Intense Emission, Third Order Non-Linear Optical Properties	Low Molecular Weight, Solution is Processing Difficult.



Poly(phenylene/silane)

Heat Resistant,
Semiconductor,
Precursor to SiC



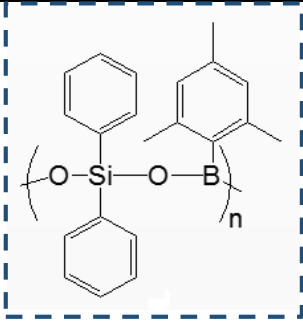
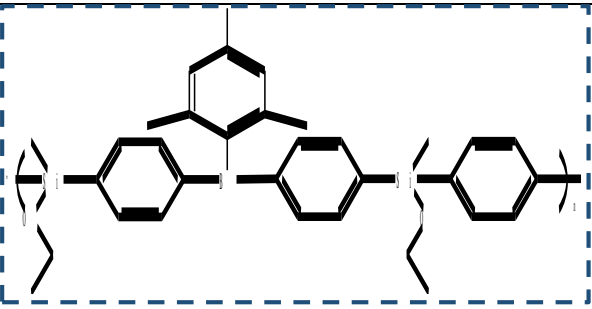
Poly(phenylene/silylene/borane)

Thermally Stable,
Intense Emission

With above mentioned ideas, we have designed three different types of boron/silicon bimetallic copolymers. In these systems, boron and silicon atoms are present in the main chain and because of their different structural compositions they possess variety of physical and chemical properties.

1.5 Survey of this Thesis

Chapter	Boron/Silicon Bimetallic Polymers	Specific Properties and Applications
2		<p>Synthesis of novel σ-p conjugated polysilylborane via dehydrocoupling polymerization was done. Further, turn on type of fluoride ion sensing was observed with micromolar concentrations of fluoride ions.</p>
		<p>Synthesis of highly alternating poly(borosiloxane) via</p>

3		<p>dehydrocoupling polymerization.</p> <p>Ultrasensitivity was achieved towards fluoride ions in water.</p>
4		<p>Defined poly(silyl/phenyl/borane) was prepared. It was found to be a first example of ultraviolet emitter via thermally activated delayed fluorescence (TADF).</p>

1.6 References

- (1) Carraher Jr, C. E. *Introduction to polymer chemistry*; CRC press, 2012.
- (2) Akelah, A.; Moet, A. *Functionalized polymers and their applications*; Springer, 1990.
- (3) Ratner, B. D. *Pergamon Press plc, Compr. Polym. Sci.* **1989**, 7, 201–247.
- (4) Williams, C. K.; Hillmyer, M. A. *Polym. Rev.* **2008**, 48, 1–10.
- (5) Corma, A.; Iborra, S.; Velty, A. *Chem. Rev.* **2007**, 107, 2411–2502.
- (6) Mark, J. E.; Allcock, H. R.; West, R. *Inorganic polymers*; Oxford University Press, 2005.
- (7) Abd-El-Aziz, A. S.; Carraher, C. E.; Pittman, C. U.; Zeldin, M. *Macromolecules Containing Metal and Metal-like Elements: Supramolecular and Self-assembled Metal-containing Materials*; John Wiley & Sons, 2009; Vol. 9.
- (8) Schlesinger, H. I.; Burg, A. B. *Chem. Rev.* **1942**, 31, 1–41.
- (9) Good, C. D.; Ritter, D. M. *J. Am. Chem. Soc.* **1962**, 84, 1162–1166.
- (10) Matsumi, N.; Naka, K.; Chujo, Y. *J. Am. Chem. Soc.* **1998**, 120, 5112–5113.
- (11) Hawthorne, M. F. *Angew. Chem. Int. Ed. Engl.* **1993**, 32, 950–984.

- (12) Matsumi, N.; Chujo, Y. *Polym. J.* **2008**, *40*, 77–89.
- (13) Brown, H. C. *Inc.: New York* **1962**.
- (14) Chujo, Y.; Tomita, I.; Hashiguchi, Y.; Tanigawa, H.; Ihara, E.; Saegusa, T. *Macromolecules* **1991**, *24*, 345–348.
- (15) Chujo, Y.; Morimoto, M.; Tomita, I. *Polym. J.* **1993**, *25*, 891–895.
- (16) Chujo, Y.; Morimoto, M.; Tomita, I. *Polym. Bull.* **1992**, *29*, 617–624.
- (17) Zweifel, G.; Clark, G. M.; Leung, T.; Whitney, C. C. *J. Organomet. Chem.* **1976**, *117*, 303–312.
- (18) Matsumi, N.; Miyata, M.; Chujo, Y. *Macromolecules* **1999**, *32*, 4467–4469.
- (19) Matsumi, N.; Chujo, Y.; Lavastre, O.; Dixneuf, P. H. *Organometallics* **2001**, *20*, 2425–2427.
- (20) Matsumoto, F.; Matsumi, N.; Chujo, Y. *Polym. Bull.* **2001**, *46*, 257–262.
- (21) Matsumi, N.; Naka, K.; Chujo, Y. *Polym. J.* **1998**, *30*, 833–837.
- (22) Matsumi, N.; Umeyama, T.; Chujo, Y. *Macromolecules* **2000**, *33*, 3956–3957.
- (23) Chujo, Y.; Tomita, I.; Saegusa, T. *Macromolecules* **1990**, *23*, 687–689.
- (24) Matsumi, N.; Kotera, K.; Chujo, Y. *Macromolecules* **2000**, *33*, 2801–2806.
- (25) Matsumi, N.; Chujo, Y. *Macromolecules* **1998**, *31*, 3802–3806.
- (26) Matsumi, N.; Naka, K.; Chujo, Y. *J. Am. Chem. Soc.* **1998**, *120*, 10776–10777.
- (27) Matsumi, N.; Umeyama, T.; Chujo, Y. *Polym. Bull.* **2000**, *44*, 431–436.
- (28) Trofimenko, S. *J. Am. Chem. Soc.* **1967**, *89*, 3165–3170.
- (29) Herdtweck, E.; Jäkle, F.; Opromolla, G.; Spiegler, M.; Wagner, M.; Zanello, P. *Organometallics* **1996**, *15*, 5524–5535.
- (30) Matsumoto, F.; Nagata, Y.; Chujo, Y. *Polym. Bull.* **2005**, *53*, 155–160.
- (31) Kamaya, E.; Matsumoto, F.; Kondo, Y.; Chujo, Y.; Katagiri, M. *Nucl. Instruments Methods Phys. Res. Sect. A: Accel. Spectrometers, Detect. Assoc. Equip.* **2004**, *529*, 329–331.
- (32) Matsumi, N.; Sugai, K.; Ohno, H. *Macromolecules* **2002**, *35*, 5731–5733.
- (33) Smith, K.; Pelter, A.; Jin, Z. *Angew. Chem. Int. Ed. Engl.* **1994**, *33*, 851–853.
- (34) Matsumi, N.; Mizumo, T.; Ohno, H. *Chem. Lett.* **2004**, *33*, 372–373.
- (35) Evans, J.; Vincent, C. A.; Bruce, P. G. *Polymer* **1987**, *28*, 2324–2328.
- (36) Yamaguchi, S.; Akiyama, S.; Tamao, K. *J. Am. Chem. Soc.* **2001**, *123*, 11372–11375.
- (37) Wade, C. R.; Broomsgrove, A. E.; Aldridge, S.; Gabbai, F. P. *Chem. Rev* **2010**,

110, 3958–3984.

- (38) Vedarajan, R.; Hosono, Y.; Matsumi, N. *Solid State Ionics* **2014**, 262, 795–800.
- (39) Tanaka, K.; Chujo, Y. *Macromol. rapid Commun.* **2012**, 33, 1235–1255.
- (40) Tokoro, Y.; Nagai, A.; Chujo, Y. *J. Polym. Sci. Part A: Polym. Chem.* **2010**, 48, 3693–3701.
- (41) Tokoro, Y.; Nagai, A.; Chujo, Y. *Appl. Organomet. Chem.* **2010**, 24, 563–568.
- (42) Guo, Y.; Zhang, F.; Yang, J.; Wang, F. *Electrochem. Commun.* **2012**, 18, 24–27.
- (43) Jones, R. G. *Silicon-containing polymers*; Royal Society of Chemistry, 1995.
- (44) Jones, R. G.; Ando, W.; Chojnowski, J. *Silicon-containing polymers: the science and technology of their synthesis and applications*; Springer Science & Business Media, 2013.
- (45) Feigl, A.; Bockholt, A.; Weis, J.; Rieger, B. In *Silicon Polymers*; Springer, 2009; pp. 1–31.
- (46) Voronkov, M. G.; Deich, A. Y. *J. Struct. Chem.* **1964**, 5, 443–448.
- (47) Kumada, M.; Tamao, K. *Adv. Organomet. Chem.* **1968**, 6, 19–117.
- (48) West, R. *Pure Appl. Chem.* **1982**, 54, 1041–1050.
- (49) Cotts, P. M. *J. Polym. Sci. Part B: Polym. Phys.* **1994**, 32, 771–778.
- (50) West, R. *J. Organomet. Chem.* **1986**, 300, 327–346.
- (51) Fehér, F.; Schinkitz, D.; Schaaf, J. *Z. für Anorg. und Allg. Chem.* **1971**, 383, 303–313.
- (52) Auner, N.; Weis, J. *Organosilicon Chemistry III: From Molecules to Materials*; John Wiley & Sons, 2008.
- (53) Kipping, F. S. *J. Chem. Soc. Trans.* **1924**, 125, 2291–2297.
- (54) Cypryk, M.; Gupta, Y.; Matyjaszewski, K. *J. Am. Chem. Soc.* **1991**, 113, 1046–1047.
- (55) Grimmond, B. J.; Corey, J. Y. *Inorganica Chim. Acta* **2002**, 330, 89–94.
- (56) Imori, T.; Tilley, T. D. *Polyhedron* **1994**, 13, 2231–2243.
- (57) Kido, J.; Nagai, K.; Okamoto, Y. *J. Alloy. Compd.* **1993**, 192, 30–33.
- (58) Fujii, A.; Yoshimoto, K.; Yoshida, M.; Ohmori, Y.; Yoshino, K. *Jpn. J. Appl. Phys.* **1995**, 34.
- (59) Yuan, C.-H.; Hoshino, S.; Toyoda, S.; Suzuki, H.; Fujiki, M.; Matsumoto, N. *Appl. Phys. Lett.* **1997**, 71, 3326–3328.
- (60) Ishikawa, M.; Kumada, M. *Adv. Organomet. Chem* **1981**, 19, 51–95.

- (61) Fang, M.-C.; Watanabe, A.; Matsuda, M. *J. Organomet. Chem.* **1995**, *489*, 15–22.
- (62) Chicart, P.; Corriu, R. J. P.; Moreau, J. J.; Garnier, F.; Yassar, A. *Chem. Mater.* **1991**, *3*, 8–10.
- (63) Fang, M.-C.; Watanabe, A.; Matsuda, M. *Macromolecules* **1996**, *29*, 6807–6813.
- (64) Ohshita, J.; Izumi, Y.; Kim, D.-H.; Kunai, A.; Kosuge, T.; Kunugi, Y.; Naka, A.; Ishikawa, M. *Organometallics* **2007**, *26*, 6150–6154.
- (65) Kim, D.-H.; Ohshita, J.; Kosuge, T.; Kunugi, Y.; Kunai, A. *Chem. Lett.* **2006**, *35*, 266–267.
- (66) Adachi, A.; Manhart, S. A.; Okita, K.; Kido, J.; Ohshita, J.; Kunai, A. *Synth. Met.* **1997**, *91*, 333–334.
- (67) Ohshita, J.; Nodono, M.; Watanabe, T.; Ueno, Y.; Kunai, A.; Harima, Y.; Yamashita, K.; Ishikawa, M. *J. Organomet. Chem.* **1998**, *553*, 487–491.
- (68) Yajima, S.; Hasegawa, Y.; Hayashi, J.; Iimura, M. *J. Mater. Sci.* **1978**, *13*, 2569–2576.
- (69) Yilgör, \. Iskender; McGrath, J. E. In *Polysiloxane Copolymers/Anionic Polymerization*; Springer, 1988; pp. 1–86.
- (70) Kawakami*, Y.; Imae, I.; Oishi, M.; Seino, M.; Liu, Y. *Mol. Cryst. Liq. Cryst.* **2004**, *415*, 75–92.
- (71) Kawakami, Y. *React. Funct. Polym.* **2007**, *67*, 1137–1147.
- (72) Sundar, R. A.; Keller, T. M. *Macromolecules* **1996**, *29*, 3647–3650.
- (73) Roesler, R.; Har, B. J.; Piers, W. E. *Organometallics* **2002**, *21*, 4300–4302.
- (74) Evans, C. E.; Lough, A. J.; Grondley, H.; Manners, I. *New J. Chem.* **2000**, *24*, 447–453.
- (75) Henderson, L. J.; Keller, T. M. *Macromolecules* **1994**, *27*, 1660–1661.
- (76) Matsumi, N.; Umeyama, T.; Chujo, Y. *Macromolecules* **2001**, *34*, 3510–3511.
- (77) Liu, Z.; Picken, S. J.; Besseling, N. A. *Macromolecules* **2014**, *47*, 4531–4537.

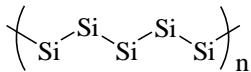
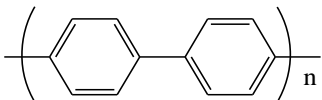
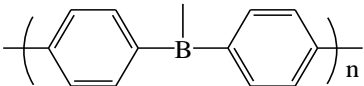
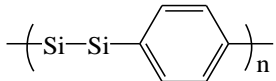
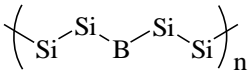
Chapter 2: σ -p Conjugated Copolymers via Dehydrocoupling Polymerization of Phenylsilane and Mesitylborane

2.1 Introduction

Conjugated polymers have been widely investigated as a key material for plastic electronics¹ and are potentially useful for versatile applications such as organic semiconductor², light emitting materials^{3,4}, sensing materials^{5,6} and so forth. In particular, conjugated polymers bearing exotic elements in their main chain were also extensively studied because of their unique electronic state under specific orbital interactions^{7–18}. In 1990, a series of π -conjugated¹⁹ organoboron systems with extended p- π conjugation through the boron was developed by several research groups, independently^{20,21}. The boron incorporation to π -conjugated systems led to unique characteristics such as n-type electrochemical activity, intense fluorescence emission, 3rd order non-linear optical property, anion sensing property and so on²².

On the other hand, the boron incorporation to σ -conjugated system has not been known to the best of our knowledge. As a unique example for orbital interaction of σ -conjugation system²³, σ - π interaction is widely known^{24–26}. Usually, σ - π interaction is more significantly observed in photo excited state than in ground state. This is due to the intramolecular charge transfer from oligosilylene moiety to aromatic moiety. σ -Electrons flow to vacant π -orbital of aromatic moiety after the excitation of valance electrons at π -level to π^* -level²⁷ (**Table 2.1**). In this context, when the boron atom bearing the vacant p-orbital is incorporated into σ -conjugated systems, there will be possibility of observing significant σ -p orbital interaction in the ground state. There have been only a few examples of perhydrogeno derivatives and low molecular weight silylboranes^{28,29}.

Table 2.1: Various Types Conjugated System.

Chemical Structure	Conjugation Type
	σ^{23}
	π^{19}
	$p-\pi^{21}$
	$\sigma-\pi^{27}$
	$\sigma-p ?$

Based on the above mentioned idea, in the present work, the synthesis of poly(phenylsilane/mesitylborane) was undertaken by dehydrocoupling polymerization of phenylsilane and mesitylborane in the presence of transition metal catalyst. Although Wurtz coupling polymerization³⁰ of chlorosilane is most common synthetic route for polysilanes, this method will not be useful for relatively unstable boron containing polymers.

In the present work, dehydrocoupling polymerization using rhodium catalyst successfully afforded the desired poly(phenylsilane/mesitylborane) whose molecular weights were several thousand g/mol. Various feed ratios of the starting materials in dehydrocoupling polymerization of mesitylborane and phenylsilane were examined in the presence of rhodium catalyst (**Scheme 2.1**).

The details of amounts of starting materials, yields and B/Si unit ratios are summarized in **Table 2.2**. The reaction was carried out under nitrogen atmosphere at room temperature with constant vigorous stirring. The obtained copolymer **1** was reprecipitated in *n*-hexane, then **1** was dried under vacuum for 3 hours. A relatively high molecular weight was observed when mesitylborane and phenylsilane were taken in molar ratio of 1:10, respectively.

2.2 Experiment

2.2.1 Materials and Methods

Phenylsilane (TCI), [tris(dimethylphenylphosphino)-(2, 5-norbornodiene) rhodium I] hexafluorophosphate (aldrich), Toluene (WAKO), Tetrabutylammonium fluoride (TCI), were purchased. Phenylsilane and toluene were dried over activated molecular sieves and used. Mesitylborane was freshly synthesized according to the literature and used. A 400 MHz Nuclear Magnetic Resonance (NMR) spectrometer (Ultrashield™ Plus Bruker, Z101355) was used to characterize polymers. Fluorescence Spectrophotometer (JASCO, FP-8200) and UV-Vis spectrometer (JASCO V-630) were used for optical measurements under solution state. Cyclic voltammetry were carried out on EC stat-100. For gel permeation chromatography (GPC) Shimadzu-LC-20AD was used. IR spectra was recorded on JASCO FT/IR-4100.

2.2.3 Synthetic Procedure

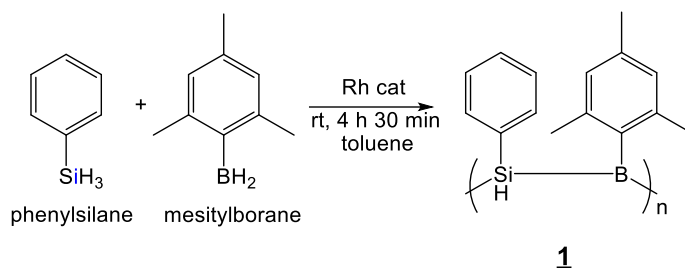
A typical polymerization procedure is as follows. Freshly prepared mesitylborane (500 mg, 3.78 mmol) was dissolved in toluene (15 mL) with metal catalyst [tris(dimethylphenylphosphino)-(2, 5-norbornodiene rhodium I)] hexafluorophosphate (15 mg, 0.019 mmol) in a 100 mL round bottom flask under nitrogen atmosphere. To this, phenylsilane (818 mg, 7.56 mmol) was added dropwise by syringe and the reaction mixture was stirred at room temperature for 12 hours. The reaction mixture was reprecipitated in *n*-hexane and the supernatant solution was removed by syringe. The resulting polymer was dried under vacuum for 3 hours to obtain the product.

2.2.4 Characterisation

The structure of the polymers were supported by ¹H-NMR, ¹¹B-NMR and FT-IR spectra (**Figure 2.1**). Presence of one peak of boron (Si-B-Si, 19 ppm) was observed in ¹¹B-NMR (**Figure 2.1 (B)**) which indicated the presence of one type of

boron in system. From the IR spectra, the broad peak assignable to Si-B stretching was observed at 680 cm^{-1} . The gel permeation chromatography (GPC) showed the number average molecular weight to be in the range of $1200\text{-}2900\text{ gmol}^{-1}$ (THF as eluent/PSt standards) having *polydispersity index* (PDI) of 1.1 - 1.4.

$^1\text{H-NMR}$: (δ , ppm, 400 MHz): 2.2 (s, 6H, CH_3), 2.3 (s, 3H, CH_3), 6.5 (s, 2H, aromatic protons); 7.0-7.9 (m, 5H, aromatic protons), $^{11}\text{B-NMR}$: (δ , ppm, 128 MHz): 19.0 (Si-B-Si), IR: 470 cm^{-1} , 680 cm^{-1} , 1033 cm^{-1} , 2164 cm^{-1} , 2960 cm^{-1} .



Scheme 2.1: Synthesis of Copolymer 1.

Table 2.2: Synthetic Results in Various Reaction Conditions.

S. No.	Mesitylborane (mg, mmol)	Phenylsilane (mg, mmol)	Rhodium cat. (mg)	Yield (mg)	B/Si** (%)	Mol. Wt. (g/mol)
1	500, 3.780	818, 7.56	15	315.0	35.7	1200
2	50, 0.378	409, 3.78	10	79.0	20.0	2300
3	370, 2.803	3030, 28.0	15	420.0	24.9	2900
4	200, 1.515	1967, 18.1	15	680.0	14.2	2100

2.3 Results and Discussion

The resultant polymers were highly fluorescent when irradiated with UV light in various solvents. Moreover, solvatochromism of the absorption was also observed in solvents of various polarity. The moderately intense fluorescence emission and the presence of Lewis acidic boron unit indicated sensing potential for various Lewis bases and anions. The density functional optimization of highest occupied molecular orbital (HOMO) and lowest unoccupied molecular orbital (LUMO) of several models of Si/B systems having two, three and nine Si/B units were carried out using Gaussian 09W DFT (basis set 6-311G, B3LYP) algorithms. These calculations suggested effective overlap of bonding orbitals in the case of long chain model which can mimic the copolymer (**Table 2.3, entry 3**). For this system, HOMO was extended through the boron atom supporting σ -p conjugation. The band gap of copolymer largely decreased with increasing Si-B based chain length. It can be explained by considering the charge

transfer between σ -electrons and p-orbital of boron. The presence of charge, each on boron and silicon atom as a result of charge transfer was implied by DFT calculation (**Table 2.3**). To confirm the intra molecular charge transfer, electronic charge distribution on boron and silicon atoms were compared for various models used for DFT calculations. The boron was found to have negative charge in longer polymer chain length. This was complementary to HOMO where orbitals were effectively overlapping in longer chain of the model (**Table 2.4**).

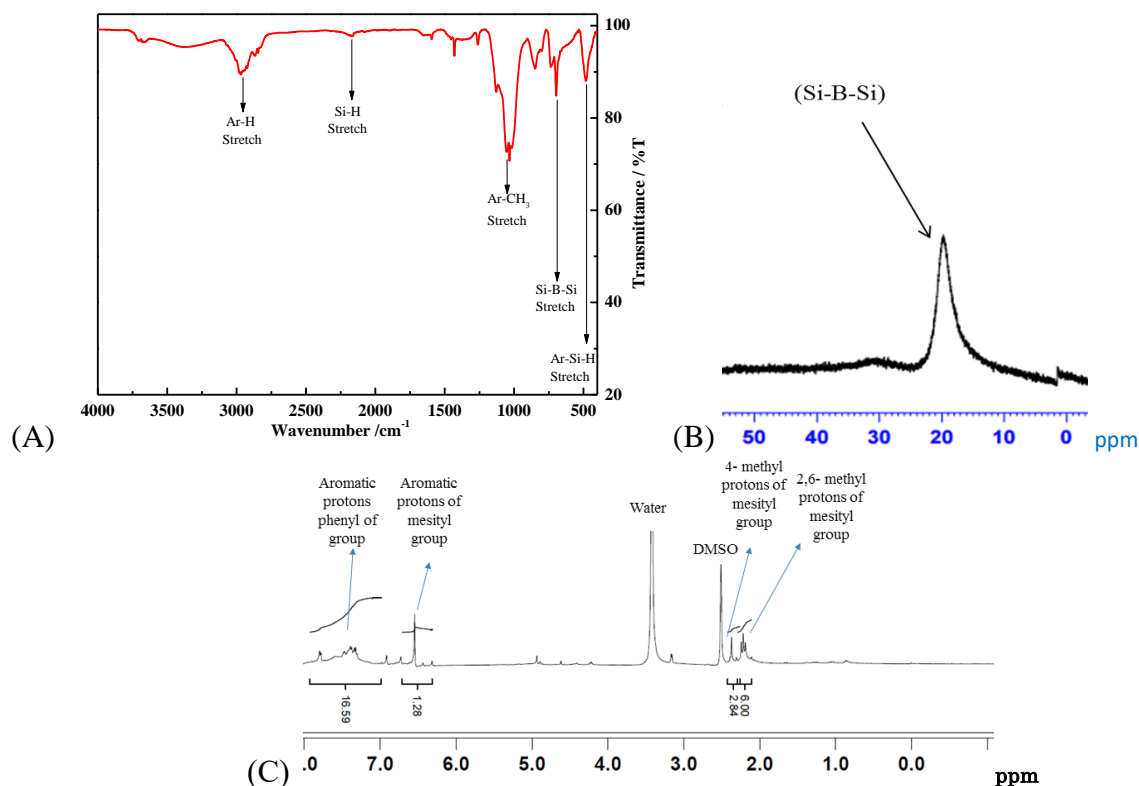


Figure 2.1: IR (A). ^{11}B -NMR (B) and ^1H -NMR (C) Spectra of **1.**

The polymer was also studied by UV-vis spectroscopy (**Figure 2.2A**) and the wavelength of maximum absorbance was around 320 nm. Also, band gap energy was calculated using method proposed by Morita et al.,³¹ (**Figure 2.2B**) and it was found to be 3.8 eV which was very close to the calculated value (3.6 eV) of polymer mimic by DFT technique. Various arylborane based fluoride anion sensors have already been studied and many of them have been reported to show good sensitivity due to extended π -conjugation through boron. In those sensors, the π -conjugation is interrupted by forming borate complex between organoboron moiety and fluoride anion, leading to quenching of fluorescence. On the other hand, in this work we have synthesized σ -p conjugated polymers showing turn on type sensitivity towards micro molar concentrations of fluoride ion. The fluoride anion sensing was examined by fluorescence emission spectroscopy using tetrabutylammonium fluoride (TBAF) as fluoride anion source. The “turn on” type of mechanism has been considered to be desirable, as it reduces the human error.

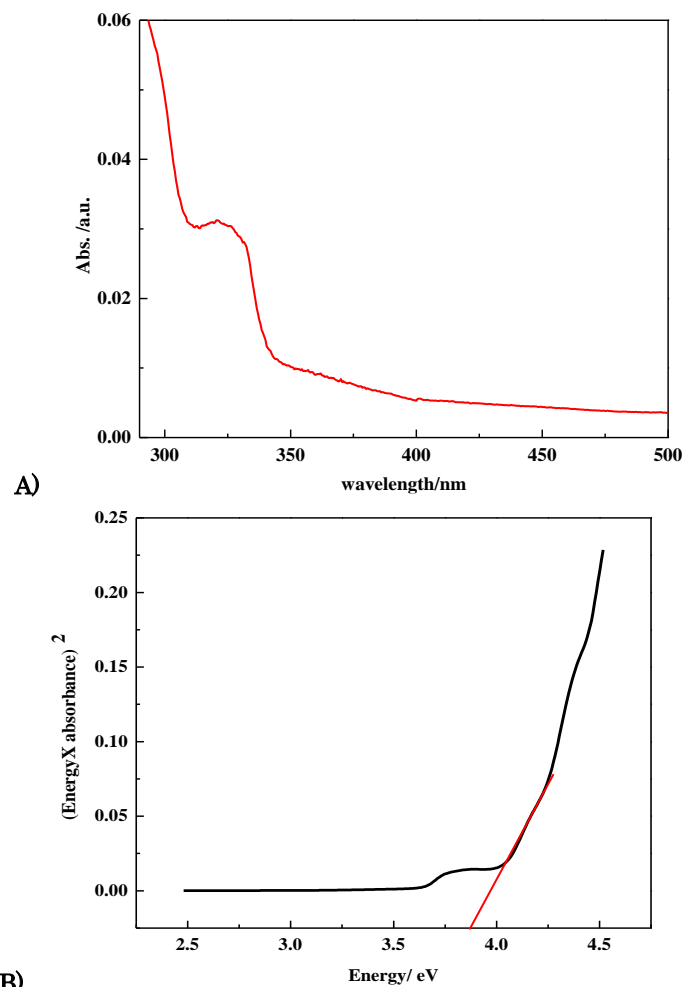


Figure 2.2: UV-Vis Absorption Spectra of **1 (A), Band Gap Energy Calculation of **1** (B).**

Table 2.3: 3D Optimised Structures, HOMO and Band Gap Energies of Models (DFT Calculation, Basis Set: 6-311G, B3LYP).

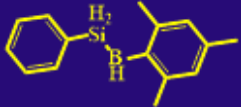
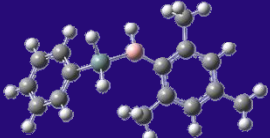
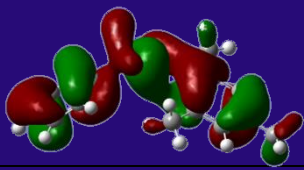

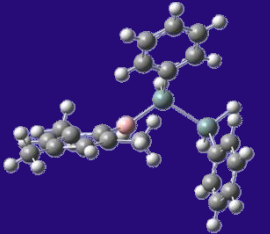
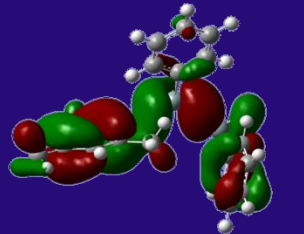
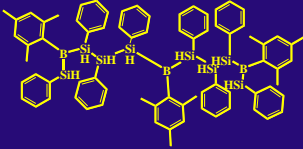
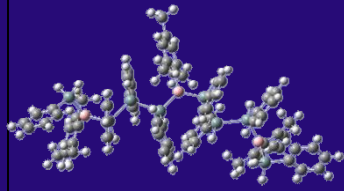
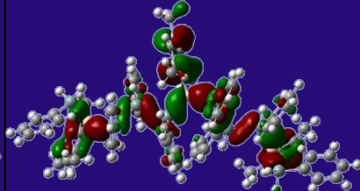

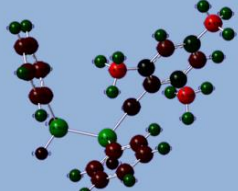
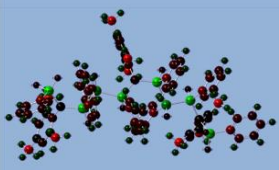
Chemical Structure	Optimized Chemical Structure	HOMO	E _{gap} (eV)
			16.9
			4.10
			3.60

Table 2.4: Charge Distribution on Boron and Silicon Atoms in Different Models of 1 Optimized by Gaussian 09 (6-311G, B3LYP, DFT).

NO. of units	2 units	3 units	11 units
Charge distribution			
Charge distribution Value (B, Si)	-0.038, 0.520	-0.086, 0.432	-0.050, 0.626

-1



+1

Mulliken Charge Distribution: -1 to +1.

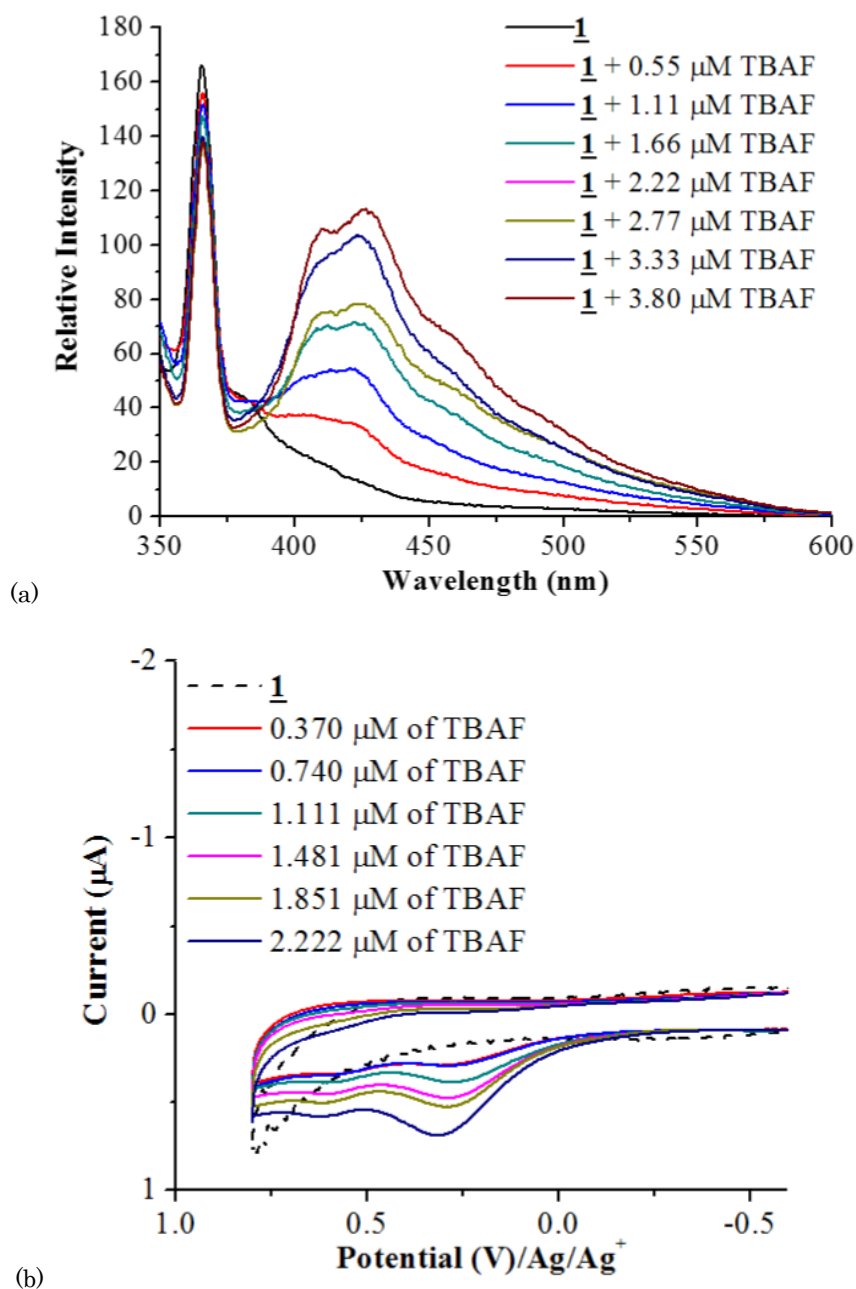


Figure 2.3. Fluoride Ion Sensing of **1 (a) in THF After the Addition of Various Conc. of TBAF by Fluorescence Emission Spectra. (Excitation wavelength = 290 nm) (b) Cyclic Voltammograms of **1** (1 mM) with Various Conc. of TBAF in TBAP (0.1 M) at a Scan Rate of 100 mV/s vs Ag/Ag⁺; WE:Pt; CE:Pt.**

The sensing behavior was found to be a “turn on” type in which a new emission peak appeared at ~425 nm and emission intensity increased linearly with increasing the concentration

of fluoride ion with a slight decrease in the intensity at ~360 nm (**Figure 2.3 (a)**, sample number **2 in Table 2.2**). In the poly(silane/borane), tricoordinate boron had more or less quenched the emission of oligosilanylene group. However, when tricoordinate boron was converted to borate, inherent fluorescence property of oligosilanylene was recovered to show “turn-on” type emission. Cyclic voltammetry was carried out to see the sensitivity of **1** towards fluoride ions. In the cyclic voltammograms, a new peak appeared at 0.3 V and the magnitude of current kept on increasing linearly with increasing the concentration of fluoride ions (**Figure 2.3 (b)**, sample number 2 in **Table 2.2**). Appearance of reduction peak at 0.3 V in the cathodic half can possibly correspond to irreversible decomposition of B⁻F-Si.

2.4 Conclusions

Experimental data and DFT calculation suggested the formation of σ -p conjugated poly (silane/borane). Design of Si/B based σ -p conjugated systems will provide a novel strategy for design of conjugated polymers. Due to their unique electronic state, versatile optical and electronic applications are expected.

2.5 Notes and references

****The B/Si ratio means the percentage ratio of boron and silicon units in the polymer sequence structure and it was calculated by integral ratio of peaks in ¹H-NMR (methyl peaks of mesityl group as well as aromatic protons of both mesityl group and phenylgroup were compared).**

- (1) Singh, T. B.; Sariciftci, N. S. *Annu. Rev. Mater. Res.* **2006**, *36*, 199–230.
- (2) Garnier, F.; Yassar, A.; Hajlaoui, R.; Horowitz, G.; Deloffre, F.; Servet, B.; Ries, S.; Alnot, P. *J. Am. Chem. Soc.* **1993**, *115*, 8716–8721.
- (3) Pei, J.; Yu, W.-L.; Huang, W.; Heeger, A. J. *Macromolecules* **2000**, *33*, 2462–2471.
- (4) Nature Volume 365 issue 6447 1993 [doi 10.1038%2F365628a0] Greenham, N. C.; Moratti, S. C.; Bradley, D. D. C.; Friend, R. H -- Efficient light-emitting diodes based on polymers with high electron affinities.
- (5) McQuade, D. T.; Pullen, A. E.; Swager, T. M. *Chem. Rev.* **2000**, *100*, 2537–2574.
- (6) Thomas, S. W.; Joly, G. D.; Swager, T. M. *Chem. Rev.* **2007**, *107*, 1339–1386.
- (7) Sohn, H.; Huddleston, R. R.; Powell, D. R.; West, R.; Oka, K.; Yonghua, X. *J. Am. Chem. Soc.* **1999**, *121*, 2935–2936.
- (8) Yamaguchi, S.; Jin, R.-Z.; Itami, Y.; Goto, T.; Tamao, K. *J. Am. Chem. Soc.* **1999**, *121*,

10420–10421.

- (9) Hong, S. Y.; Marynick, D. S. *Macromolecules* **1995**, *28*, 4991–4995.
- (10) Kim, B.-H.; Woo, H.-G. *Organometallics* **2002**, *21*, 2796–2798.
- (11) Boydston, A. J.; Yin, Y.; Pagenkopf, B. L. *J. Am. Chem. Soc.* **2004**, *126*, 3724–3725.
- (12) Lucht, B. L.; Buretea, M. A.; Tilley, T. D. *Organometallics* **2000**, *19*, 3469–3475.
- (13) Sohn, H.; Sailor, M. J.; Magde, D.; Trogler, W. C. *J. Am. Chem. Soc.* **2003**, *125*, 3821–3830.
- (14) Hay, C.; Hissler, M.; Fischmeister, C.; Rault-Berthelot, J.; Toupet, L.; Nyulászi, L.; Réau, R. *Chem. - Eur. J.* **2001**, *7*, 4222–4236.
- (15) Hay, C.; Fave, C.; Hissler, M.; Rault-Berthelot, J.; Réau, R. *Org. Lett.* **2003**, *5*, 3467–3470.
- (16) Naka, K.; Umeyama, T.; Chujo, Y. *J. Am. Chem. Soc.* **2002**, *124*, 6600–6603.
- (17) Umeyama, T.; Naka, K.; Nakahashi, A.; Chujo, Y. *Macromolecules* **2004**, *37*, 1271–1275.
- (18) Umeyama, T.; Naka, K.; Chujo, Y. *Macromolecules* **2004**, *37*, 5952–5958.
- (19) Synthetic Metals, *4* (1981) 99 - 112 99.
- (20) Matsumi, N.; Chujo, Y. *Polym. J.* **2008**, *40*, 77–89.
- (21) Matsumi, N.; Naka, K.; Chujo, Y. *J. Am. Chem. Soc.* **1998**, *120*, 10776–10777.
- (22) Jäkle, F. *Chem. Rev.* **2010**, *110*, 3985–4022.
- (23) Miller, R. D.; Michl, J. *Chem. Rev.* **1989**, *89*, 1359–1410.
- (24) Horn, K. A.; Grossman, R. B.; Thorne, J. R. G.; Whitenack, A. A. *J. Am. Chem. Soc.* **1989**, *111*, 4809–4821.
- (25) Sakurai, H.; Tasaka, S.; Kira, M. *J. Am. Chem. Soc.* **1972**, *94*, 9285–9286.
- (26) Sakamaki K., Ohshita J., Kunai A., Nakao H., Adachi. A., Whitenack A. A., *J. Am. Chem. Soc.* **2001**, *123*, 604–612.
- (27) Fang, M.-C.; Watanabe, A.; Matsuda, M. *Macromolecules* **1996**, *29*, 6807–6813.
- (28) Buynak, J. D.; Geng, B. *Organometallics* **1995**, *14*, 3112–3115.
- (29) Suginome, M.; Matsuda, T.; Ito, Y. *Organometallics* **2000**, *19*, 4647–4649.
- (30) Ishikawa, M.; Hongzhi, N.; Matsusaki, K.; Nate, K.; Inoue, T.; Yokono, H. *J. Polym. Sci. Polym. Lett. Ed.* **1984**, *22*, 669–671.
- (31) Morita S., Akashi T., Fujji A., Yoshida M., Ohmori Y., Yoshimoto K., *Synth. Met.*, **1995**, *69*, 433.

Chapter 3: Synthesis and Applications of Poly(borosiloxane)

3.1 Introduction

Three dimensional polyborosiloxanes (PBS) have been studied extensively in recent past as ceramic materials¹. These polymers may also fall in the class of organic-inorganic hybrid² materials known for excellent virtues such as, high temperature resistance, high mechanical strength, flame-retardancy, coating materials and so on³. A few report in literature detail about the slow burning and high char yields of this class of polymer⁴. In addition, it also forms a good homogeneous mixture with various commercially useful polymeric materials like polyethyl terephthalate (PET)⁵, polypropylene (PP)⁶, etc. These properties makes PBS a qualified candidate for replacing environmentally less favorable halogenated flame retardants.

The properties of hybrid materials largely depend upon the intrinsic microstructure⁷, molecular arrangements and absolute morphology^{8,9} which in turn depend on synthetic procedure. Designing and synthesis of a well-defined PBS would allow fine tuning chemical, thermal and rheological properties. Sol-gel synthesis², condensation of boric acid with various functional silanes and siloxanes at elevated temperatures⁴, simultaneous hydrolysis of alkoxyboranes and alkoxysiloxanes¹⁰, dehydrocarbon condensation using Piers-Rubinsztajin reaction¹¹, enzyme catalyzed green method at slightly elevated temperature¹², are a few of the synthesis processes already in use.

In this study, linear and well defined poly(borosiloxane) was for the first time prepared by dehydrocoupling polymerization. The polymer obtained showed highly alternating sequence.

In spite of wide availability of three dimensional borosilicate glass (**Figure 3.1**), no example of one dimensional counterpart has been ever reported to the best of our knowledge. Further in our studies, we have designed a linear highly alternating poly(borosiloxane) (PBS). Also, the obtained polymer exhibited unexpected high stability to water and air.

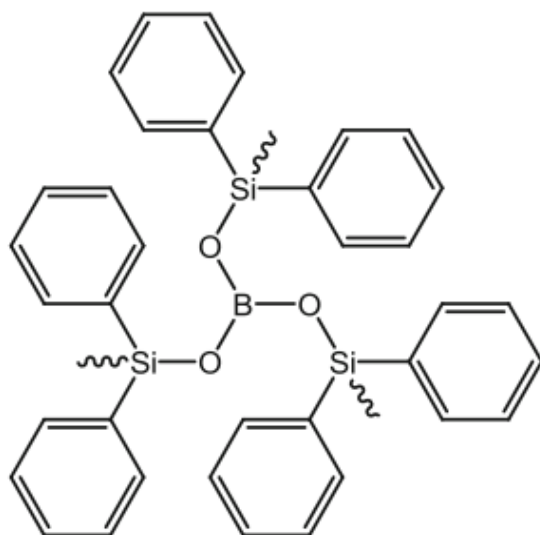


Figure 3.1: Three Dimensional Network of Polyborosiloxane¹³.

The prepared poly(borosiloxane) were found to be useful in variety of applications. Few of them are studied in detail here:

3.1.1 Solid State Ultra-sensitivity Towards Fluoride Ions in Aqueous Media

Nowadays, fluoride ion is extensively used in drugs for the treatment of psychiatric diseases and osteoporosis¹⁴. According to World Health Organization (WHO), concentration of fluoride ion in drinking water in the range of 0.8-1.2 mg/l is beneficial for teeth and bones. However, exposure to 1.5-10.0 mg/l or above can cause serious ailments such as pitting of tooth enamel, deposition in bones and crippling skeletal fluorosis¹⁵. Therefore, the minimal concentration of fluoride ion detection is desirable in aqueous media. But it is challenging because of its high affinity towards water (hydration enthalpy $\Delta H = -504$ KJ/mol)¹⁶. Over the years, researchers have comprehensively studied various types of organoboron low molecular weight and polymeric sensors showing prodigious visible and/or spectroscopic responses¹⁷⁻¹⁹. But most of them work in organic media and gives reversible reaction in water¹⁶. In order to achieve higher affinity towards fluoride ions in aqueous media, cationic organoboron compounds were studied by Găbbai et. al. with varying hydrophilicity of the receptors¹⁶. Sensing was possible up to 4 ppm of fluoride ions with optical methods (UV-Vis, PL) but there happens to be a detection limit in these methods as large amount of change in reaction mixture is required to generate the response. Also, the presence of strong chromophore is a requisite in chemical structure. In the recent past, various electrochemical techniques were developed in the field of sensing such as electrochemical impedance spectroscopy (EIS), open circuit potential (OCP) and cyclic voltammetry (CV)²⁰. These electrochemical techniques do require very diminutive changes in electronic structure in the reaction mixture to trigger the signal. The advantage of solid state sensing over solution state sensing is because the reaction occurs at the electrode-electrolyte interface which leads to very high responses and facile sensing in aqueous media.

Our newly designed linear highly alternating poly(borosiloxane) (PBS) demonstrated strong affinity towards fluoride ions in solid state under aqueous conditions.

3.1.2 Self-Healing Properties of Poly(borosiloxane)

These days polymeric materials are extensively used in various applications such as surface coatings²¹, photoresist materials²², moulded engineering components and so on. But, continuous exposure of these materials to extreme conditions may cause physical degradation which may result in diminishing effect of the existing useful properties. The polymers which are capable of repairing the physical damage themselves can drastically enhance the durability²³. The ability of the polymers to repair themselves is known as self-healing behavior.

Self-healing (SH) polymers were developed after taking inspiration from biological systems where automatic response for reconstruction is triggered immediately after damage. To achieve SH in polymers, a number of reports are available in the literature with different methods^{24–26} such as using chemical reaction, chain-interdiffusion, intermolecular interactions and so on. Healing methods using chemical reactions (Diels-Alder Reaction)²⁷ and intermolecular interactions^{28–30} (hydrogen-bonding, ionic interaction π - π stacking interaction) are widely studied. These methods, however, are expensive in terms of industrial applications.

The SH method involving chain-interdiffusion²⁵, possible only in the polymeric materials, are proven to be cost-effective and are achievable by just keeping in time or by gentle heating. A behavior to recover mechanical damage beyond glass transition temperature (T_g) is well known for long time among polymers. Polyurethane networks with a lot of dangling chains exhibiting SH at the temperature above T_g has been studied by Yamaguchi et al.³¹ In a gel, dangling chains are the polymer chains having one end free to move and can show interdiffusion via reptile motion. Therefore, soft gel like poly(borosiloxane) can be a promising candidate for SH behavior.

Furthermore, according to Wool et al.^{25,32}, there are four stages of healing in chain-interdiffusion (**Figure 3.2**):

- 1) Surface approaching
- 2) Wetting
- 3) Diffusion
- 4) Randomization

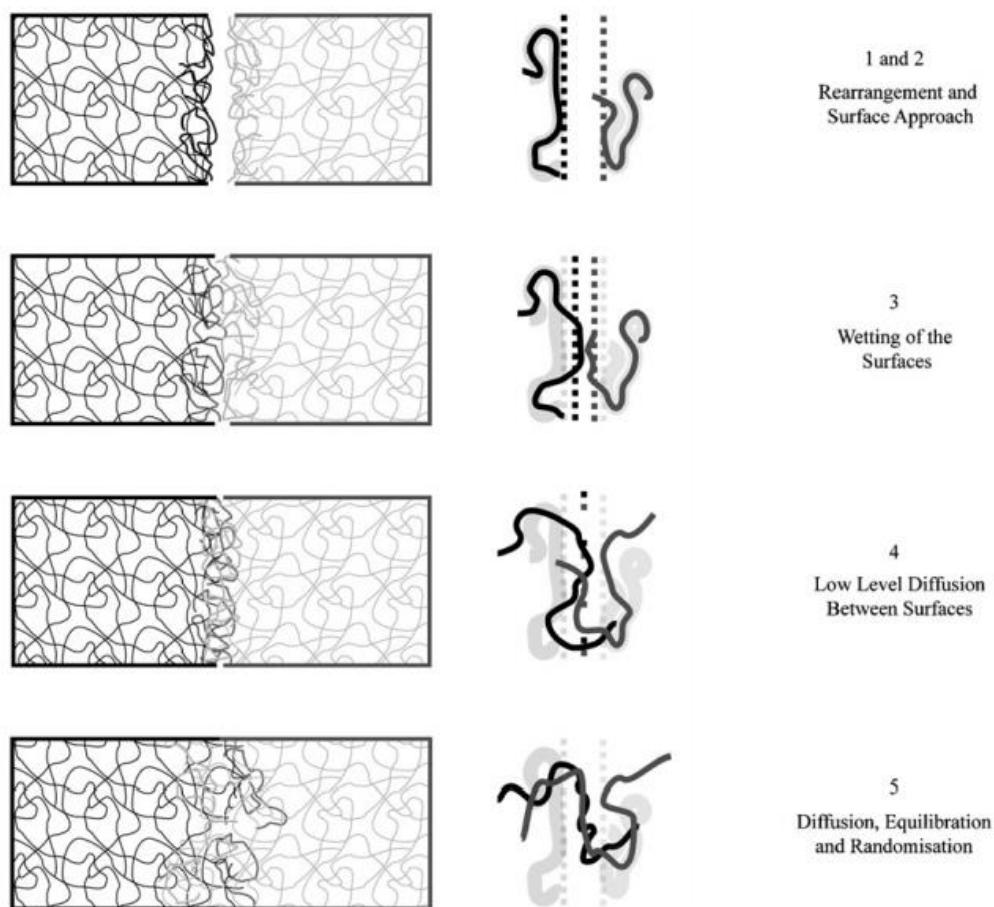


Figure 3.2: Mechanism of Healing with Chain-Interdiffusion.

In this method, the two damaged surfaces are wet together to form interface prior to inter-diffusion. Also, Brown et al.,³³ found that at least 200 nm of diffusion distance is required in order to achieve good mechanical strength.

Herein, the poly(borosiloxane) was examined as a self-healing polymer in which the wetting of damaged surface was not required and the diffusion distance up to a few micrometers (μm) was observed.

3.1.3 Ion Conductive Properties of Ion-Gels with Poly(borosiloxane) Polymer Support

Lithium ion batteries (LIBs) have already cemented its place industrially because of its massive energy density compared to other metal batteries such as Ni-Cd and Ni-hydrogen batteries³⁴. However, apart from excellent performance, the safety concerns are still associated with it³⁵. Researchers have distinctly focused on the further development of components in LIBs for safe utilization, among them design of electrolytes has been the area of interest³⁶. Conventional electrolytes like ethylene carbonate and diethylene carbonate show excellent properties³⁷ but are highly flammable and there is always a risk of leakage from the cell. To overcome above mentioned problems focus was shifted towards the development of gel type electrolytes. Gel type electrolytes provide certain advantages to LIBs³⁸ such as lower degree of dendrite formation, reduced reactivity with lithium, enhanced safety and ease of processing. Different approaches have been employed in order to develop such ion-gel electrolytes. Firstly, the addition of gelator^{39,40} to the liquid electrolyte which could harden the organic liquids smoothly. Thus prepared ion-gel electrolytes showed enhanced ionic conductivity in the presence of carrier ions.

Also, among gel type systems, electrolytes based on poly(ethyleneoxide)(PEO)⁴¹ and poly(acrylonitrile)(PAN)⁴² have been extensively studied. Further, to introduce non-flammability to the electrolytes, incorporation of ionic liquids were employed and studied vastly⁴³. Ionic liquids not only have non-flammable nature but it also possess excellent ionic conductivity and good thermal stability.

In order to prepare such gel type electrolytes with ionic liquid, sol-gel condensation was carried out to synthesize organic-inorganic hybrid materials with *in-situ* polymerization of ionic liquids. Borosilicates, which are considered to be softer than silicate, were studied by Ohno et al⁴⁴. Here, boron incorporation helped the lithium salt dissociation and also, it was able to trap anions. As a result, improved ionic conductivity was observed. Brosilicate network based ion-gels with monomeric ionic liquids were prepared and studied as electrolyte had exhibited good electrolytic properties⁴⁵. In this case, significant ionic conductivity of 2.0 mS cm^{-1} was achieved with moderate lithium ion transference number (t_{Li^+}) up to 0.16.

In the present work, a one dimensional linear and alternating poly(borosiloxane) was used in the combination of various lithium salts and low viscous ionic liquids and was studied as ion-

gel electrolytes. Alternating poly(borosiloxane) with higher number of boron units in the main chain of the polymer, is expected to trap anions efficiently and increase the selective cation transport.

3.2 Experiment

3.2.1 Synthesis and Characterization

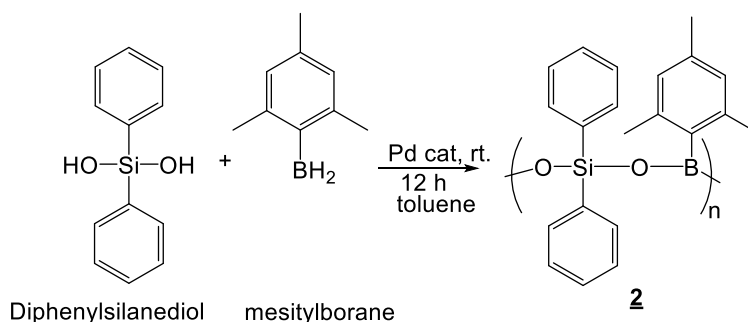
The synthesis of poly(borosiloxane) was carried out by dehydrocoupling polymerization of bifunctional silanol and mesitylborane in the presence of rhodium or palladium catalyst using tetrahydrofuran as a solvent (**Scheme 3.1**). The polymerization was successful under various reaction time, monomer concentrations and temperatures (**Table 3.1**). The synthesized polymers were characterized by ^1H -NMR (**Figure 3.3**), ^{11}B -NMR and ^{29}Si -NMR spectra. ^{11}B -NMR spectrum showed single peak at 30 ppm, highlighting only one atomic environment of boron atom (**Figure 3.4**). ^{29}Si -NMR spectrum supported alternating nature of the polymer with single peak at -21 ppm (**Figure 3.5**). Among the numerous possible polymer sequences, single peak in ^{11}B -NMR and ^{29}Si -NMR can be observed only with a high degree of alternating nature. In order to further confirm alternating nature, a model reaction was designed (**Table 3.2, entry 4**). The monomer diphenylsilanediol was modified to triphenylsilanol possessing a single reaction site. Triphenylsilanol was reacted with half equivalents of mesitylborane under same reaction conditions. A competition between (1) formation of dimer bis(triphenylsiloxane) vs (2) an adduct with a mesitylborane and two triphenylsilanol units could exist (**3**) (**Table 3.2, entry 4**). High yields (93%) of **3** firmly supported alternating sequence structure. Characterization of **3** was done by using ^1H -NMR, ^{11}B -NMR and ESI-MS (**Figure 3.7**) measurements. Single peak in ^{11}B -NMR and the integration ratios of ^1H -NMR supported the chemical structure of **3**. Further, homo polymerization of both the monomers, mesitylborane and diphenylsilanediol were also attempted under similar conditions, which yielded no product (**Table 3.2, entry 1,2**). The study of model reactions inferred that the presence of both the monomers were necessary for the chain propagation step. The need for every other monomers at the chain propagation step can be attributed as the driving force for such highly alternating sequence in polymer chain.

Also, the IR spectra of these polymers confirmed the formation of Si-O-B linkages (814 cm^{-1}) in the polymer chain (**Figure 3.6**). Broad peaks corresponding to Si-O and B-O linkages were also observed but interestingly, peaks for B-OH and Si-OH were absent. It suggests minimum

residual hydroxyl groups in the polymers backbone which can be handy for various applications. The gel permeation chromatographic (GPC) analysis of polymer **2** using THF as eluent (PSt standards, Isocratic flow of 1 mL/min, 35 °C) indicated the number average molecular weight of higher than 40000 g/mol.

The DFT calculations (Gaussian 09, 6-311G, B3LYP, d, p) were done for specifically designed models with Si-O-B and C-O-B linkages and bonding properties were compared (**Table 3.3**). The optimised structure showed partial multiple bonds in Si-O and also, the bond angle $\angle\text{SiOB}$ was larger (137.45°) than that of $\angle\text{COB}$ (131.23°). This presence of a partial double bond in the optimized structure evince the partial delocalization of oxygen lone pair to Si, which in turn allows an increase in bond angle. Also, a shorter B-O bond length was found in Si-O-B model (1.36 \AA) than that of C-O-B model (1.38 \AA). Hence, it can postulated that oxygen donates it's lone pair to the 3d orbital of silicon to form a donor-acceptor $p\pi-d\pi$ back-bonding which suitably exposes the boron atom for reaction with fluoride anion.

To confirm the stability of the polymer in water, polymer sample was immersed in water for 2 h and subjected of GPC analysis. No change in molecular weight was observed, showing high stability in water. The stability in water can be explained by hydrophobicity induced from diphenylsilanediol unit and electron rich groups on boron along with bond strengthening effect of $p\pi-d\pi$ interaction of Si-O adjacent to B-O bond.



Scheme 3.1. Synthesis of Poly(borosiloxane).

Table 3.1: Synthetic Results with Various Reaction Conditions.

S.No.	Catalyst	Time (h)	Temp (°C)	Yield (%)	Mn	PDI
1	A	8	rt	24	8700	1.6
2	A	8	70	56	900	1.0
3	B	8	rt	95	12900	1.5
4	B	48	rt	80	42500	1.2
5	B	48	70	77	1500	1.0
6	B	8	rt	66	700	1.0
7	C	8	rt	61	400	2.1
8	D	8	rt	72	900	1.1

A: [Tris(dimethylphenylphosphino)-(2,5-norbornodiene)rhodium(I), B: Bis(triphenylphosphino)-palladium(II) chloride, C: Chloroplatinic acid hexahydrate, D: Chloroplatinic acid.

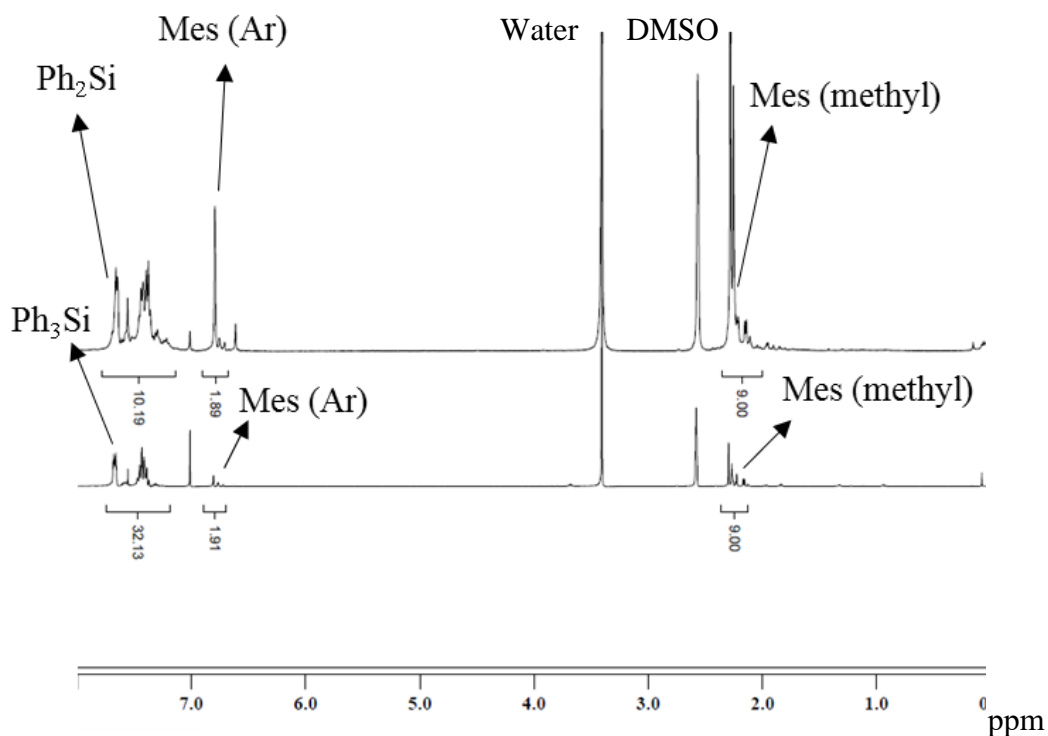


Figure 3.3: ¹H-NMR Spectra of **2 (above) and Model **3** (below).**

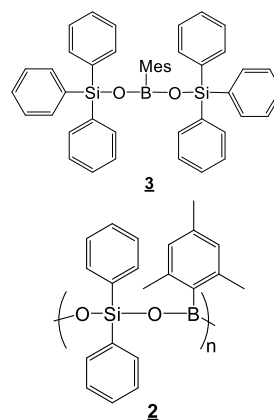
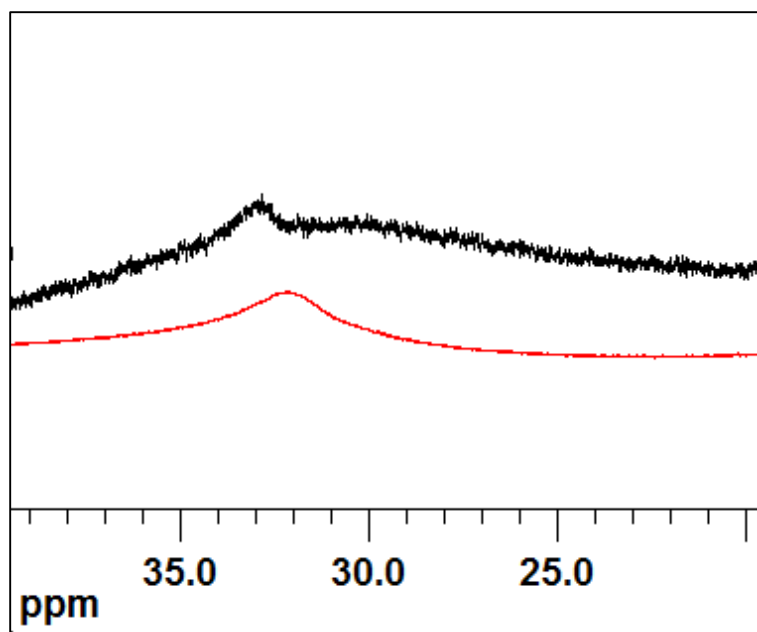


Figure 3.4: ^{11}B -NMR of **2** (below) and **3** (above).

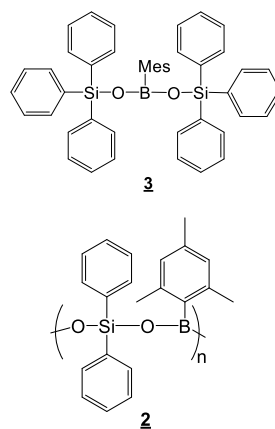
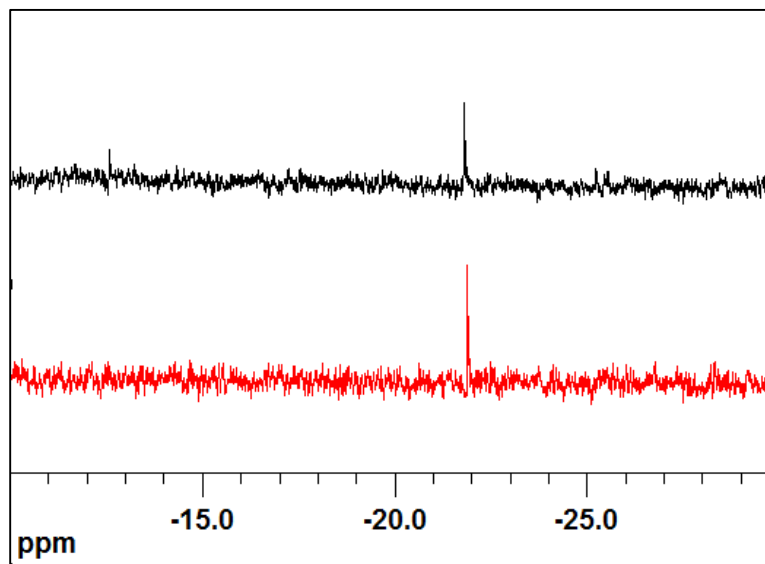
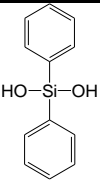
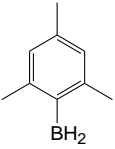
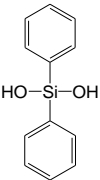
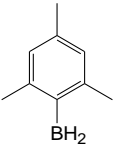
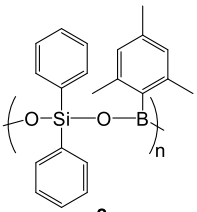
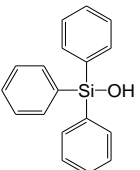
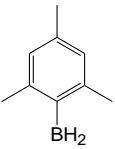
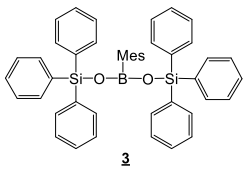


Figure 3.5: ^{29}Si -NMR of **2** (below) and **3** (above).

Table 3.2: Synthetic Results of Model Reactions.

S. No.	Silicon Moiety	Boron Moiety	Product
1	 Diphenylsilanediol	-	No Polymerization
2	-	 mesitylborane	No Polymerization
3	 Diphenylsilanediol	 mesitylborane	 2 81%
4	 Triphenyl-silanol	 mesitylborane	 3 93%

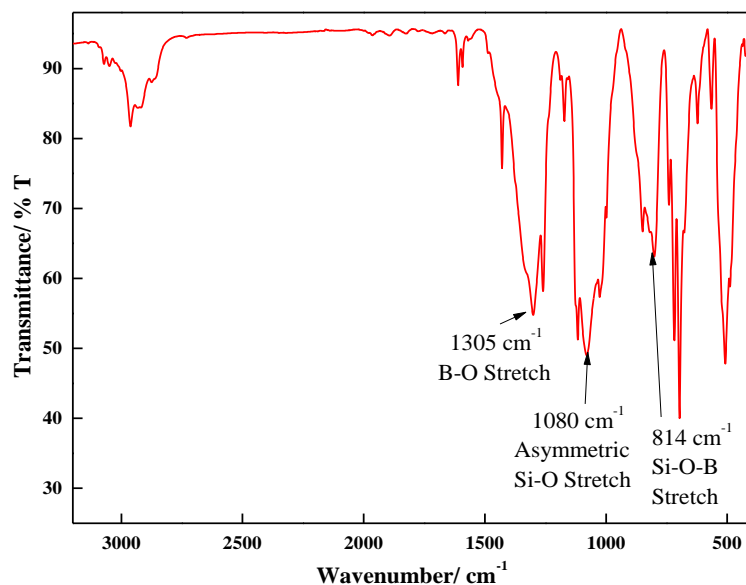


Figure 3.6: IR Spectra of Polymer 2.

Table 3.3: DFT Calculation of COB and SiOB Model.

Model	Chemical Structure	Optimized Structure	Bond Angle/ ^o	Bond length (B-O)/ Å ^o
COB			$\angle\text{COB} = 131.23$	1.38
SiOB			$\angle\text{SiOB} = 137.45$	1.36

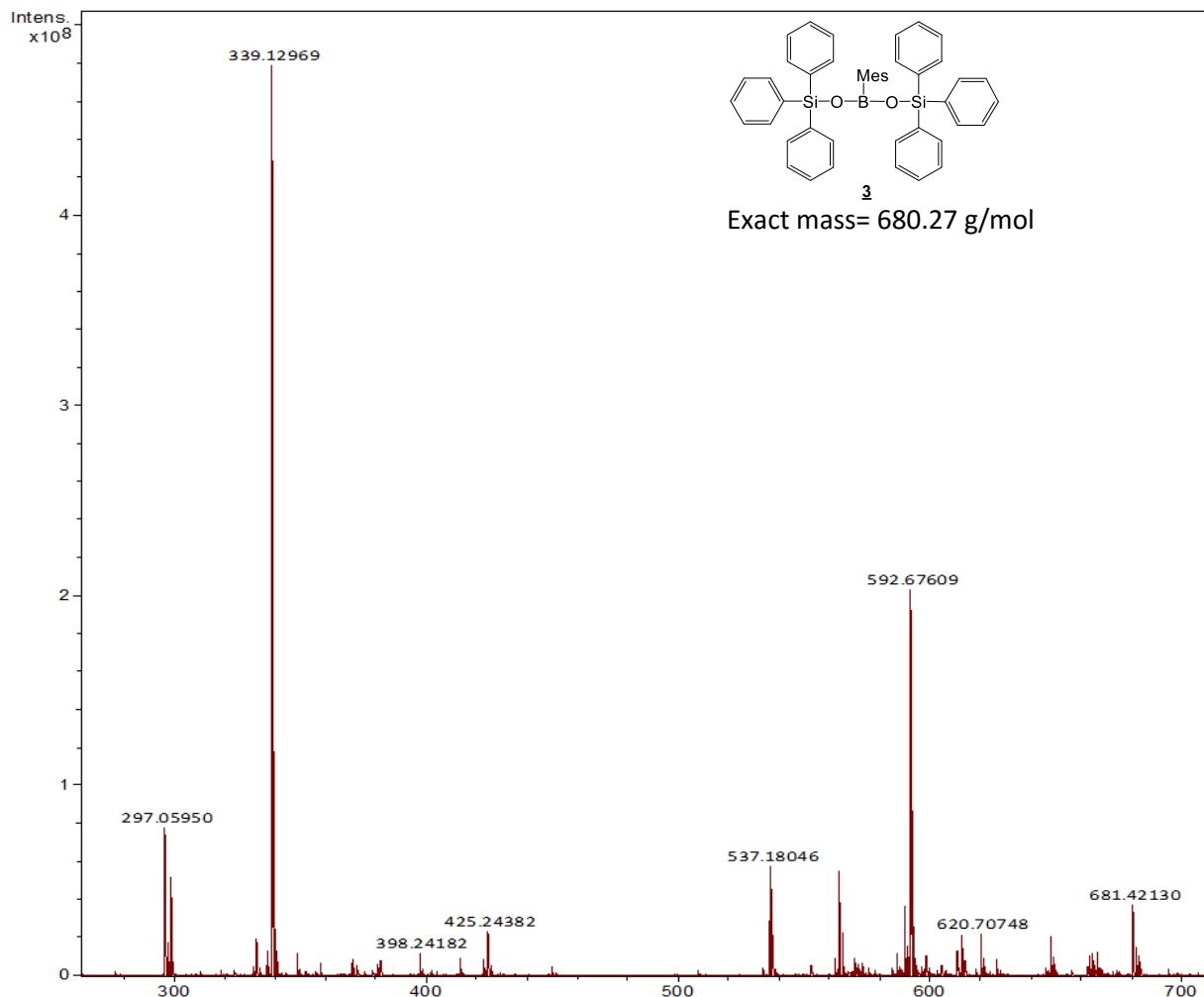


Figure 3.7: ESI-MS Mass Spectrum (Positive Mode) of Model 2.

Synthetic Procedure of Poly(borosiloxane): The synthesis of poly(borosiloxane) was carried out by dehydrocoupling polymerization of bifunctional silanol and mesitylborane in the presence of transition metal catalyst using tetrahydrofuran as a solvent (**Table 3.1**). A 100 ml round bottom flask was charged up with diphenylsilanediol (491 mg, 2.2 mmol) and bis(triphenylphosphino)-palladium(II) chloride (78 mg, 5 mol %) under nitrogen atmosphere. To this was added a THF solution of freshly prepared mesitylborane (300 mg, 2.2 mmol) with constant stirring. Effervescence due to evolution of H₂ gas confirms the progress of the reaction. The reaction mixture was allowed to stir at room temperature for 48 hours. THF was removed under reduced pressure and the product was extracted with *n*-hexane. *n*-Hexane was removed under reduced pressure and the polymer was dried in vacuum. (Yield = 81%)

Polymer **2**: ^1H -NMR: (δ , ppm, 400 MHz): 2.25 (s, 3H, CH_3), 2.28 (s, 6H, CH_3), 6.79 (s, 2H, aromatic protons); 7.30-7.49 (m, 6H, aromatic protons), 7.50-7.71 (m, 4H, aromatic protons), ^{11}B -NMR: (δ , ppm, 128 MHz): 32.0 (Si-O-B), ^{29}Si -NMR: (δ , ppm, 79.5 MHz): -22.0 (Si-O-B).

Synthetic Procedure of Model 3: The synthesis of **3** was carried out by dehydrocoupling of bifunctional silanol and mesitylborane in the presence of transition metal catalyst using tetrahydrofuran as a solvent. A 100 ml round bottom flask was charged up with triphenylsilanol (418 mg, 1.5 mmol) and bis(triphenylphosphino)-palladium(II) chloride (26 mg, 0.757 mol %) under nitrogen atmosphere. To this was added a THF solution of freshly prepared mesitylborane (100 mg, 0.74 mmol) with constant stirring. The reaction mixture was allowed to be stirred at room temperature for 48 hours. THF was removed under reduced pressure and the product was extracted with *n*-hexane. *n*-Hexane was removed under reduced pressure and the desired compound was dried in vacuum. (Yield = 93 %)

Model **3**: ^1H -NMR: (δ , ppm, 400 MHz): 2.25 (s, 3H, CH_3), 2.28 (s, 6H, CH_3), 6.80 (s, 2H, aromatic protons); 7.30-7.48 (m, 18H, aromatic protons), 7.50-7.75 (m, 12H, aromatic protons) ^{11}B -NMR: (δ , ppm, 128 MHz): 32.8 (Si-O-B). ^{29}Si -NMR: (δ , ppm, 79.5 MHz): -22.0 (Si-O-B). $m/z = 681.42$ g/mol.

3.3 Application of Poly(borosiloxane)

3.3.1 Solid State Ultra-sensitivity Towards Fluoride Ions in Aqueous Media

Solid state fluoride ion sensitivity was examined by electrochemical impedance spectroscopy (EIS), open circuit potential (OCP) measurements and cyclic voltammetry (CV) (**Figure 3.8, Figure 3.9, Figure 3.10**) using ammonium fluoride as fluoride ion source. For the electrochemical measurements, polymer film was solution casted over glassy carbon electrode and was immersed in aqueous electrolyte (**Figure 3.11**). Significant sensitivity towards fluoride ions was observed up to the concentration of 10^{-10} M. The magnitude of impedance linearly decreased with addition of fluoride ions. This decrease in impedance can be assigned to the reaction at the electrode-electrolyte interface. Also, the OCP profile was very stable and showed a staircase type profile with increasing aliquot of fluoride ions. The reaction at electrode-electrolyte interface was not saturated even after several additions of fluoride ions (10^{-10} M). Saturation in OCP was observed only at a fluoride ion concentration of 10^{-7} M (**Figure 3.10 (b)**). Cyclic voltammograms complemented the sensing behavior showing turn-on type of curves. The magnitude of current augmented with appendage of fluoride ions at -0.43 V in cathodic scan.

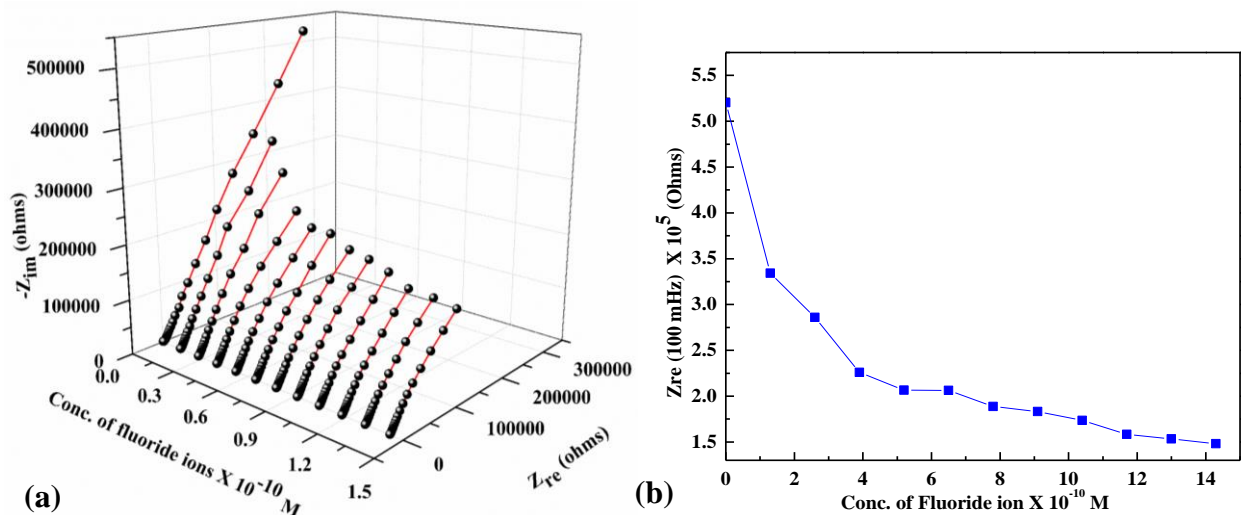


Figure 3.8: (a) Electrochemical Impedance Analysis of 2 with Titration of Fluoride Ions, (b) Graph of Real Impedance at 100 mHz vs Concentration of Fluoride Ions. Supporting Electrolyte (0.1 M): Disodium Hydrogen Phosphate aq., RE: Ag/AgCl, WE: GC, CE: Pt.

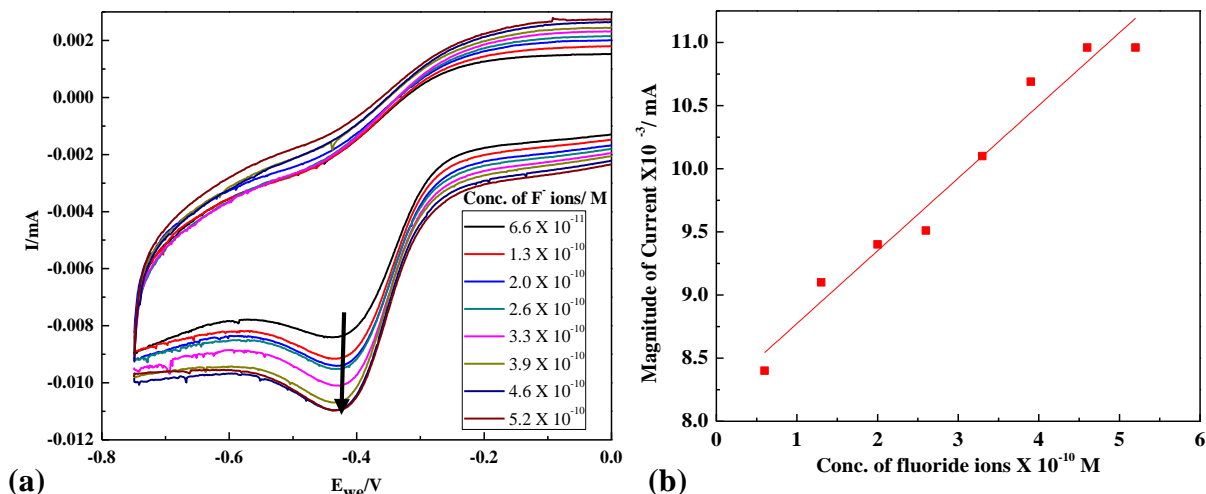


Figure 3.9: (a) Cyclic Voltammograms Open Circuit Potential Measurement of 2 with Titration of Fluoride Ions, (b) Magnitude of Current vs Conc. of Fluoride Ions. Supporting Electrolyte (0.1 M): Disodium Hydrogen Phosphate aq., RE: Ag/AgCl, WE: GC, CE: Pt.

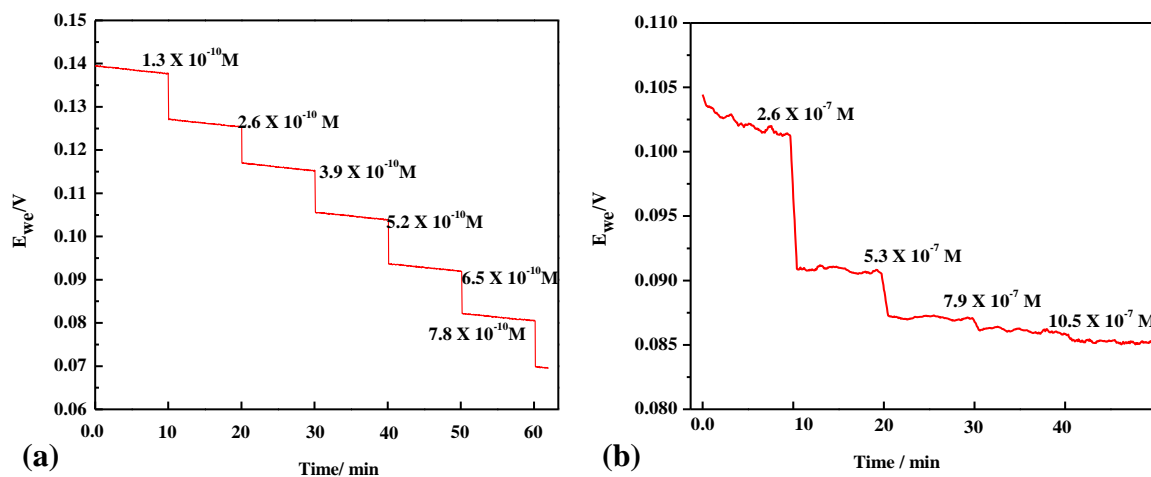


Figure 3.10: Open Circuit Potential Measurement of 2 with Titration of Fluoride Ions. (a) Concentration of Fluoride Ions 7.8×10^{-10} - 1.3×10^{-10} , (b) Concentration of Fluoride Ions 10.5×10^{-7} - 1.3×10^{-7} . Supporting Electrolyte: Disodium Hydrogen Phosphate, RE: Ag/AgCl, WE: GC, CE: Pt.

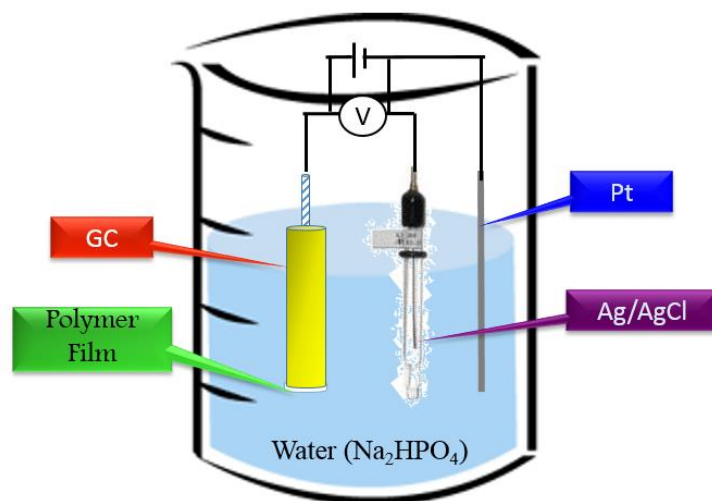
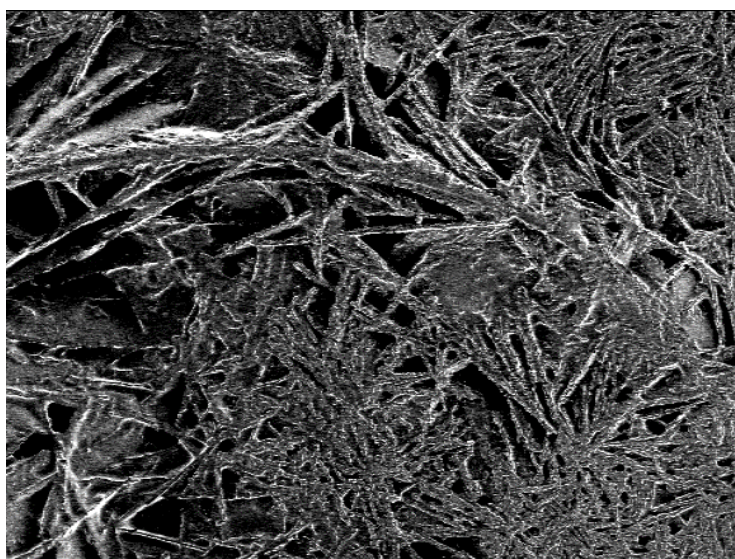


Figure 3.11: A Schematic Representation of Electrochemical Cell Setup.

Further, the polymer film was coated over exfoliated graphite and was immersed into an aqueous solution of ammonium fluoride for 10 minutes. The film was analyzed with SEM before and after the reaction with fluoride ions (**Figure 3.12**). The dendrimer type of morphology was transformed into perforated globules. This change in morphology was evinced for the binding of fluoride ions efficiently.

(a)



167 nm

(b)

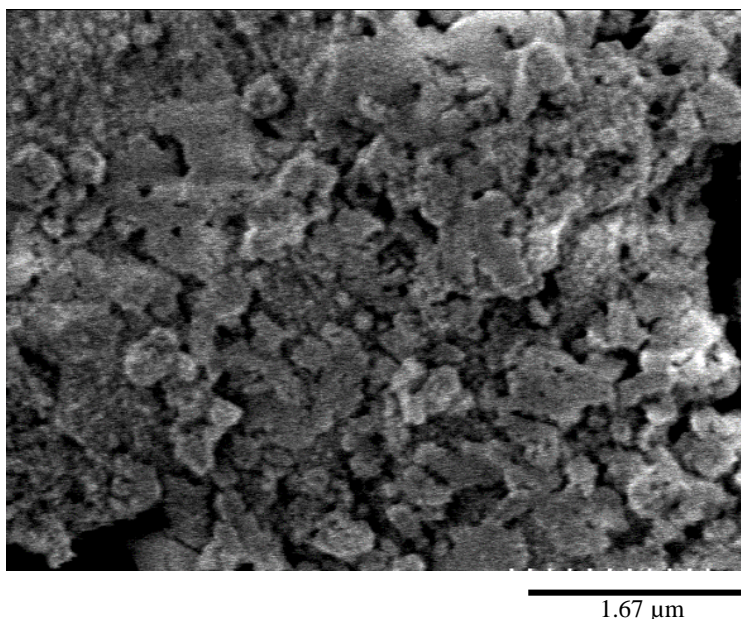
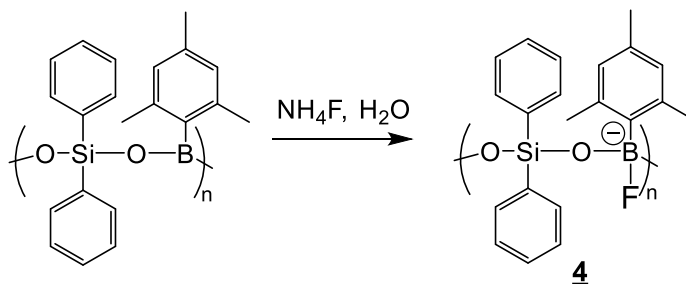


Figure 3.12: The SEM Images of Polymer Film Before (A) and After (B) the Reaction with Fluoride Ions.

In order to study the reaction pathway between polymer and fluoride anion, poly(borosiloxane) was reacted with equimolar quantity of ammonium fluoride in water (**Scheme 3.2**) and the ^{11}B -NMR spectra were measured before and after the polymer reaction (**Figure 3.13**). Although the polymer was not soluble in water, but the solid/liquid reaction proceeded smoothly showing strong affinity towards fluoride ions. The resultant product was analyzed by ^{11}B -NMR and ^{19}F -NMR spectra (**Figure 3.14**). Appearance of a new peak at -138 ppm in ^{19}F -NMR and a shift of peak in ^{11}B -NMR from 30 ppm to 1 ppm were observed. The shift in peaks apparently confirms the effective binding of boron with fluoride anion to form borate complex quantitatively.



Scheme 3.2: Polymer Reaction of Poly(borosiloxane) with Ammonium Fluoride.

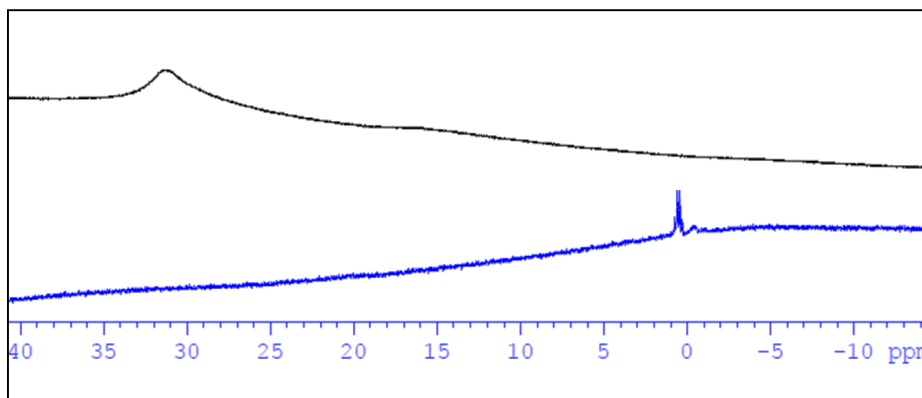


Figure 3.13: ^{11}B -NMR of 2 Before (black) and After (Blue) the Polymer Reaction with Fluoride Anion.

The polymer reaction with the poly(borosiloxane) was carried out with ammonium fluoride in water. The 20 mg of 1 was immersed into 1.0 M solution of ammonium fluoride in water at room temperature and stirred for 6 hours. The product was filtered and dried under vacuum.

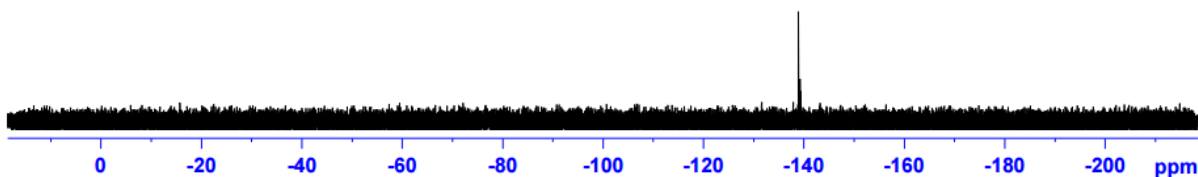


Figure 3.14: ^{19}F -NMR of 4 After the Polymer Reaction with Fluoride Anion.

The molecular weight analysis was done before and after the reaction with fluoride ions by GPC (**Figure 3.15**). There appeared to be a small change in the molecular weight from 42500 g/mol (2) to 43000 g/mol (4). This small increase in the molecular weight can be assigned to formation of borate with the binding of fluoride ions.

There are various kinds of organoboron fluoride anion sensors present in the literature which can bind with fluoride ions. But most of them can work only in organic solvents and give reversible reaction in the presence of water. Also the sensitivity towards concentration of fluoride ions were limited in the range 10^{-3} - 10^{-6} M in aqueous media. Gabbai et. al developed ammonium and phosphonium based low molecular weight organoboron compounds which can detect fluoride ions in aqueous media maximum up to 10^{-6} M. In the present work we have developed

poly(borosiloxane) which can detect up to 10^{-10} M concentration of fluoride ions in aqueous media which is most sensitive to date.

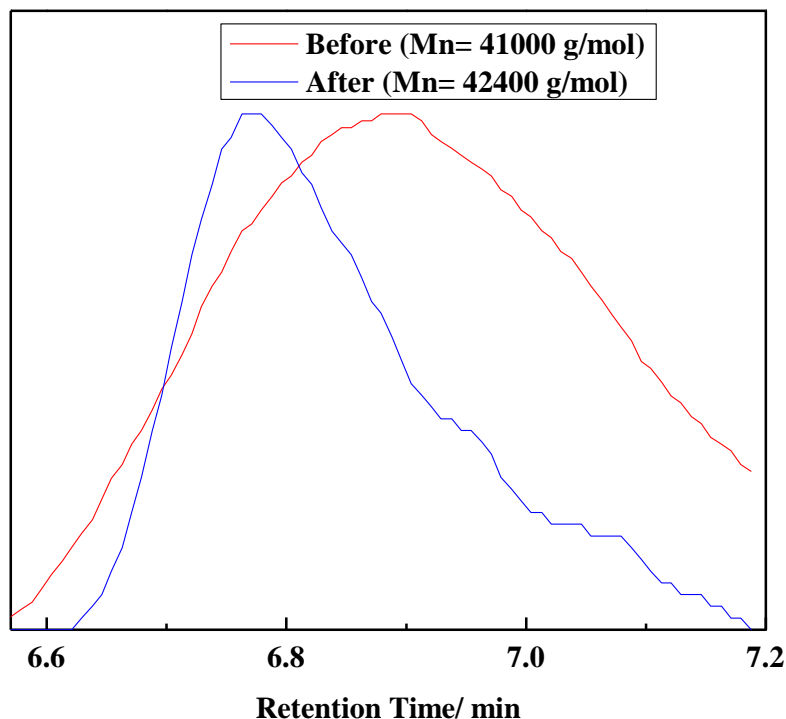


Figure 3.15: GPC Traces of Polymers 2 and 4.

3.3.1.1 Conclusion

Thus, in this study synthesis of highly alternating poly(borosiloxane) by dehydrocoupling polymerization was successfully carried out. The polymer sequence structure was understood by various model reactions. The fluoride anion sensing was examined and it was established to be highly sensitive (10^{-10} M of fluoride anion). Detection of such low concentration was possible by the synergistic contributions of both, the solid state electrochemical sensing measurements and the Si-O back-bonding in the polymer chain exposing boron atom in a suitable conformation for reaction with fluoride. The kind of sensing behavior being presented here, is unprecedented under these conditions to the best of our knowledge which will open a new window for the development of fluoride anion sensing methods and materials.

3.3.2 Self-Healing Properties of Poly(borosiloxane)

The thermal stability of poly(borosiloxane) was analyzed by thermo-gravimetric analysis (TGA). The polymer was found to be stable up to 140 °C and started decomposing after further increase in temperature (**Figure 3.16**). The char yield was observed to be more than 20 % at 750 °C. Such a high char yield can be assigned to the silicon-carbide and boron carbide formation at 750 °C. Further, in the differential scanning calorimetry (DSC) analysis, the glass transition temperature (T_g) and decomposition temperature (T_D) were determined to be -5 °C and 125 °C, respectively (**Figure 3.17**).

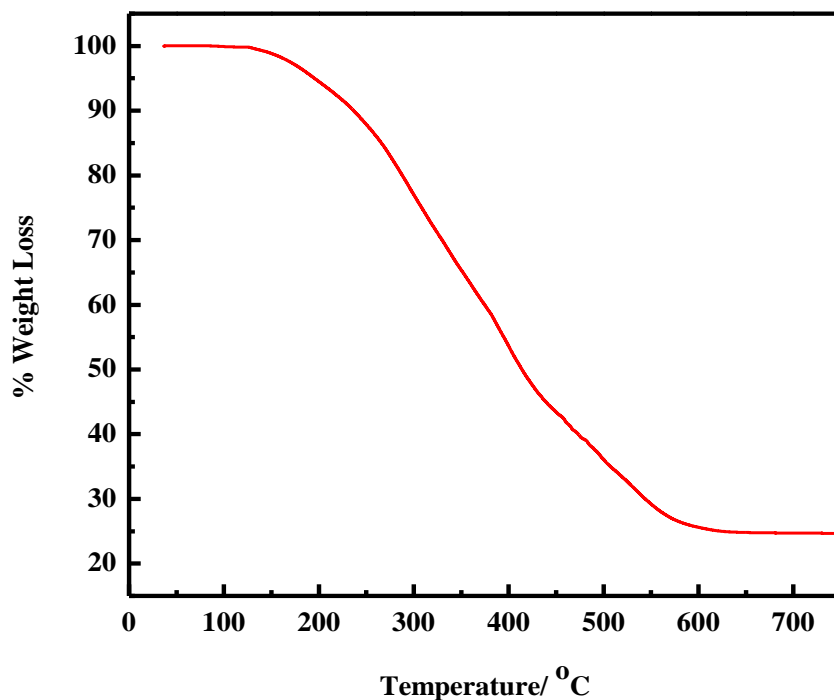


Figure 3.16: Thermo-gravimetric Analysis of Poly(borosiloxane) 2.

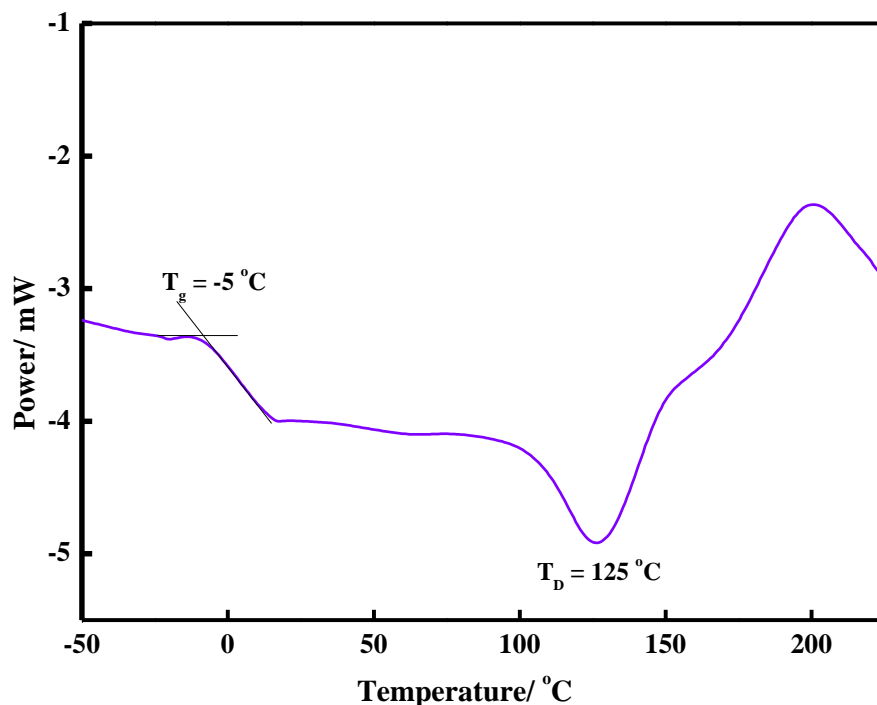


Figure 3.17: Differential Scanning Calorimetry Analysis of Poly(borosiloxane) 2.

In order to examine the SH propertis of 2, the polymer film was coated over Ti-metal by solution casting method and was dried thoroughly. A scratch was made to the polymer film to damage it physically and the polymer was heated over hot plate for 1 minute at 45 °C. The healing of damage was evident from visual observation (**Figure 3.18**). An extremely quick response (30 sec) to heal the physical damage was observed at a temperature higher than T_g . This SH behavior was thought to be a result of enhanced free movement of polymer segments at 45 °C. As already discussed earlier, the free movement of polymer segment can lead to reptile motion which might be the mechanism of self-healing property observed here. In order to further confirm the healing phenomenon, scanning electron microscopy (SEM) was employed to monitor the healing behavior (**Figure 3.19**). A deliberate indentation in the range of 70-75 μm was created and partial healing of the polymer surface was observed to cover the scratch gradually. The dangling chains which are created at both the damaged edges of the film, believed to move towards each other to cover the scratch on subjecting the elevated temperature.



Figure 3.18: Visual Observation of Self-healing Property of 2.

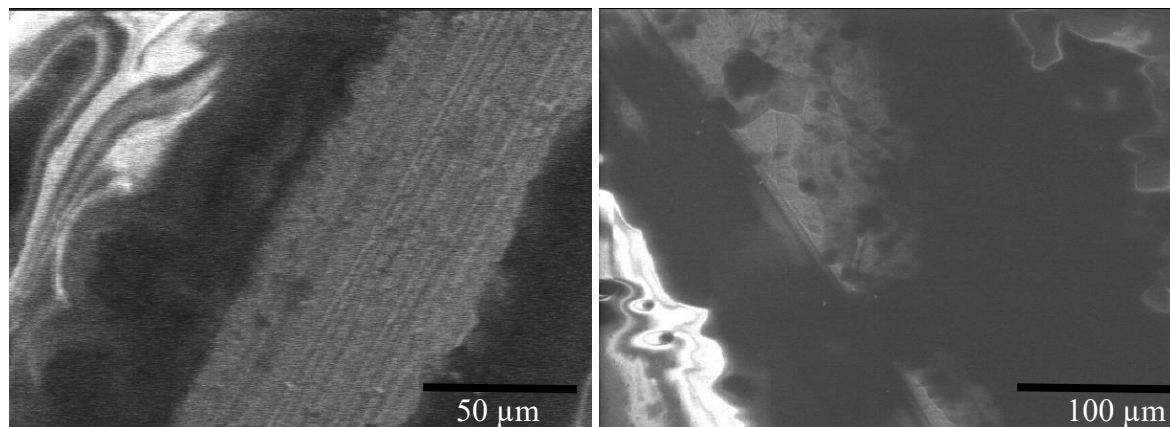


Figure 3.19: SEM Micrographs of Polymer Film Coated Over Ti-Metal with Scratch (Left) and After Partial Healing (Right).

The SH behavior was evident visually as well as with SEM analysis. Also, the prepared polymer exhibited good stability towards water and air. The polymer coat may possibly act as a corrosion protection to metal. Hence, in order to examine the corrosion protection ability of the healed surface, electrochemical impedance measurements were carried out. The polymer was coated on Ti-metal and immersed into a 3% NaCl aq. solution (Electrolyte). The electrochemical impedance of the polymer coated Ti-metal, polymer coat with scratch and polymer coat after healing were measured. A conventional three electrode system was used for this measurement. The Ti-metal with/without polymer coat was used as working electrode, Pt as counter electrode and Ag/AgCl as reference electrode in all the measurements. The Nyquist plots showed the high impedance of polymer coated Ti-metal even after immersing it to the 3% NaCl aq. solution for 1 hour 30 minutes proving it a good surface protecting polymer coat. The magnitude of impedance decreased as expected after scratch. The impedance after self-healing of the polymer coat was similar to the completely coated Ti (**Figure 3.20**). The closure of the scratch was evident. The

observed magnitude of impedance was plotted at different stages of self-healing and it evinced SH behavior beyond doubt. Also, in order to avoid the misperception that the formation of TiO_2 at the scratched surface can also cause the enhancement in magnitude of impedance, the impedance were measured for bare Ti-metal and after immersing it to the electrolyte for 2 hours and 30 minutes. The enhancement of impedance appeared be minimal as compared to polymer self-healing (**Figure 3.21, Figure 3.22**).

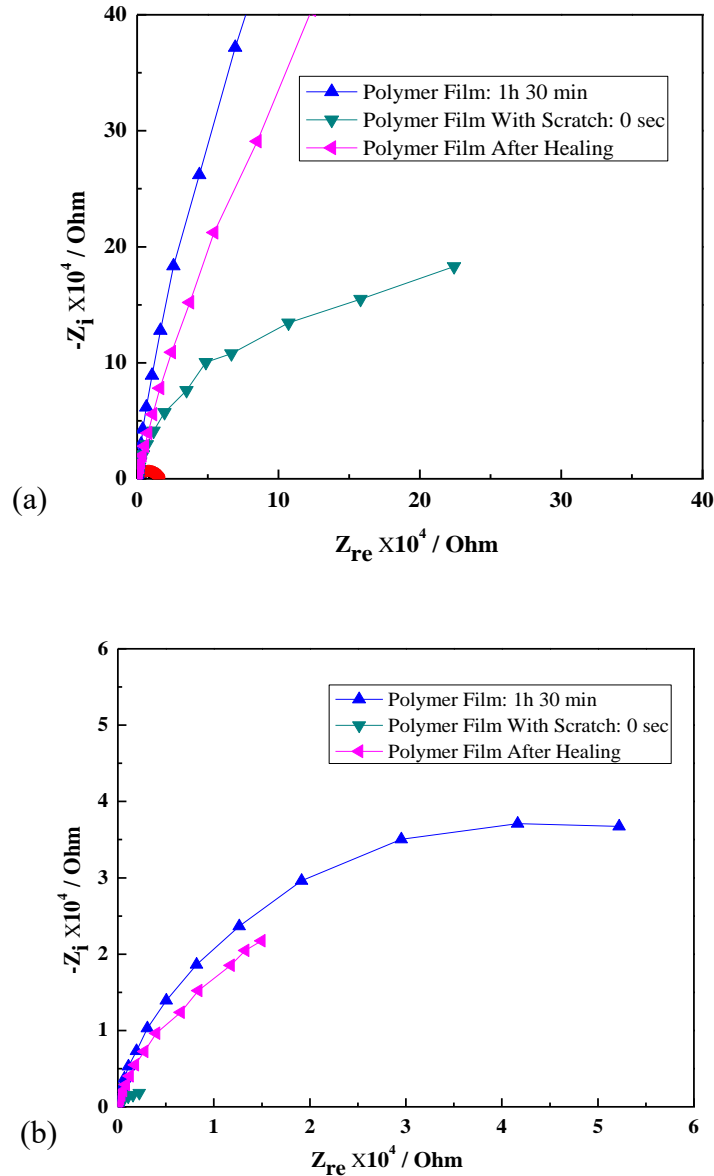


Figure 3.20: Nyquist Plots of Impedance to Observe Self-Healing Behavior (a), Enhanced In (b). Supporting Electrolyte: 3% NaCl, RE: Ag/AgCl, WE: Ti, CE: Pt.

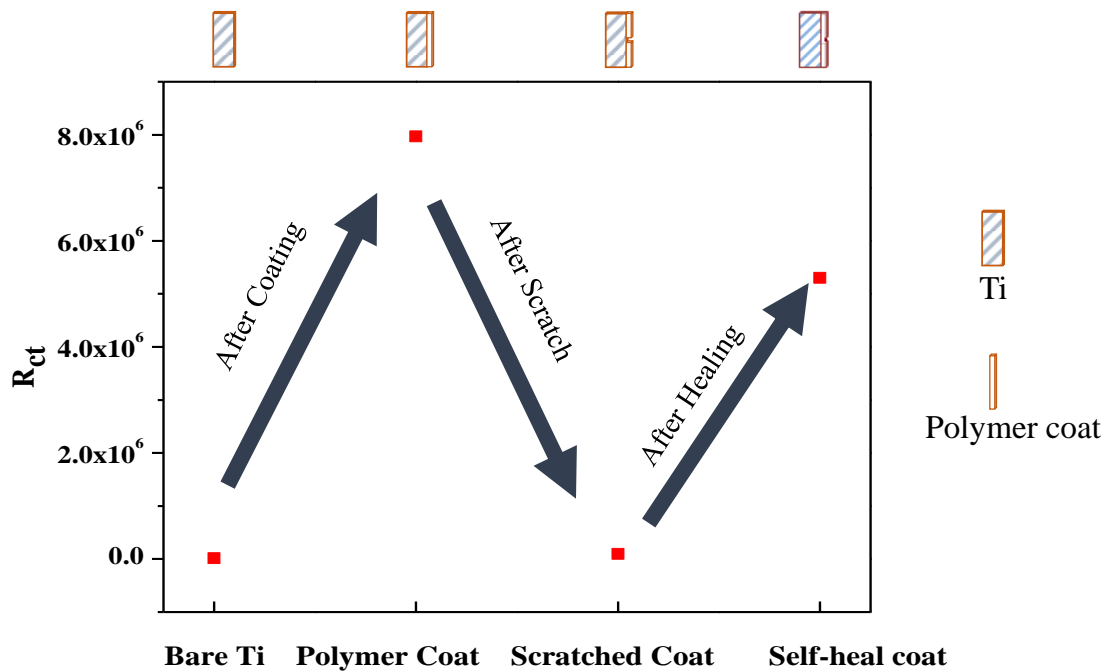


Figure 3.21: Magnitude of Impedance at Each Step of Self-Healing Behavior.

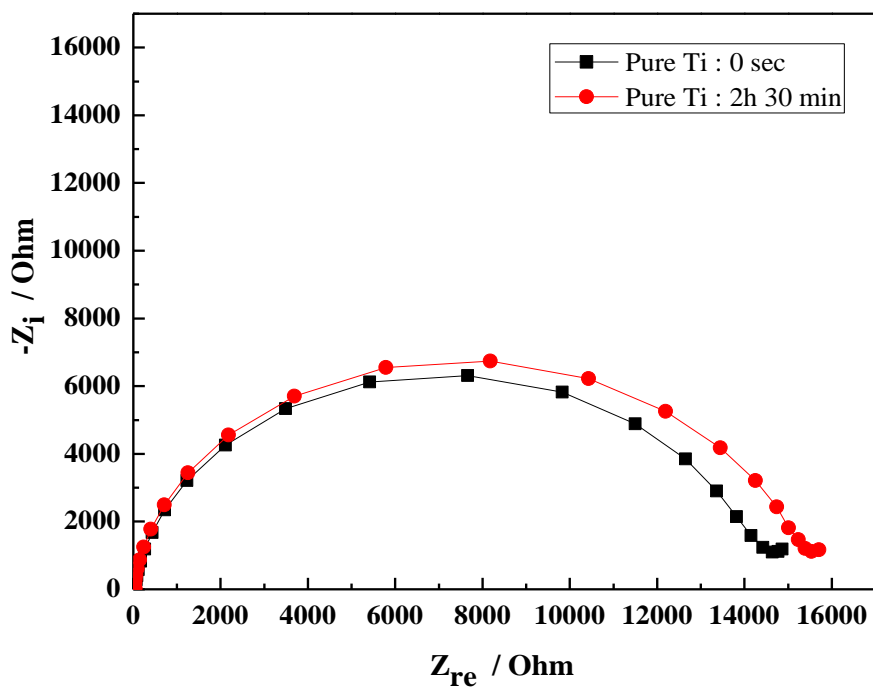


Figure 3.22: Nyquist Plots of Impedance to Observe Self-Healing Behavior.

Supporting Electrolyte: 3% NaCl, RE: Ag/AgCl, WE: Ti, CE: Pt.

The Bode plots for three different samples are shown in **Figure 3.23** and **Figure 3.24** of three different samples viz. (i) after coating the polymer on metal (ii) after inducing a scratch on the polymer coat and (iii) after healing the scratch.

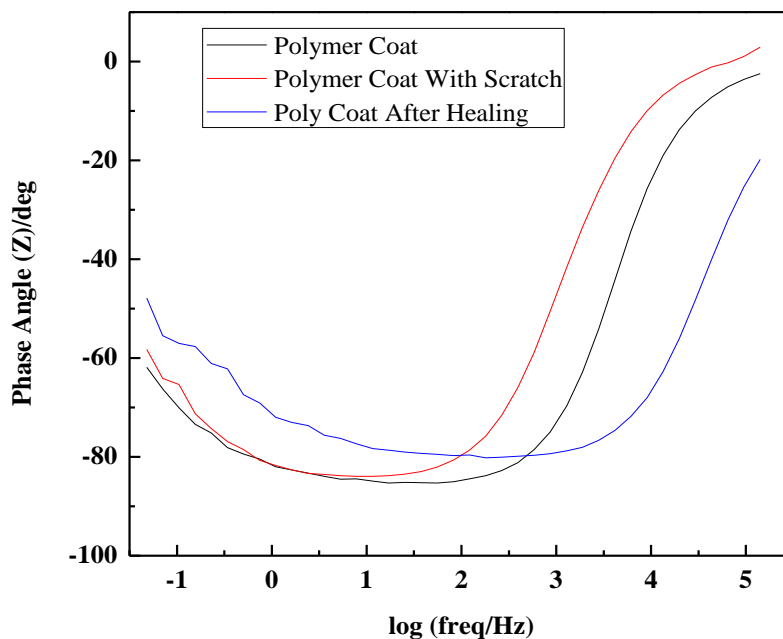


Figure 3.23: Bode Phase Angle Plot of Investigation of Self-Healing Property of Polymer.

Supporting Electrolyte: 3% NaCl, RE: Ag/AgCl, WE: Ti, CE: Pt.

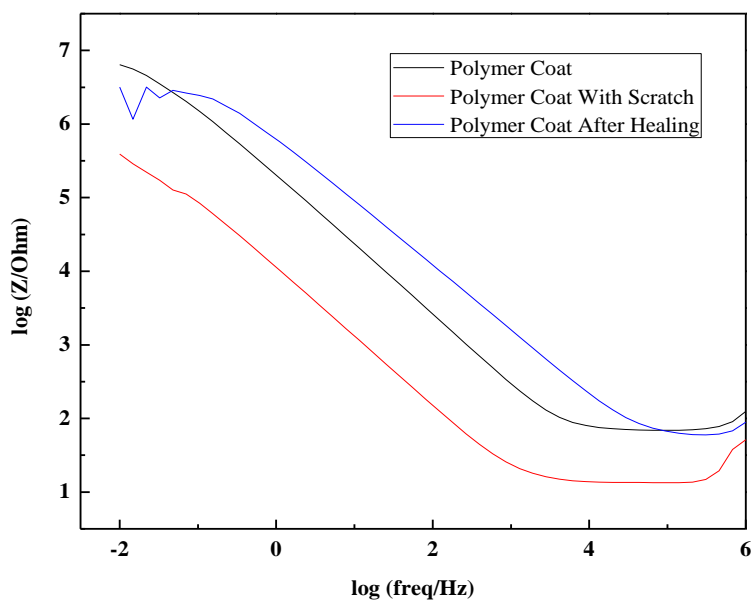


Figure 3.24: Bode-impedance plots of Each Step of Self-Healing. Supporting Electrolyte:

3% NaCl, RE: Ag/AgCl, WE: Ti, CE: Pt.

Seeing the phase angle behavior from right to left, it is noted that the polymer coated metal shows a stable phase angle -80° in the intermediate frequency range. Though the phase angle is similar after inducing the scratch, it can be seen that there is a considerable shift in the onset of the change in phase angle. Again, after healing the scratch, it can be seen that the onset of the change in phase angle starts at higher frequency unlike the one in scratched surface. The phase angle reaches a value -75° at the most stable part. This can be attributed to the thinning of the polymer due to overall stretching of the coat during healing.

Also, bode impedance complements the SH behavior of the polymer. Again seeing the plot from right to left, we observed that the impedance corresponding to the lowest frequency is high in the case of samples with the polymer coat and after healing compared to the sample with scratch. This clearly indicated the metal dissolution from the scratched part, which makes the resistance lower which is totally arrested after healing, leading to regain of the higher impedance.

The corrosion experiment to observe polarization curves, was carried out using linear sweep voltammetry (LSV). Similar to the above mentioned experiments, the polymer was coated over Ti-metal and immersed into the 3% Na_2SO_4 aq. solution (Electrolyte). The Ti-metal was used as working electrode, Pt as counter electrode and Ag/AgCl as reference electrode in all the measurements. The results of corrosion experiments of polymer coat, polymer coat with scratch and polymer coat after healing are presented in **Figure 3.25**. It was comprehended that even after immersing the polymer coat in the electrolyte for 14 hours, the corrosion current (I_{corr}) did not change drastically, whereas corrosion potential (E_{corr}) changed from 0.537 V to 0.053 V. After inducing a scratch to the polymer coat the E_{corr} decreased to -0.051 V indicating active metal dissolution. After partial healing, the E_{corr} reached to -0.011 V and after complete healing E_{corr} was observed to be very similar to fresh polymer coat (0.454 V). Although the I_{corr} did not change to give a very good idea of self-healing but it was significantly seen by monitoring E_{corr} (**Table 3.4. Figure 3.25**).

Table 3.4: Results of Corrosion Experiment.

Sample No.	Sample	E_{corr}/V	$I_{\text{corr}}/\text{mA}$
1	Ti (0 sec)	-0.054	-4.26
2	Ti (14 h)	-0.006	-4.17
3	Polymer Coat (0 sec)	0.537	-7.25
4	Polymer Coat (14 h)	0.053	-6.96
5	After Scratch	-0.051	-6.08
6	Partial Heal	-0.011	-6.52
7	Complete Heal	0.454	-6.34

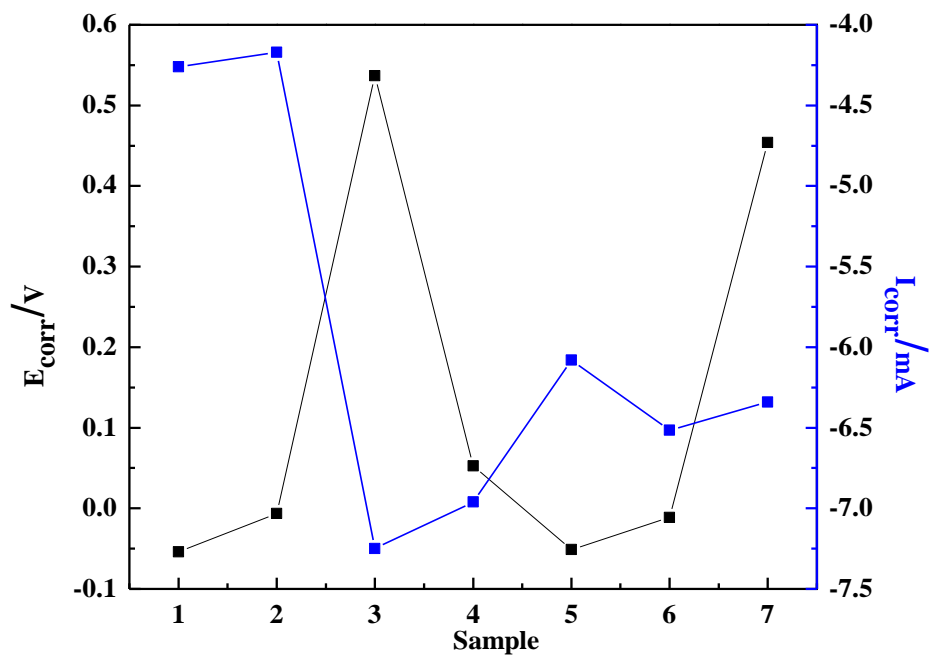


Figure 3.25: Results of Corrosion Experiment.

3.3.2.1 Conclusion:

Therefore, the self-healing behavior of poly(borosiloxane) achieved by heating to 45 °C, was observed visually. A reptile motion of the polymer was believed to be the mechanism for self-healing and thus was confirmed by SEM micrographs. The polymer coat behaved as a remarkable corrosion protectant to the metal surface. The self-healing property was also observed by monitoring electrochemical impedance measurements and depolarization studies. Good protection was observed after self-healing in samples which were subjected to scratch-heal test. This proved that the healing process was complete in all the facets.

3.3.3 Ion Conductive Properties of Ion-Gels with Poly(borosiloxane) Polymer Support

Polymer **2** was dissolved in tetrahydrofuran (THF) with various ratios of lithium bis(trifluoromethanesulfonylimide)(LiTFSI)/lithium bis(fluoromethanesulfonylimide)(LiFSI) with allylmethylimidazolium bis(trifluoromethanesulfonylimide)(AMImTFSI) and the mixtures were stirred for 5 hours at room temperature. THF was evaporated under reduced pressure and the sample was dried thoroughly under vacuum at 50 °C.

A variety of ion-gel electrolyte were prepared by doping the synthesized poly(borosiloxane) with a low viscous ionic liquid AMImTFSI and two different lithium salts (LiTFSI/LiFSI). The details of composition of each sample is tabulated in **Table 3.5**. In this study, the linear and alternating poly(borosiloxane) system were employed as a polymer support having higher borane content. Boron atom can interact with anions and help in the salt dissociation which might be useful for enhancement of ionic conductivity and selective cation transport.

Ionic conductivity measurements were carried out using ac impedance method in order to examine the temperature dependence of ionic conductivities of the prepared samples. With this method linear increase in the ionic conductivity was observed except a slight change of slope in the Arrhenius plots after 44-47 °C (**Figure 3.26**). By the measurements of ionic conductivity of various samples, the composition of ion-gel electrolytes were optimized to achieve highest ionic conductivity. For this, two sets of sample were prepared under different doping carriers, firstly the samples were doped with LiTFSi (Samples 1-4, **Table 3.5**) and secondly the samples were doped with LiFSI (Samples 5-7). The maximum ionic conductivity achieved was $7.3 \times 10^{-4} \text{ Scm}^{-1}$ (Sample 4, **Table 3.5**) and $1.8 \times 10^{-3} \text{ Scm}^{-1}$ (Sample 7, **Table 3.5**) at 51 °C among each set of prepared sample, respectively.

The samples prepared by doping with LiFSI showed relatively higher ionic conductivity than that of samples prepared by doping with LiTFSI. In order to attain better understanding of ionic conductivity behavior, the linear regression equation of the VFT (Vogel-Fulcher-Tammann) plots were fitted (**Figure 3.27**). The numeric values of activation energy and carrier ion numbers were obtained with this method (**Table 3.5**, Column 7, 8). However, the carrier ion numbers were observed to be relatively higher and the activation energy were found to be lower in the case of samples doped with LiFSI. This infers the better interaction of FSI anion with borane. A strong

interaction between borane and FSI anion would allow better salt dissociation resulting in the decrease of activation energy and increase in carrier ion numbers.

Also, in the case of samples doped by LiTFSI similar phenomena was observed. Though the ionic conductivities observed were relatively lower, however, these values were comparable to the previously reported ion-gel electrolytes reported by our group where three dimensional network of polyborosilane was employed with LiTFSI. Moreover, in present study, the carrier ion numbers and the activation energy were improved compared to the previous reports.

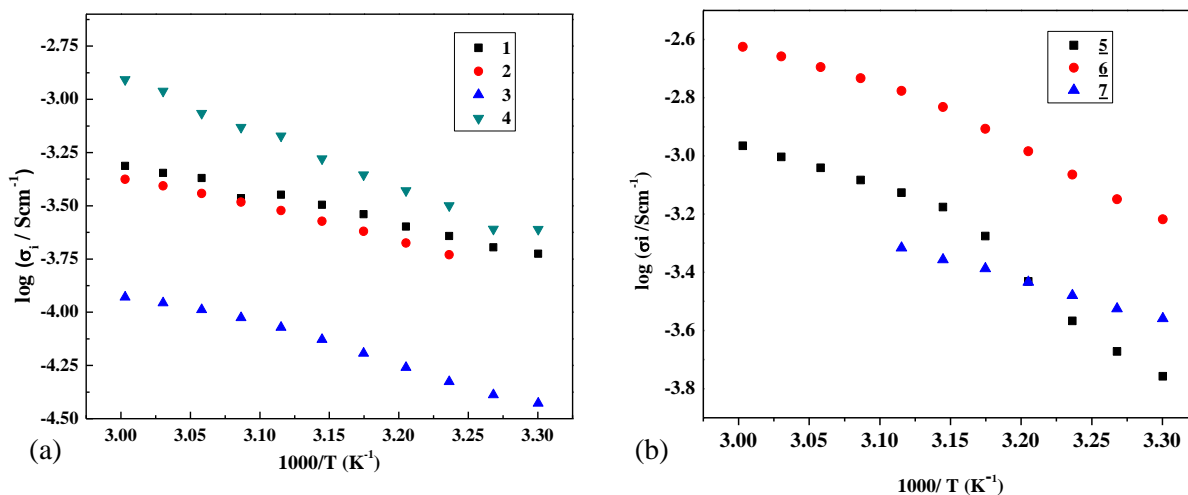


Figure 3.26: Arrhenius Plots of Ionic Conductivity (a) Samples 1-4, (b) Samples 5-7.

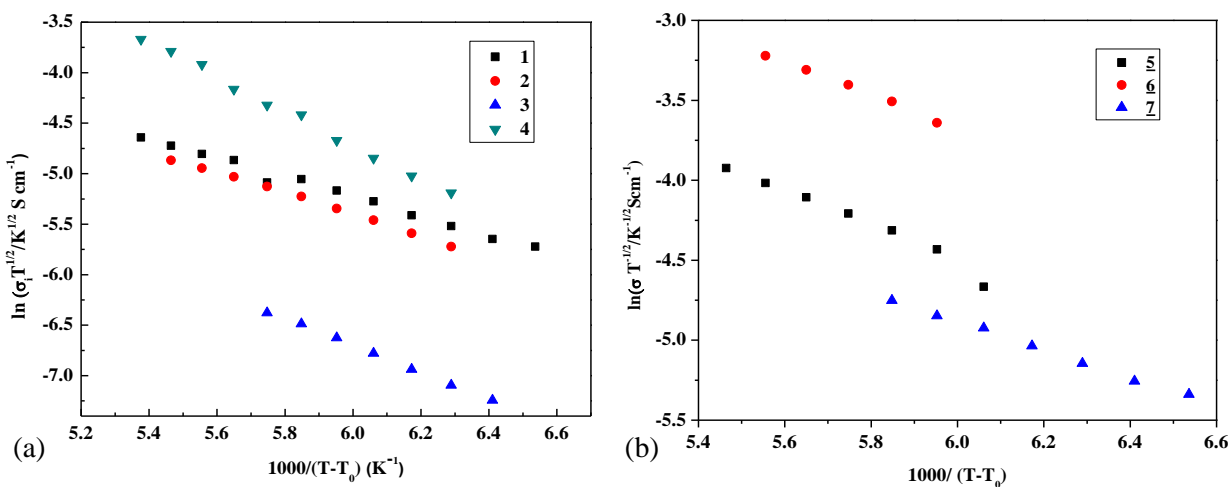
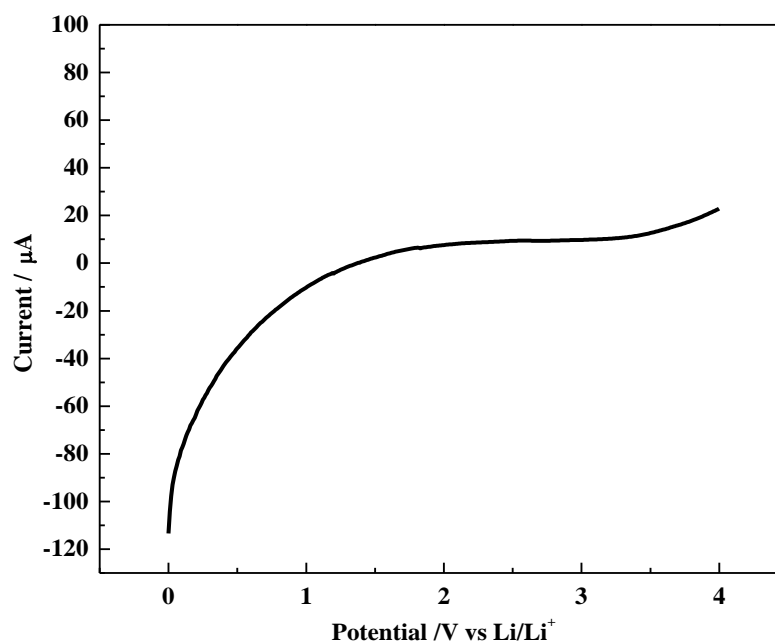


Figure 3.27: Arrhenius Plots of Ionic Conductivity (a) Samples 1-4, (b) Samples 5-7.

Table 3.5: Parameters of Ionic Conductivity Measurements of Various Samples.

Sample	Molar Ratio			$\sigma(51\text{ }^{\circ}\text{C})(\text{Scm}^{-1})$	B (K)	A ($\text{SK}^{1/2}\text{cm}^{-1}$)	R^2
	Polymer	LiTFSI	LiFSI AMImTFSI				
1	1.0	1.0	1.5	3.0×10^{-4}	936.5	1.40	0.996
2	1.0	1.0	1.0	3.2×10^{-4}	1042	2.30	0.997
3	1.0	1.0	0.5	9.4×10^{-5}	1188	1.50	0.999
4	0.5	1.0	1.0	7.3×10^{-4}	1565	106	0.990
5	1.0		1.0	5.2×10^{-4}	872.1	2.23	0.999
6	1.0		1.0	8.2×10^{-4}	104.5	316	0.997
7	0.5		1.0	1.8×10^{-3}	117.9	346	0.996

Further, the electrochemical stability of prepared ion gel (Sample 4) was examined by linear sweep voltammetric measurement (**Figure 3.28**). The potential window was observed to be 3.1 V vs Li/Li^+ exhibiting moderate stability.

**Figure 3.28: Linear Sweep Voltammogram of samples 4.**

The lithium ion transference number (t_{Li^+}) was measured according to the technique given by Evans et al., using dc polarization and ac impedance analysis. The sample 4 and sample 7 were chosen to be analyzed because of the relatively higher ionic conductivity observed for these systems. The t_{Li^+} values of sample 4 and sample 7 were found to be 0.23 and 0.40, respectively, at

room temperature (**Table 3.6**). The plot of dc current profiles and impedance before and after polarization are given in **Figure 3.29** and **Figure 3.30**, respectively. Moderately enhanced selective lithium cation transport was observed for the sample prepared by doping with LiTFSI and significant enhancement was observed in the sample prepared by doping with LiFSI. This observation is coherent with the observed values of ionic conductivity and it also supports the better interaction of borane with FSI anion in this case.

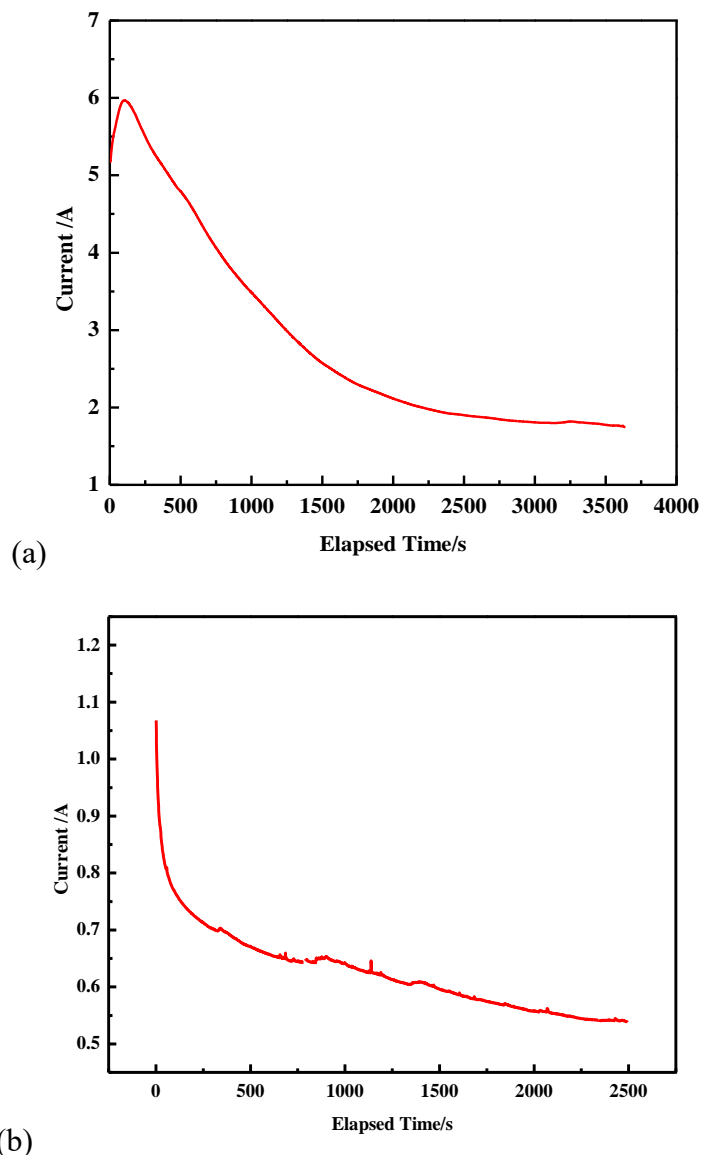


Figure 3.29: DC Current Profile During Polarization of (A) Sample 4 And (B) Sample 7 in Li/electrolyte/Li Type Cells with Applied Potential Difference of 30 mV.

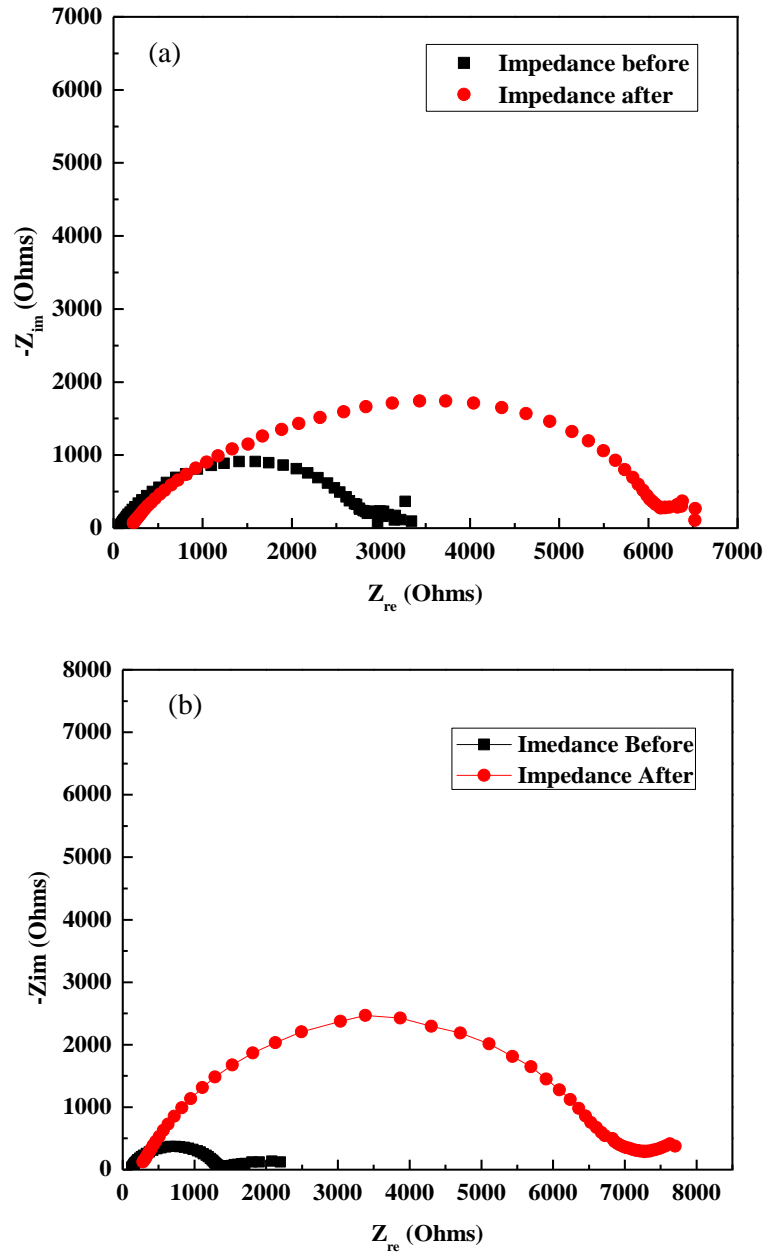


Figure 3.30: Nyquist Plots of Impedance Measured Before and After the Polarization Under DC Current. (a) Sample 4 and (b) Sample 7.

Table 3.6: Parameters of Lithium Ion Transference Number Measurement.

Sample	R_0 (Ohm)	R_s (Ohm)	I_0 (A)	I_s (A)	V (V)	t_{Li^+}
4	439.7	1578	6.38×10^{-5}	1.75×10^{-5}	0.03	0.23
7	587.0	123.0	1.71×10^{-5}	1.26×10^{-5}	0.03	0.40

3.3.3.1 Conclusion:

Novel ion-gel electrolytes were prepared by doping the synthesized poly(borosiloxane) with low viscous ionic liquid and lithium salts. The ionic conductivity of the prepared samples was in the range of 10^{-5} - 10^{-3} Scm^{-1} . Also, the lithium ion transference number was found to be in range of 0.23-0.40. The samples prepared by doping with LiFSI showed relatively enhanced ionic conductivity as well as lithium ion transference number than samples with LiTFSi because of better interaction of borane with FSI anions.

3.4 References

- (1) Bai, H. W.; Wen, G.; Huang, X. X.; Han, Z. X.; Zhong, B.; Hu, Z. X.; Zhang, X. D. *J. Eur. Ceram. Soc.* **2011**, *31*, 931–940.
- (2) Bonhomme, C.; Coelho, C.; Baccile, N.; Gervais, C.; Azais, T.; Babonneau, F. *Accounts Chem. Res.* **2007**, *40*, 738–746.
- (3) Liu, Z.; Picken, S. J.; Besseling, N. A. *Macromolecules* **2014**, *47*, 4531–4537.
- (4) Yajima, S.; Hayashi, J.; Okamura, K. *Nature* **1977**, 521.
- (5) Huo, Y.; Fan, Q.; Dembsey, N. A.; Patra, P. K. In *MRS Proceedings*; 2007; Vol. 1007, pp. 1007–1012.
- (6) Lai, X.; Zeng, X.; Li, H.; Zhang, H. *J. Macromol. Sci. Part B* **2014**, *53*, 721–734.
- (7) Oh, E. O.; Chakrabarti, K.; Jung, H. Y.; Whang, C. M. *Mater. Sci. Eng.* **2002**, *90*, 60–66.
- (8) Wang, B.-L.; Hu, L.-L. *Mater. Chem. Phys.* **2005**, *89*, 417–422.
- (9) Huang, H. H.; Orlor, B.; Wilkes, G. L. *Macromolecules* **1987**, *20*, 1322–1330.
- (10) Zhu, B. *Polyborosiloxane and Method of Preparing Same*, 2008.
- (11) Cella, J.; Rubinsztajn, S. *Macromolecules* **2008**, *41*, 6965–6971.
- (12) Mosurkal, R.; Kirby, R.; Muller, W. S.; Soares, J. W.; Kumar, J. *Green Chem.* **2011**, *13*, 659–665.
- (13) Rubinsztajn, S. *J. Inorg. Organomet. Polym. Mater.* **2014**, *24*, 1092–1095.
- (14) Horowitz, H. S. *J. Public Health Dent.* **2003**, *63*, 3–8.

- (15) Simon, M. J.; Beil, F. T.; Riedel, C.; Lau, G.; Tomsia, A.; Zimmermann, E. A.; Koehne, T.; Ueblacker, P.; R  ther, W.; Pogoda, P. *Clin. oral Investig.* **2016**, 1–10.
- (16) Kim, Y.; Gabbai, F. P. *J. Am. Chem. Soc.* **2009**, *131*, 3363–3369.
- (17) Wade, C. R.; Broomsgrove, A. E.; Aldridge, S.; Gabbai, F. P. *Chem. Rev* **2010**, *110*, 3958–3984.
- (18) Yamaguchi, S.; Akiyama, S.; Tamao, K. *J. Am. Chem. Soc.* **2001**, *123*, 11372–11375.
- (19) Matsumi, N.; Kawaguchi, K.; Hirota, Y.; Aoi, K. *J. Organomet. Chem.* **2009**, *694*, 1776–1779.
- (20) Vedarajan, R.; Hosono, Y.; Matsumi, N. *Solid State Ionics* **2014**, *262*, 795–800.
- (21) Kissel, D. J.; Brinker, C. J. Durable polymer-aerogel based superhydrophobic coatings: a composite material, 2016.
- (22) Kweon, S.; Song, K. H.; Park, H.; Choi, J.-C.; Doh, J. *ACS Appl. Mater. & interfaces* **2016**.
- (23) Cho, S. H.; White, S. R.; Braun, P. V. *Adv. Mater.* **2009**, *21*, 645–649.
- (24) Bergman, S. D.; Wudl, F. *J. Mater. Chem.* **2008**, *18*, 41–62.
- (25) Wool, R. P. *Soft Matter* **2008**, *4*, 400–418.
- (26) Wu, D. Y.; Meure, S.; Solomon, D. *Prog. Polym. Sci.* **2008**, *33*, 479–522.
- (27) Chujo, Y.; Sada, K.; Saegusa, T. *Macromolecules* **1990**, *23*, 2636–2641.
- (28) Feldman, K. E.; Kade, M. J.; Meijer, E. W.; Hawker, C. J.; Kramer, E. J. *Macromolecules* **2009**, *42*, 9072–9081.
- (29) Kalista, S. J.; Ward, T. C. *J. R. Soc. Interface* **2007**, *4*, 405–411.
- (30) Burattini, S.; Colquhoun, H. M.; Fox, J. D.; Friedmann, D.; Greenland, B. W.; Harris, P. J.; Hayes, W.; Mackay, M. E.; Rowan, S. J. *Chem. Commun.* **2009**, 6717–6719.
- (31) Yamaguchi, M.; Ono, S.; Terano, M. *Mater. Lett.* **2007**, *61*, 1396–1399.
- (32) Wool, R. P.; O’connor, K. M. *J. Appl. Phys.* **1981**, *52*, 5953–5963.
- (33) Brown, H. R.; Yang, A. C. M.; Russell, T. P.; Volksen, W.; Kramer, E. J. *Polymer* **1988**, *29*, 1807–1811.
- (34) Tarascon, J.-M.; Armand, M. *Nature* **2001**, *414*, 359–367.
- (35) Armand, M.; Tarascon, J.-M. *Nature* **2008**, *451*, 652–657.
- (36) Zhang, S. S. *J. Power Sources* **2006**, *162*, 1379–1394.

- (37) Aurbach, D.; Markovsky, B.; Weissman, I.; Levi, E.; Ein-Eli, Y. *Electrochimica Acta* **1999**, *45*, 67–86.
- (38) Song, J. Y.; Wang, Y. Y.; Wan, C. C. *J. Power Sources* **1999**, *77*, 183–197.
- (39) Van Esch, J. H.; Feringa, B. L. *Angew. Chem. Int. Ed.* **2000**, *39*, 2263–2266.
- (40) Bonhote, P.; Dias, A.-P.; Papageorgiou, N.; Kalyanasundaram, K.; Grätzel, M. *Inorg. Chem.* **1996**, *35*, 1168–1178.
- (41) Borghini, M. C.; Mastragostino, M.; Passerini, S.; Scrosati, B. *J. Electrochem. Soc.* **1995**, *142*, 2118–2121.
- (42) Watanabe, M.; Kanba, M.; Matsuda, H.; Mizoguchi, K.; Shinohara, I.; Tsuchida, E.; Tsunemi, K. *Chem-Rapid* **1981**, *2*.
- (43) Fuller, J.; Breda, A. C.; Carlin, R. T. *J. Electrochem. Soc.* **1997**, *144*, L67–L70.
- (44) Mizumo, T.; Watanabe, T.; Matsumi, N.; Ohno, H. *Polym. Adv. Technol.* **2008**, *19*, 1445–1450.
- (45) Smaran, K. S.; Vedarajan, R.; Matsumi, N. *Int. J. Hydrog. Energy* **2014**, *39*, 2936–2942.

Abbreviations

OLED: Organic Light Emitting Diodes

OPV: Organic-Photovoltaic Cells

OFET: Organic Field-Effect Transistors

EQE: External Quantum Efficiency

T₁: Lowest Triplet Excited State; S₀: Singlet Ground State

RISC: Reverse Intersystem Crossing

TTA: Triplet–Triplet Annihilation

T_m: Up-Converted Triplet State; S_n: Up-Converted Singlet State

HLCT: Hybridized Local and Charge-Transfer

LE: Local Excited; CT: Charge Transfer;

T_{CT}: CT-Based Triplet Excited State; S_{CT}: CT-Based Singlet Excited State

IC: Internal Conversion

TADF: Thermally Activated Delayed Fluorescence

ΔE_{ST} : Singlet-Triplet Energy Splitting

VR: Vibrational Relaxation;

PF: Prompt Fluorescence; DF: Delayed Fluorescence

NR: Non-Radiative Relaxation

UV-LED: Ultraviolet Light Emitting Diode,

DFT: Density Functional Theory; TD: Time-Dependent

PL: Photoluminescence

HOMO: Highest Occupied Molecular Orbitals

LUMO: Lowest Unoccupied Molecular Orbitals

Chapter 4: Poly(silylene/phenylene/borane) as Ultraviolet Emitter via Thermally Activated Delayed Fluorescence

4.1 Introduction

In the recent past, organic electronic materials have shown remarkable series of utility in organic semiconductors, conductors and light emitters. Their tunable optical and electronic properties have drawn a lot of attention in the field of organic light emitting diodes (OLED)^{1,2}, organic-photovoltaic cells (OPV)³ and organic field-effect transistors (OFET)⁴. A variety of organic electronic compounds can be produced using variety of synthetic strategy in organic chemistry unlikely of conventional inorganic counterparts. Consequently, a wide range of organic semiconductors have come in to existence which considerably took the development of organoelectronics to the next level.

The massive potential of OLEDs has made it peccable in smart phones and other electronic displays⁵, widespread research is going on in this field in order to understand fundamental processes⁶ and further possible modifications⁷. The major limitation of limited efficiency of OLEDs can be overcome by harvesting the non-radiative triplet excitons⁸. The singlet excitons and triplet excitons formed under electrical excitation are naturally present in the ratio of 1:3⁹. Whereas 75% of the electrically generated energy get wasted via triplet excitons in non-radiative decay resulting in theoretical maximum limit of external quantum efficiency (EQE) to be 5%. Number of efforts were made in order to harvest the non-emissive triplet excitons and achieve high efficiency.

A) Incorporation of Heavy Metals

The incorporation of heavy metals in organic aromatic frameworks enhances the spin-orbit interactions. As a result lowest triplet excited state (T_1) to the ground state (S_0) transition ($T_1 \rightarrow S_0$) occurs via effective intersystem crossing (ISC) for phosphorescence luminescence^{9,10} (**Figure 4.1**). Using this phenomena internal quantum efficiency nearly 100% and EQE of about 30% have been achieved in doped phosphorescent OLED. But, the incorporation of heavy metals such as Iridium (Ir) and Platinum (Pt) makes this process expensive and its utilization has been limited.

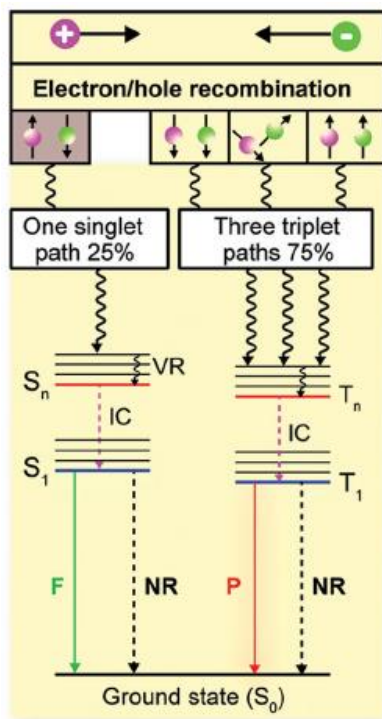


Figure 4.1¹¹: A Schematic of Employed In Harvesting The Triplet Excitons For Luminescence in OLED Devices by Metal Incorporation.

F: Fluorescence, P: Phosphorescence, IC: Internal Conversion, ISC: Intersystem Crossing, RISC: Reverse Intersystem Crossing, VR: Vibrational Relaxation, NR: Non-Radiative Relaxation, ΔE_{ST} The Singlet-Triplet Energy Splitting.

B) Triplet-Triplet Annihilation (TTA)

In the triplet-triplet annihilation (TTA) process, two triplet excitons get converted to one singlet exciton provided a large energy gap (ΔE_{ST}) between the S_1 and T_1 states ($2T_1 > S_1$)¹² (**Figure 4.2**). This process is possible via an up-conversional TTA process which brings the up-converted triplet state (T_m) close to singlet one (S_n) for RISC because of additional singlet excitons formed by the triplet excitons. Also, luminescence efficiency can be achieved from 15 to 37.5% and EQE of TTA OLED devices can be further improved to a maximum 62.5% depending on extent of up-conversion¹³. The associated problem in TTA process is that large driving voltages or high concentrated sensitizers are required to promote up-conversion.

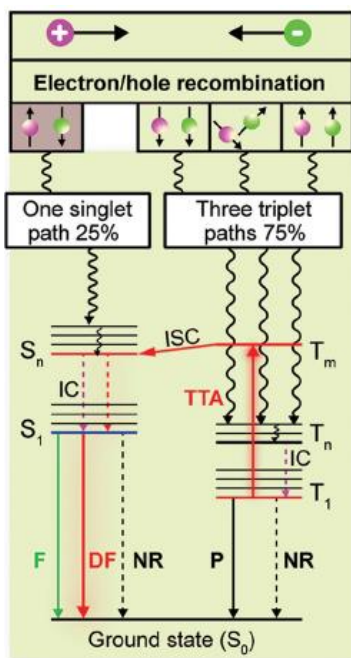


Figure 4.211: A Schematic of Employed In Harvesting The Triplet Excitons For Luminescence in OLED Devices by Triplet-Triplet Annihilation (TTA).

F: Fluorescence, P: Phosphorescence, IC: Internal Conversion, ISC: Intersystem Crossing, RISC: Reverse Intersystem Crossing, VR: Vibrational Relaxation, NR: Non-Radiative Relaxation, ΔE_{ST} The Singlet-Triplet Energy Splitting.

C) Hybridized Local and Charge-Transfer (HLCT)

In hybridized local and charge-transfer (HLCT) excited states, the intersystem crossing of excitons between T_m and S_n having similar energy levels may also occur (**Figure 4.3**). In this case, by the combination of both local excited (LE) and charge transfer (CT) states to a special excited state, the phenomenon holds two combined and compatible physiognomies^{14,15}:

- 1) A large transition moment from the LE state (cold exciton): Radiative decay of fluorescence with large efficiency is observed with LE state.
- 2) A weakly bound exciton from the CT state (hot exciton): The CT state contributes in the creation of singlet excitons in high yield via RISC from high-lying CT-based triplet excited state (T_{CT}) back to the CT-based singlet excited state (S_{CT}).

All the non-luminescent triplet excitons may be transferred to singlet excitons by RISC if the internal conversion (IC) from T_{CT} to T_{LE} is restricted. This results into the enhanced S_{CT} and S_{LE} (after IC) as well as enhanced fluorescence from $S_{LE} \rightarrow S_0$ with EQE of the OLED device as good as of the conventional metal-complex devices. Nevertheless, Kasha's rule states that the

restriction of the internal conversion process is quite difficult and challenging. Also, more of the molecules have a tendency to reside in the lowest singlet or triplet states rather than the high level S_n or T_n excited states. Thus, the design and synthesis of such systems with a HLCT excited state structure is a rather challenging.

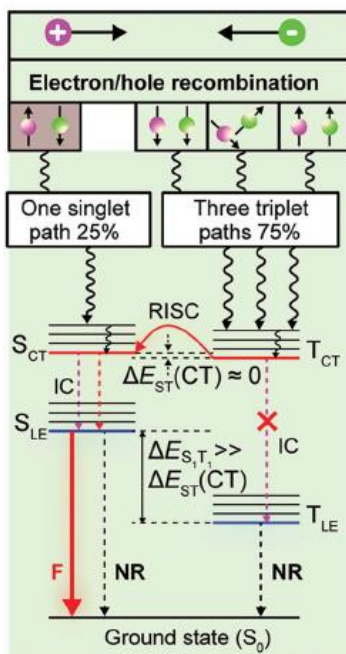


Figure 4.3¹¹: A Schematic of Employed In Harvesting The Triplet Excitons For Luminescence in OLED Devices by Hybridized Local And Charge-Transfer (HLCT).

F: Fluorescence, P: Phosphorescence, IC: Internal Conversion, ISC: Intersystem Crossing, RISC: Reverse Intersystem Crossing, VR: Vibrational Relaxation, NR: Non-Radiative Relaxation, ΔE_{ST} The Singlet-Triplet Energy Splitting.

D) Thermally Activated Delayed Fluorescence (TADF)

A relatively better and efficient phenomena to harvest triplet excitons is utilization of RISC¹⁶ process from T_1 to S_1 as shown in **Figure 1.4**. Level of T_1 is always lower than S_1 (Hund's rule), therefore, RISC can be achieved by stimulation or activation. Also, such RISC can be facile if energy levels of T_1 and S_1 are close to each other. In other words the singlet-triplet energy splitting (ΔE_{ST}) must be smaller so that endothermic RISC process may overcome the energy barrier by the thermal motions of atoms. Non-radiative triplet excitons (because of spin-forbidden $T_1 \rightarrow S_0$ transition) can be converted to singlet excitons via RISC in TADF process^{17,18}. As a result greatly enhanced luminescence from delayed fluorescence ($S_1 \rightarrow S_0$) were achieved by metal-free TADF process.

Four key steps for TADF emission are as follows:

- 1) Generation of singlet and triplet excitons after the recombination electron/hole in the ratio of 1:3⁹.
- (2) Transfer of higher exciton states to the lowest exciton states (S_1 or T_1) by vibrational relaxation (VR) and internal conversion (IC).
- (3) The transfer of triplet excitons T_1 back to S_1 by RISC with the help of thermal activation^{11,16}.
- (4) Radiative deactivation of singlet excitons at S_1 (to S_0) generated either by after conventional excitation or by back-transfer from T_1 follows different mechanism. Therefore, different luminescence lifetimes of prompt fluorescence (PF) and delayed fluorescence (DF) are observed, respectively^{19,20}.

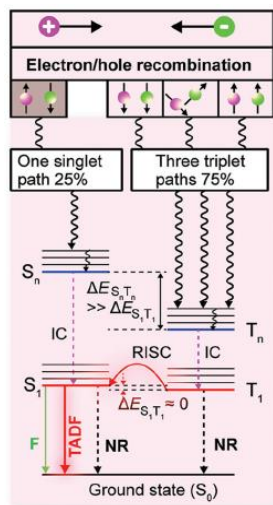


Figure 4.4¹¹: A Schematic of Employed in Harvesting the Triplet Excitons for Luminescence in OLED Devices by Thermally Activated Delayed Fluorescence (TADF). F: Fluorescence, P: Phosphorescence, IC: Internal Conversion, ISC: Intersystem Crossing, RISC: Reverse Intersystem Crossing, VR: Vibrational Relaxation, NR: Non-Radiative Relaxation, ΔE_{ST} The Singlet-Triplet Energy Splitting.

Among above mentioned processes, TADF has been found to attract significant attention. Important developments of TADF materials was shown in **Figure 4.5**. Firstly, discovery of TADF, which was earlier named as *E*-type delayed fluorescence, was done in 1961 by Parker and Hatchard in the eosin dye²¹. The first metal-containing TADF material was developed by Blasse and co-workers in 1980²². Further, in the late 1990s, the efficient delayed fluorescence was discovered in fullerenes by Berberan-Santos and co-workers²³. Research on TADF OLEDs gained interest in 2012, thanks to the pioneering work of Adachi and co-workers in order to achieve EQE

of 30% in OLED device. Such breakthrough achievement had overcome the limitation of fluorescent OLEDs.

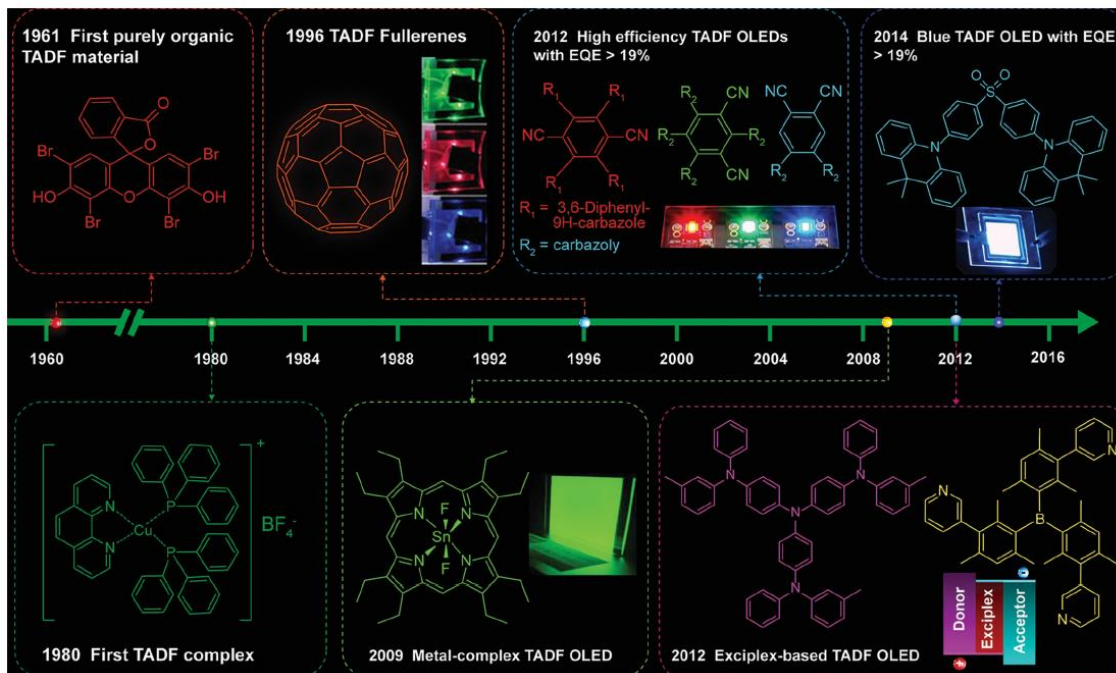


Figure 4.5¹¹: History in the Development of TADF Materials.

As discussed earlier, TADF process is dependent on the RISC which is temperature dependent phenomena. Also, it largely depends on ΔE_{ST} according to Boltzmann distribution relation (**Equation 1**)²⁴.

$$k_{RISC} \propto \exp(-\Delta E_{ST}/k_B T) \quad \text{Equation 1}$$

where k_{RISC} is RISC rate constant, k_B is Boltzmann constant and T is temperature.

It is clear that the higher k_{RISC} can be achieved if ΔE_{ST} is smaller and T is higher. Also, it is necessary to mention that at much higher temperature quantum efficiency of delayed fluorescence might decrease because of thermally enhanced non-radiative decay.

The design of emitting materials possessing smaller ΔE_{ST} is rather difficult and requires special approaches.

Principally, lowest singlet (E_S) and lowest triplet excited (E_T) states are dependent on exchange energy (J), electron repulsion energy (K) and orbital energy (E) of the two unpaired electrons in the excited states (**Equation 2, Equation 3**)¹¹. But, because of the same spin states of unpaired electrons in T_1 , E_T is lowered than E_S in S_1 .

$$E_S = E + J + K \quad \text{Equation 2}$$

$$E_T = E + J - K \quad \text{Equation 3}$$

$$\Delta E_{ST} = E_S - E_T = 2J \quad \text{Equation 4}$$

According to **Equation 4**, ΔE_{ST} is twice of J . The unpaired electrons of S_1 and T_1 having the same J value independent of the spin states, are arranged on the highest occupied molecular orbitals (HOMO) and lowest unoccupied molecular orbitals (LUMO). Thus, the exchange energy is computed by **Equation 5**²⁵.

$$J = \iint \Phi_L(1) \Phi_H(2) \{e^2/r_{1-2}\} \Phi_L(2) \Phi_H(1) dr_1 dr_2 \quad \text{Equation 5}$$

Here, Φ_L and Φ_H are the wave-functions of LUMO and HOMO respectively. It is clear by **Equation 5** that in order to achieve smaller ΔE_{ST} , large separation of HOMO and LUMO wave-functions is desirable. In other words, overlap of HOMO and LUMO must be smaller.

Further, a number of TADF molecules have been designed by various groups in the past with largely separated HOMO and LUMO using twisted donor-acceptor or through-space interaction phenomena^{26,27}. Triarylborane based molecules are also investigated utilizing vacant p-orbital as efficient acceptor and more than 20% of EQE was achieved²⁸. Also, there were only a few attempts made to transfer TADF to solution processable stage. Blending of TADF emitters with hosts were used. However, such host-guest blend method suffers problems related to poor film morphology, diffusion of small molecules into neighboring layers and aggregation of emitters to clusters. Polymeric TADF materials could ideally overcome such problems and well suited for solution processing. Only one report on polymeric TADF emitter is available in the literature to date and are called as “intermonomer TADF”²⁹.

In addition, ultraviolet light emitting diode (UV-LED) are in lime-light these days because of its promising applications in UV lamps, high resolution light sources for microscopes, medical and biotechnological applications, currency note identification, DNA chips and so on³⁰. The colour range achieved by TADF emitters is from skyblue to red and no example of UV-LED via TADF has been reported so far to the best of our knowledge.

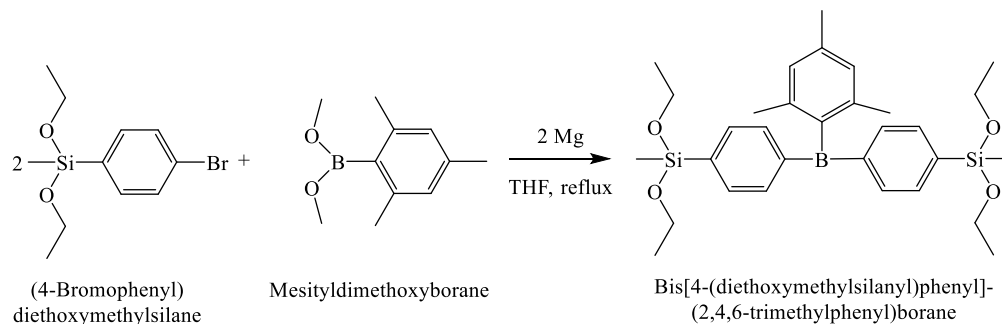
Under the current study, we have developed a triarylboron based poly(silylene/phenylene/borane) which is found to possess the attributes as an UV-TADF emitter which is first of its kind. Thus prepared defined copolymer is expected to show enhanced performance on fabrication of OLED device.

4.2 Experiment

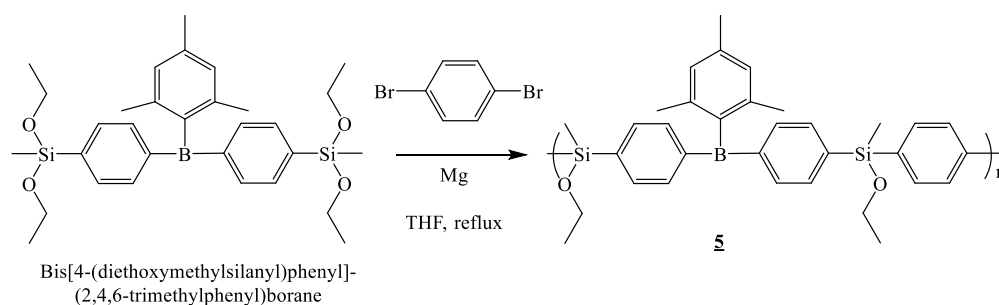
Synthesis and Characterization:

The synthesis of bis[4-(diethoxymethylsilanyl)phenyl] (2,4,6-trimethylphenyl)borane (**BDSPB**) was carried out according to **Scheme 4.1** by in-situ generation of Grignard reagent. The homo-polymerization of (4-bromophenyl) diethoxymethylsilane was already reported by J. Ohshita et al.³¹ under similar reaction conditions over the period of 65 hours. However, in the presence of more reactive mesityldimethoxyborane, **BDSPB** was yielded selectively. The isolated product was analyzed by ^1H -NMR, ^{11}B -NMR, ^{29}Si -NMR and mass spectroscopy. Single peaks in ^{29}Si -NMR and ^{11}B -NMR spectra indicated high purity of the product. All the peaks in ^1H -NMR were in accordance with the expected structure (**Figure 4.6**).

Further, the **BDSPB** was reacted with in-situ generated Grignard reagent of 1,4-dibromobenzene to yield defined and alternating poly(silylene/phenylene/borane) (**5**) (**Scheme 4.2**). Thus, prepared polymer was analyzed by ^1H -NMR, ^{11}B -NMR, ^{29}Si -NMR and IR spectroscopy (**Figure 4.6-4.9**). By the analysis of ^1H -NMR, the chemical structure of polymer **5** was confirmed. ^{29}Si -NMR and ^{11}B -NMR exhibited single peaks at -21.9 ppm and 31.1 ppm respectively, indicating the presence of only one type of boron environment in the polymer sequence. IR spectrum revealed the presence of all the expected chemical bonds such as Si-R (1607 cm^{-1} , 1259 cm^{-1}), Si-O-R (1015 cm^{-1}), B-R (1320 cm^{-1}) and so on (**Figure 4.9**). The Gel permeation chromatography (GPC, Pst Std.in THF) showed that the molecular weight of the polymer reached upto 10000 g/mol.



Scheme 4.1: Synthesis of **BDSPB.**



Scheme 4.2: Synthesis of 5.

Synthesis of Bis[4-(diethoxymethylsilyl)phenyl] (2,4,6-trimethylphenyl)borane (BDSPB):

The freshly synthesized mesityldimethoxyborane (66.35 mg, 0.35 mmol), magnesium (16 mg, 0.69 mmol) and dehydrated tetrahydrofuran (THF) (4 mL) were added in a 100 ml two neck round bottom flask under nitrogen atmosphere. To this mixture freshly prepared (4-Bromo-phenyl) diethoxymethylsilane (200 mg, 0.69 mmol) was added dropwise and the reaction mixture was refluxed for 3 hours at °C. After the completion of the reaction, the THF was evaporated and the residual gum was dissolved in chloroform. The undissolved part was filtered through a short plug of activated alumina. Chloroform was removed under reduced pressure and product was dried thoroughly. (Yield = 67 %)

$^1\text{H-NMR}$ (δ , ppm, 400 MHz, CDCl_3): 0.29 (s, 3H, MeSi), 1.15 (t, 12H, CH_3CH_2), 2.04 (s, 3H, Me-Ar), 2.19 (s, 3H, Me-Ar), 2.25 (s, 3H, Me-Ar), 3.73 (m, 8H, CH_3CH_2), 6.80 (s, 2H, Ar-B), 7.24-7.7 (m, 8H, Ar). $^{11}\text{B-NMR}$ (δ , ppm, 128 MHz, CDCl_3 , Standard: Trimethoxyborane): 31.2 ppm. $^{29}\text{Si-NMR}$ (δ , ppm, 79.5 MHz, CDCl_3): -21.84. $m/z = 549$ g/mol,

Synthesis of poly(silylene/phenylene/borane) (5):

The synthesized **BDSPB** (400 mg, 0.73 mmol) was mixed with 1,4-dibromobenzene (172 mg, 0.73 mmol) and magnesium (35 mg, 1.44 mmol) in dehydrated THF (4 mL) and the resulting mixture was refluxed for 24 hours at 75 °C. After the completion of the reaction, the THF was removed and the residual gum was dissolved in chloroform. The undissolved part was filtered through a short plug of activated alumina. Chloroform was evaporated under reduced pressure and the product was dried thoroughly. (Yield = 46 %)

$^1\text{H-NMR}$ (δ , ppm, 400 MHz, CDCl_3): 0.29 (s, 3H, MeSi), 0.54 (s, 3H, MeSi), 1.15 (m, 6H, CH_3CH_2), 2.05 (s, 6H, Me-Ar), 2.25 (s, 3H, Me-Ar), 3.71 (m, 4H, CH_3CH_2), 6.79 (s, 2H, Ar-B), 7.20-7.84 (m, 12H, Ar). $^{11}\text{B-NMR}$ (δ , ppm, 128 MHz, CDCl_3 , Standard: Trimethoxyborane): 31.1 ppm. $^{29}\text{Si-NMR}$ (δ , ppm, 79.5 MHz, CDCl_3): -21.9.

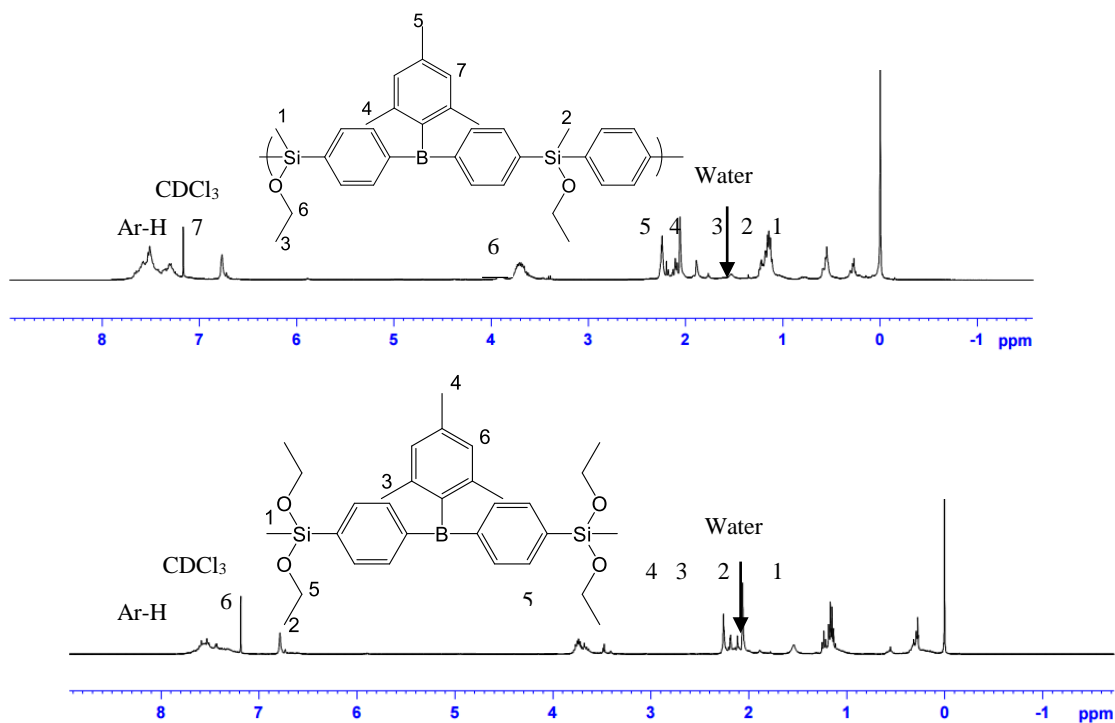


Figure 4.6: ^1H -NMR spectra of **5** (above) and BDSPB (Below).

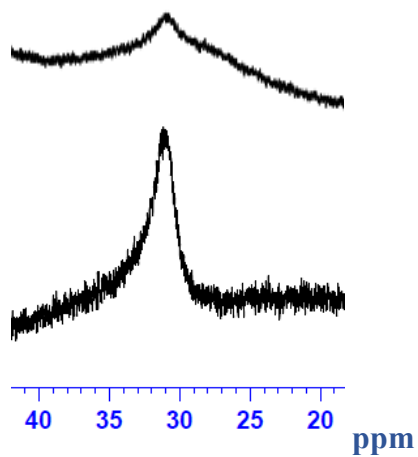


Figure 4.7: ^{11}B -NMR spectra of **5** (above) and BDSPB (Below).

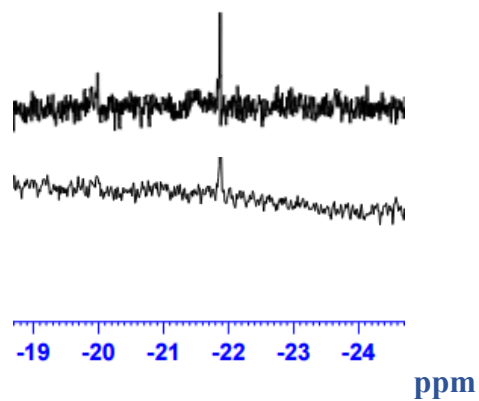


Figure 4.8: ^{29}Si -NMR spectra of **5** (below) and BDSPB (above).

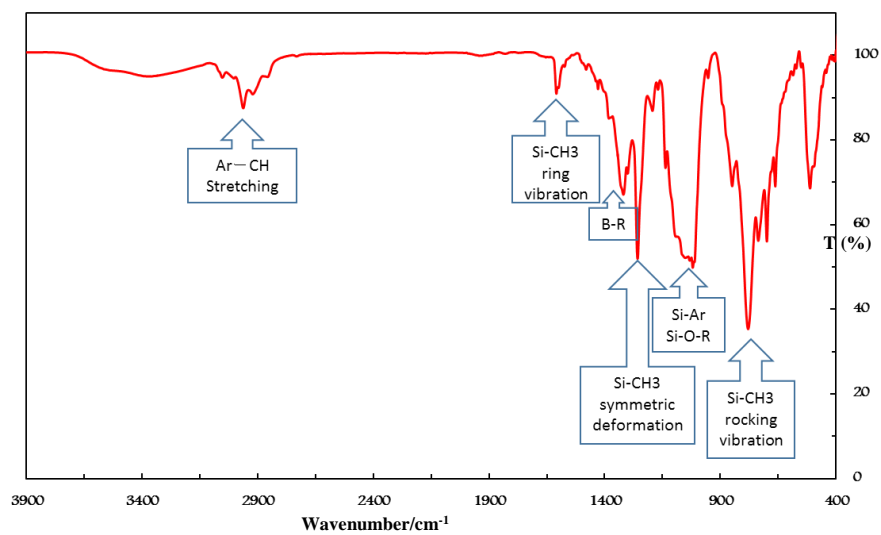


Figure 4.9: IR spectra of 5.

4.3 Results and Discussion

In order to validate the existence of the TADF behavior of **5**, a detailed optical and quantum mechanical investigation was carried out for **5** and **BDSPB**. As mentioned earlier, the smaller ΔE_{ST} is desirable for the efficient RISC which can be achieved by larger separation of HOMO and LUMO. To examine the extent of overlap of HOMO and LUMO, ground state calculation for the geometry optimization was performed at B3LYP6-311G using density functional theory (DFT) in Gaussian09 software. The BDSBPB monomer and polymer mimic model were used. The HOMO and LUMO appeared to be largely separated in both the models studied (**Table 4.1**). The chemical structures of models used are given in **Chart 4.1**.

Also, the ΔE_{ST} and oscillator strength (f) of BDSBPB and **4** were calculated using time-dependent (TD)-DFT calculations³² at B3LYP6-311G (**Table 4.2**) and were observed to be minimal. Such low ΔE_{ST} (140 meV) and f (0.0004) were expected to fulfill the requirement for efficient RISC process in TADF. UV-Vis absorbance spectrum showed the λ_{max} at 285 nm with the band gap (E_{gap}) of 3.7 eV (**Figure 4.10**). The cyclic voltammetric analysis revealed the energy of LUMO (E_{LUMO}) (- 4.37 eV) (**Figure 4.11**) which corresponds to the first reduction potential in the cathodic scan (**Equation 6**). With these values the energy of HOMO (E_{HOMO}) were evaluated (**Equation 7**).

$$\begin{aligned} E_{LUMO} &= - (4.80 + E_{red} - E_{1/2}(\text{Ferrocene})) \\ &= - (4.80 - 0.372 - 0.05) = - 4.37 \text{ eV} \end{aligned} \quad \text{Equation 6}$$

$$\begin{aligned} E_{HOCO} &= E_{LUCO} - E_{gap} \\ &= -4.37 - 3.70 = -8.07 \text{ eV} \end{aligned} \quad \text{Equation 7}$$

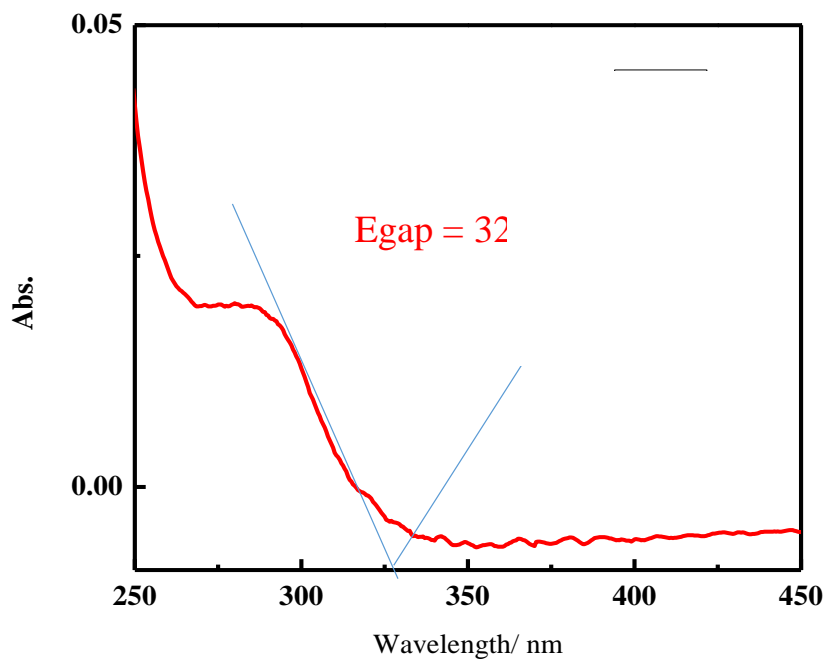


Figure 4.10: UV-Vis Spectra of **5** in Methanol.

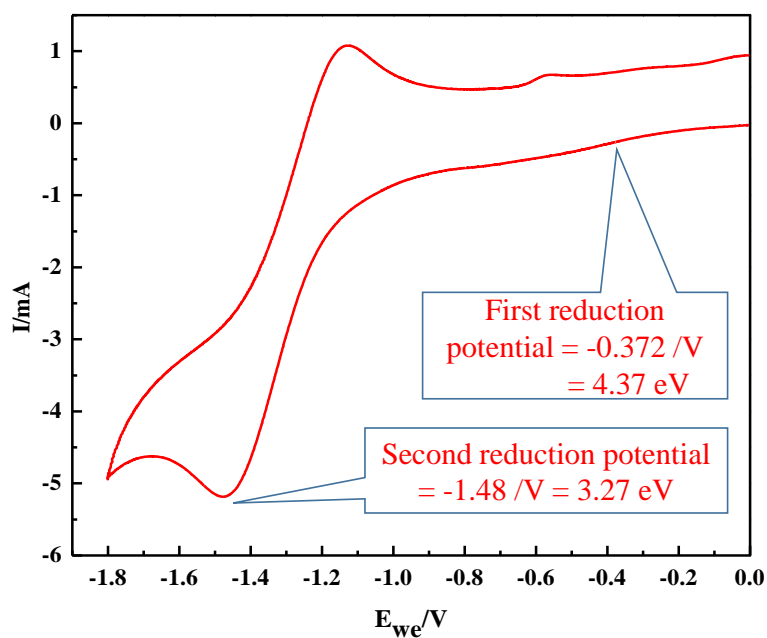
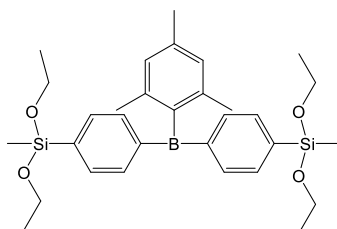
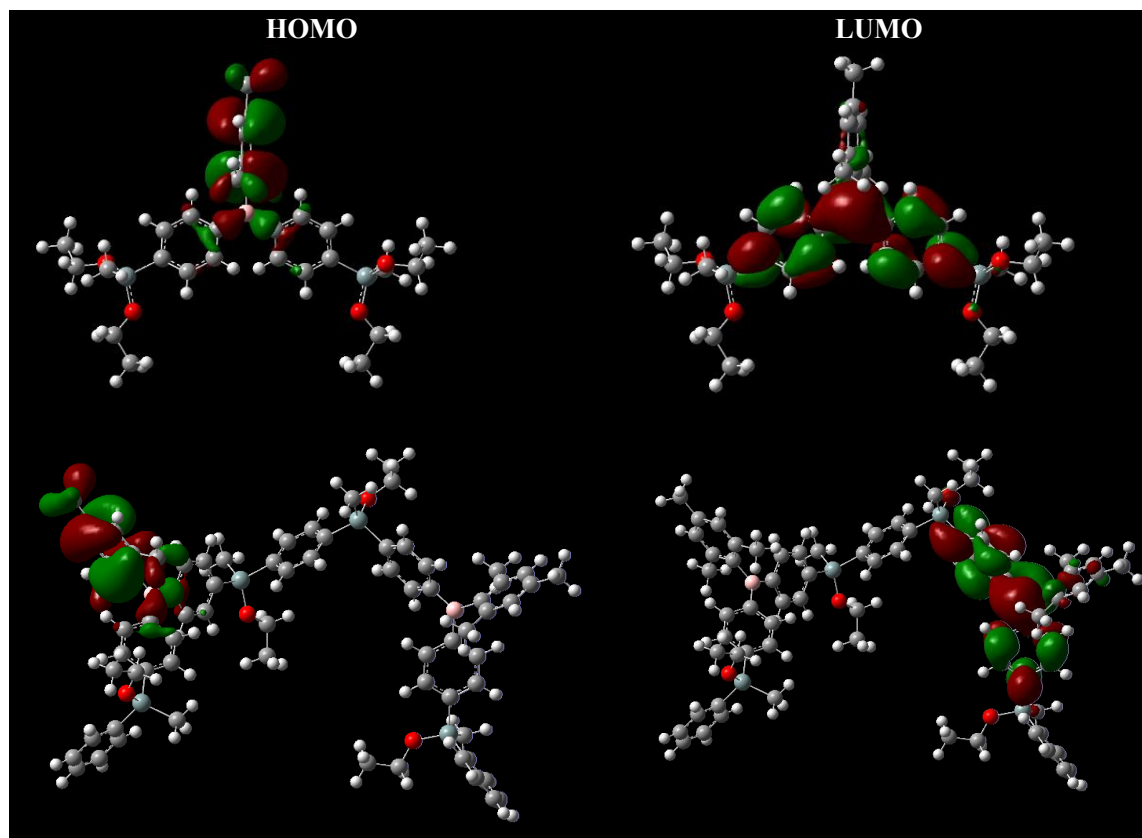
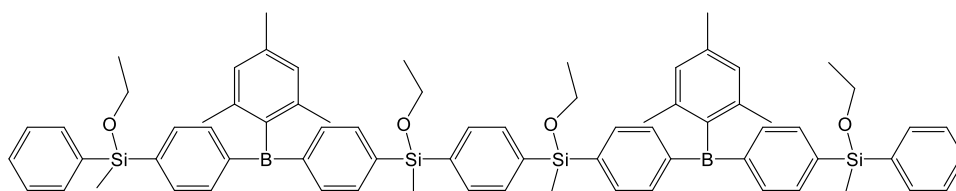


Figure 4.11: Cyclic Voltammogram of **5**; WE=Pt, CE=Pt, RE=Ag/AgNO₃; Scan Rate = 30 mV/s; Supporting Electrolyte: TBAP (Acetonitrile).

Table 4.1: Distribution of HOMO and LUMO of BDSPB (row 1) and Polymer Mimic Model (row 2)



BDSPB



Polymer Mimic Model

Chart 4.1: Chemical Structures of the Models Shown in Table 4.1.

Table 4.2: Photophysical Properties of 5 and BDSPB.

Sample	$E_{\text{gap}}^{\text{a}}$ (eV)	$\lambda_{\text{max}}^{\text{b}}$ (nm)	$\lambda_{\text{max}}^{\text{c}}$ (nm)	$\phi_{\text{PL}}^{\text{d}}$ (%)	$\Delta E_{\text{ST}}^{\text{e}}$ (meV)	f^{f}
<u>5</u>	3.7	285	350	93	140	0.0002
BDSPB	4.6	274	341	89	57	0.0004

a: By ground state DFT calculation; b: UV-VIS spectra; c: PL emission spectra; d: relative quantum yield was calculated using the following formulae : $\Phi_{\text{unk}} = \Phi_{\text{std}} [\{A_{\text{std}} - F_{\text{unk}}\} / \{A_{\text{unk}} - F_{\text{std}}\}] \{n_{\text{D,unk}} / n_{\text{Dstd}}\}^{*2}$ using 9-carboxylic anthracene as a standard; e and f: By TD-DFT calculations.

Further, photoluminescence (PL) emission spectra were measured after dissolving the polymer 5 in different solvents under excitation at various wavelengths (**Figure 4.12 – Figure 4.15**). The prompt fluorescence emission of these polymer were largely dependent of the excitation wavelength. In all the cases, the maximum emission was observed in ultraviolet range (340-350 nm) with the excitation wavelength in the range of 280-290 nm. Also, a red shift was observed in emission maxima of 5 by increase in the polarity of the solvent. The λ_{max} of emission in diethylether (polarity index = 2.8) was increased from 343 nm to 349 nm in tetrahydrofuran (polarity index 4.8)(**Figure 4.16**). However, with additional increase in polarity of solvent did not result in further red shift of the λ_{max} . The PL emission spectra for the monomer **BDSPB** were also measured (**Figure 4.17**). The emission maxima was appeared at 340 nm with large dependency of emission intensity with excitation wavelength.

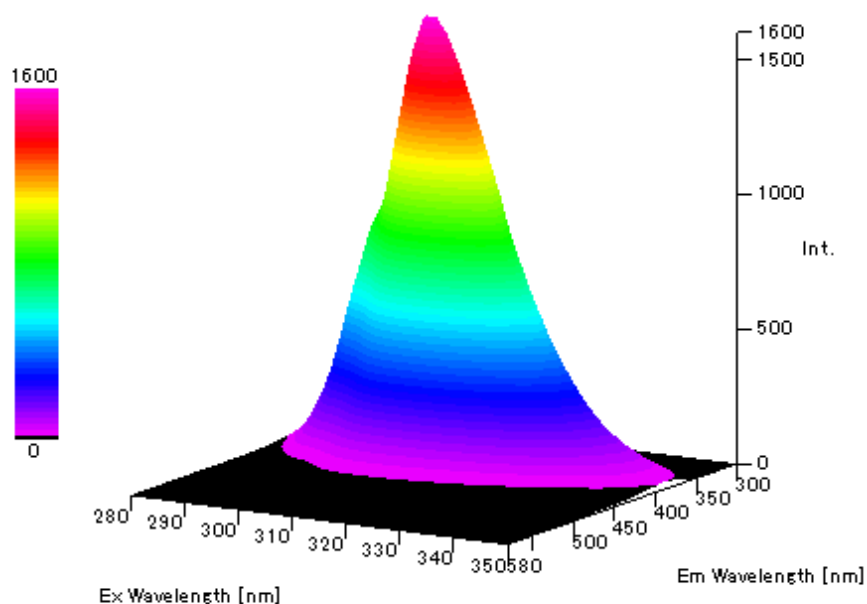


Figure 4.12: Excitation Wavelength Dependence of Photoluminescence of **5 in Methanol (10^{-5} M).**

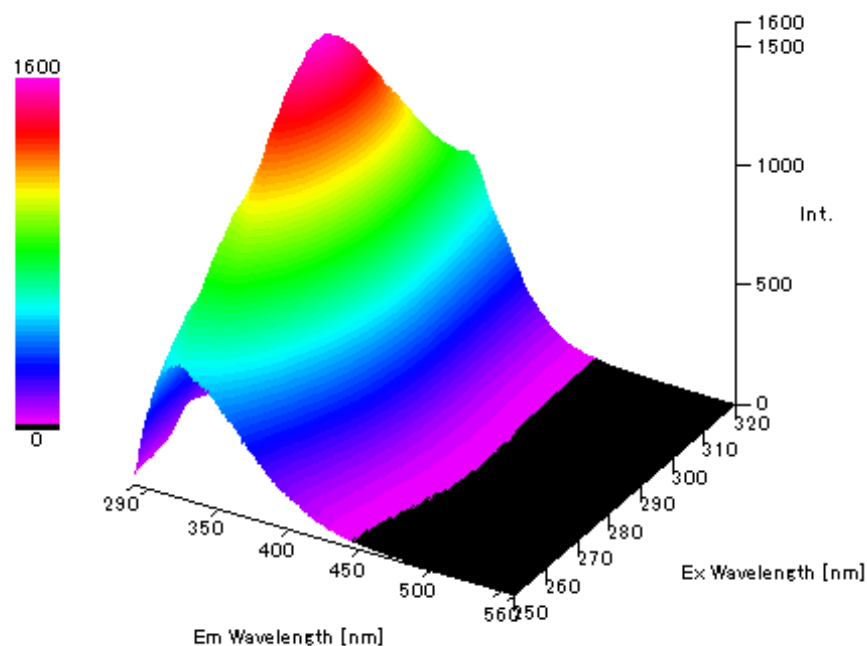


Figure 4.13: Excitation Wavelength Dependence of Photoluminescence of **5 in Acetonitrile (10^{-5} M).**

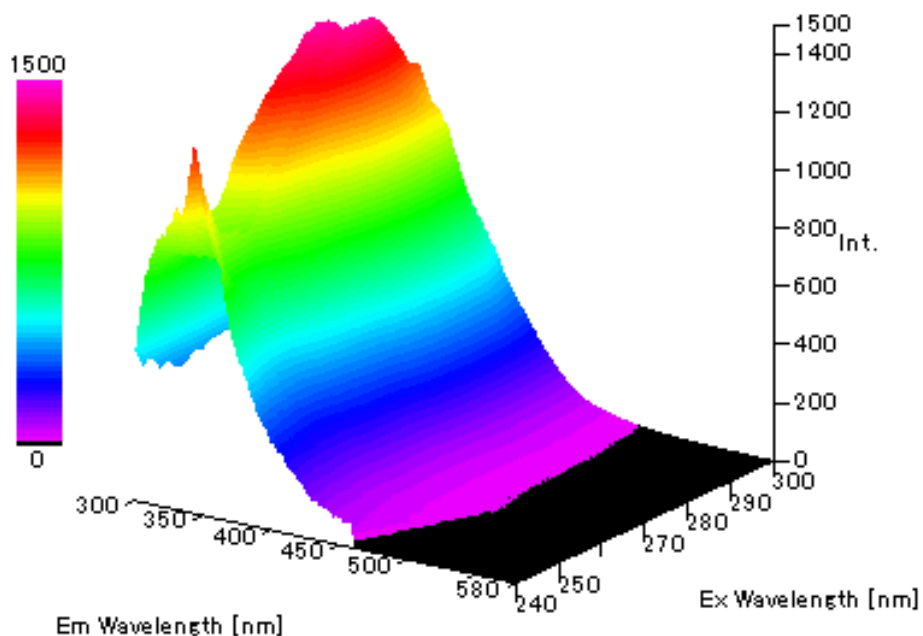


Figure 4.14: Excitation Wavelength Dependence of Photoluminescence of **5 in Diethylether (10^{-5} M).**

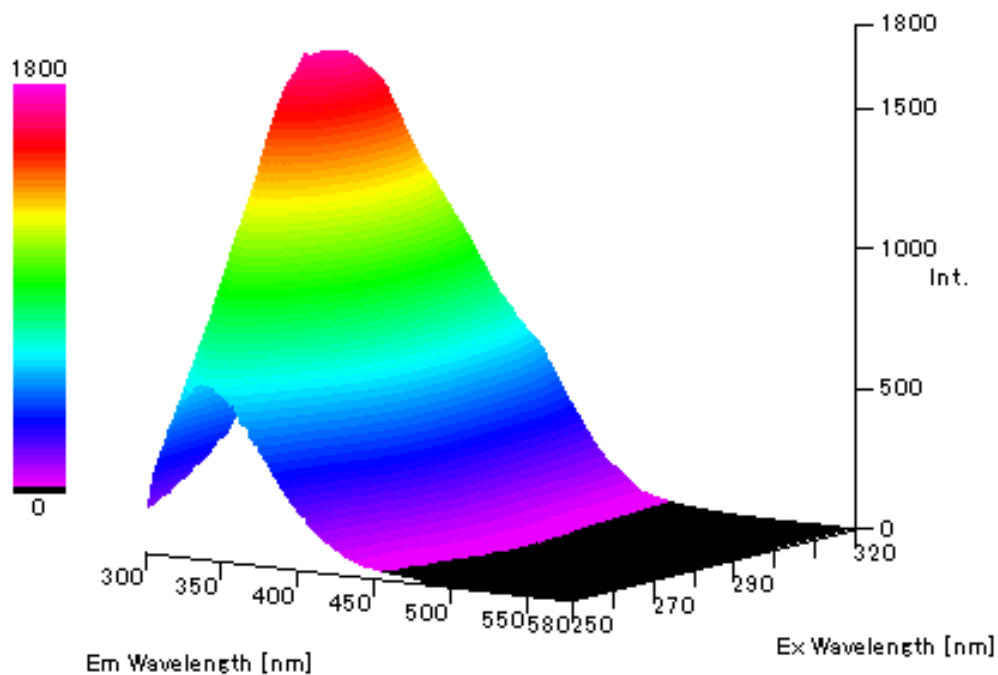


Figure 4.15: Excitation Wavelength Dependence of Photoluminescence of **5 in THF (10^{-5} M).**

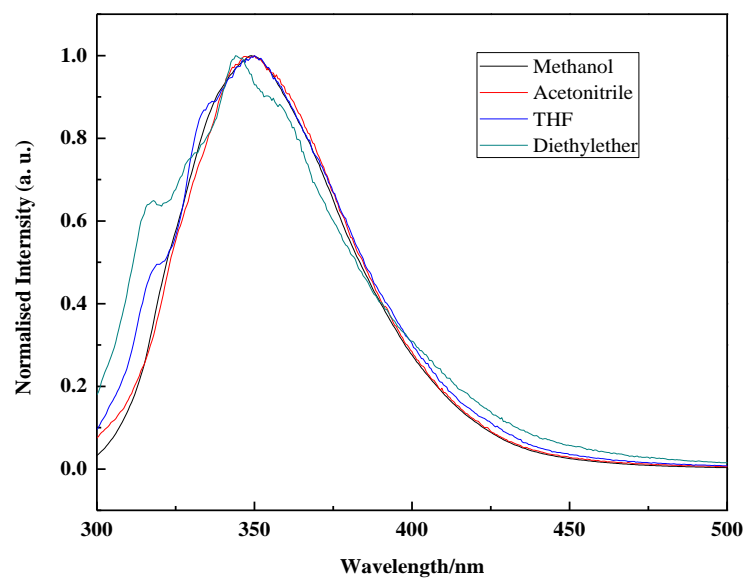


Figure 4.16: Photoluminescence Spectra of 5 in Different Solvents (10^{-5} M).

Excitation Wavelength = 290 nm

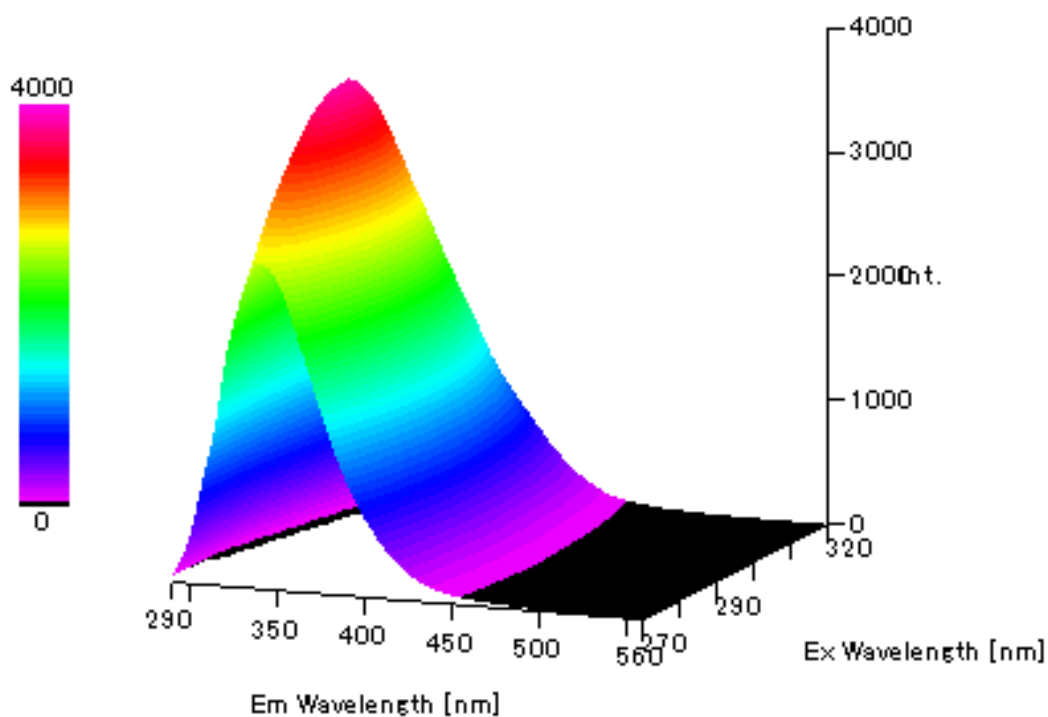


Figure 4.17: Excitation Wavelength Dependence of Photoluminescence of BDSPB in (10^{-5} M).

The delayed fluorescence (DF) was also measured for **5** in solvents of different polarities. The emission maxima in PF and DF were observed to be the similar. To collect more information to prove that the DF is originated via triplet states, the DF time decay measurements were performed (**Figure 4.18**). The decay-time found was in the range of ~ 3 ms (25-28) (sample was saturated with N_2) which is much higher than general fluorescence decay (10^{-9} - 10^{-7} s) and suggested the involvement of triplet state in the DF. Further, the decay-time measurement was performed with sample saturated with oxygen. The relative intensity decreased drastically as expected. This happened due to the quenching of T_1 excitons by dissolved oxygen. From the PF and DF spectra, the energies of singlet ($S_1 = 3.838$ eV) (**Figure 4.19**) and triplet ($T_1 = 3.886$ eV) (**Figure 4.20**) were extracted from the energy corresponding to the half maxima in high energy side²⁹. The T_1 energy observed to be exceeding the S_1 in this case. It should be pointed out here that these measurements were carried out at room temperature (298 K). The ΔE_{ST} barrier which was calculated by DFT calculations (0 K) was overcome by T_1 by the aid of temperature. This opens the possibility of RISC process which converts the triplet state to singlet following TADF phenomenon.

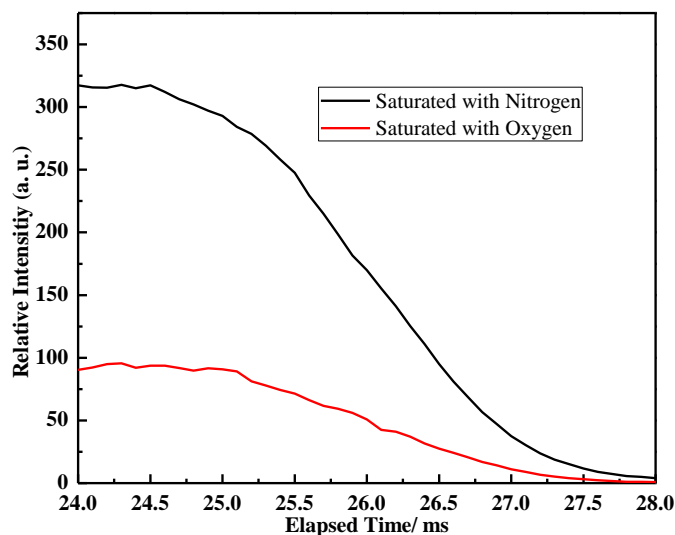


Figure 4.18: Delayed Fluorescence Decay Time Spectra of **5 in Methanol.**

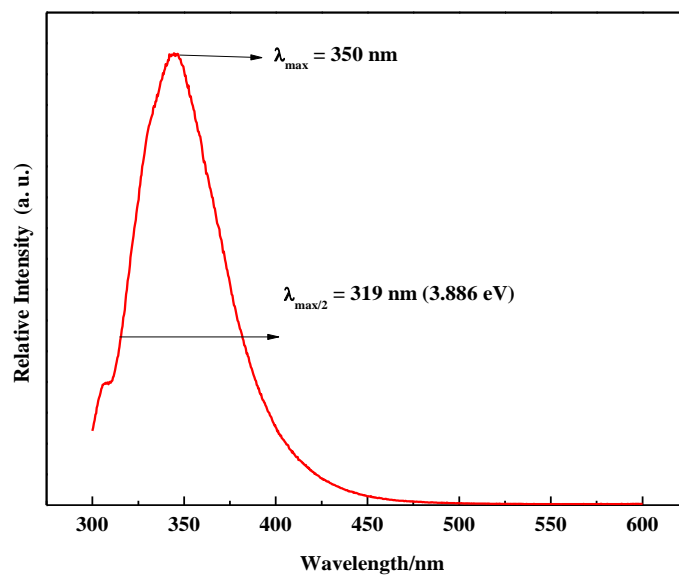


Figure 4.19: Determination of Triplet (T_1) Energy from Delayed Fluorescence Spectrum.

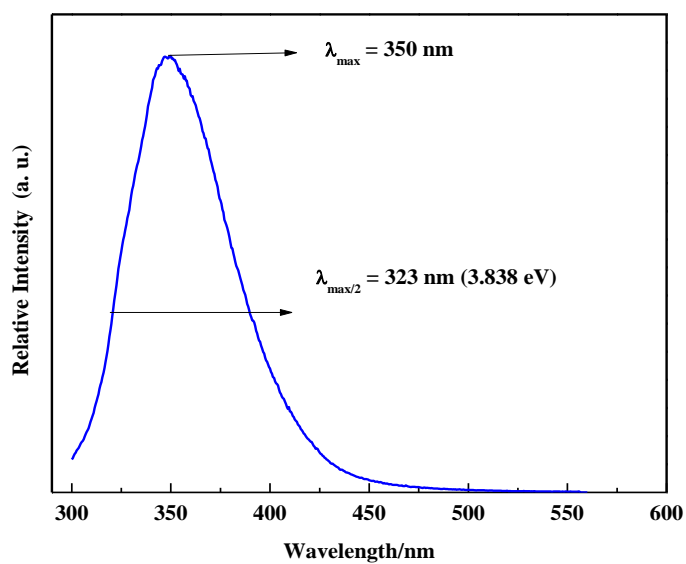


Figure 4.20: Determination of Singlet (S_1) Energy from Prompt Fluorescence Spectrum.

4.4 Conclusion

The polymeric ultraviolet emitter via thermally activated delayed fluorescence was successfully synthesized. The largely separated HOMO and LUMO was observed in DFT calculations with smaller ΔE_{ST} . The molecule was successfully designed to have large band gap to get emission in ultraviolet range. The quenching of PL was observed with dissolved oxygen, which confirmed the involvement of triplet excitons in PL. Prediction of triplet and singlet energies at room temperature provided a strong evidence of RISC by thermal activation. Thus prepared material is first example of solution processable ultraviolet emitter via TADF and can provide valuable dimension to the design of OLED emitters.

4.5 References

- (1) Figueira-Duarte, T. M.; Müllen, K. *Chem. Rev.* **2011**, *111*, 7260–7314.
- (2) Xie, L.-H.; Yin, C.-R.; Lai, W.-Y.; Fan, Q.-L.; Huang, W. *Prog. Polym. Sci.* **2012**, *37*, 1192–1264.
- (3) You, J.; Dou, L.; Yoshimura, K.; Kato, T.; Ohya, K.; Moriarty, T.; Emery, K.; Chen, C.-C.; Gao, J.; Li, G. *Nat. Commun.* **2013**, *4*.
- (4) Wang, E.; Mammo, W.; Andersson, M. R. *Adv. Mater.* **2014**, *26*, 1801–1826.
- (5) *Chem. & Eng. News* **2002**, *80*, 7.
- (6) Scholz, S.; Kondakov, D.; Lüssem, B.; Leo, K. *Chem. Rev.* **2015**, *115*, 8449–8503.
- (7) Choy, W. C.; Chan, W. K.; Yuan, Y. *Adv. Mater.* **2014**, *26*, 5368–5399.
- (8) Brütting, W.; Frischeisen, J.; Schmidt, T. D.; Scholz, B. J.; Mayr, C. *Phys. Status solidi* **2013**, *210*, 44–65.
- (9) Baldo, M. A.; O'Brien, D. F.; You, Y.; Shoustikov, A.; Sibley, S.; Thompson, M. E.; Forrest, S. R. *Nature* **1998**, *395*, 151–154.
- (10) Adachi, C.; Baldo, M. A.; Thompson, M. E.; Forrest, S. R. *J. Appl. Phys.* **2001**, *90*, 5048–5051.
- (11) Tao, Y.; Yuan, K.; Chen, T.; Xu, P.; Li, H.; Chen, R.; Zheng, C.; Zhang, L.; Huang, W. *Adv. Mater.* **2014**, *26*, 7931–7958.
- (12) Chiang, C.-J.; Kimyonok, A.; Etherington, M. K.; Griffiths, G. C.; Jankus, V.; Turksoy, F.; Monkman, A. P. *Adv. Funct. Mater.* **2013**, *23*, 739–746.
- (13) Kondakov, D. Y.; Pawlik, T. D.; Hatwar, T. K.; Spindler, J. P. *J. Appl. Phys.* **2009**, *106*.

- (14) Li, W.; Liu, D.; Shen, F.; Ma, D.; Wang, Z.; Feng, T.; Xu, Y.; Yang, B.; Ma, Y. *Adv. Funct. Mater.* **2012**, *22*, 2797–2803.
- (15) Yao, L.; Zhang, S.; Wang, R.; Li, W.; Shen, F.; Yang, B.; Ma, Y. *Angew. Chem.* **2014**, *126*, 2151–2155.
- (16) Sun, J. W.; Baek, J. Y.; Kim, K.-H.; Moon, C.-K.; Lee, J.-H.; Kwon, S.-K.; Kim, Y.-H.; Kim, J.-J. *Chem. Mater.* **2015**, *27*, 6675–6681.
- (17) Uoyama, H.; Goushi, K.; Shizu, K.; Nomura, H.; Adachi, C. *Nature* **2012**, *492*, 234–238.
- (18) Adachi, C. *Jpn. J. Appl. Phys.* **2014**, *53*.
- (19) Valeur, B.; Berberan-Santos, M. N. *Molecular fluorescence: principles and applications*; John Wiley & Sons, 2012.
- (20) Parker, C. A. *Photoluminescence of Solutions*, 1968.
- (21) Parker, C. A.; Hatchard, C. G. *Trans. Faraday Soc.* **1961**, *57*, 1894–1904.
- (22) Blasse, G.; McMillin, D. R. *Chem. Phys. Lett.* **1980**, *70*, 1–3.
- (23) Berberan-Santos, M. N.; Garcia, J. M. *J. Am. Chem. Soc.* **1996**, *118*, 9391–9394.
- (24) Niwa, A.; Kobayashi, T.; Nagase, T.; Goushi, K.; Adachi, C.; Naito, H. *Appl. Phys. Lett.* **2014**, *104*.
- (25) Méhes, G.; Nomura, H.; Zhang, Q.; Nakagawa, T.; Adachi, C. *Angew. Chem. Int. Ed.* **2012**, *51*, 11311–11315.
- (26) Ishimatsu, R.; Matsunami, S.; Kasahara, T.; Mizuno, J.; Edura, T.; Adachi, C.; Nakano, K.; Imato, T. *Angew. Chem. Int. Ed.* **2014**, *53*, 6993–6996.
- (27) Lee, S. Y.; Yasuda, T.; Nomura, H.; Adachi, C. *Appl. Phys. Lett.* **2012**, *101*.
- (28) Suzuki, K.; Kubo, S.; Shizu, K.; Fukushima, T.; Wakamiya, A.; Murata, Y.; Adachi, C.; Kaji, H. *Angew. Chem.* **2015**, *127*, 15446–15450.
- (29) Nikolaenko, A. E.; Cass, M.; Bourcet, F.; Mohamad, D.; Roberts, M. *Adv. Mater.* **2015**, *27*, 7236–7240.
- (30) Muramoto, Y.; Kimura, M.; Nouda, S. *Semicond. Sci. Technol.* **2014**, *29*.
- (31) Ohshita, J.; Yamashita, A.; Hiraoka, T.; Shinpo, A.; Kunai, A.; Ishikawa, M. *Macromolecules* **1997**, *30*, 1540–1549.
- (32) Kawasumi, K.; Wu, T.; Zhu, T.; Chae, H. S.; Van Voorhis, T.; Baldo, M. A.; Swager, T. M. *J. Am. Chem. Soc.* **2015**, *137*, 11908–11911.

Chapter 5: General Conclusion

5.1 General Conclusion

Organosilicon polymers and organoboron polymers have been widely investigated because of their unique electronic states and characteristics. However, there has been few studies on polymers including both elements in the main chain. It appears to be an attractive approach to design such a novel bimetallic copolymers whose properties are unknown. Keeping this in mind we have synthesized different type of silicon/boron bimetallic polymers in order to use them as chemosensors, polymer support for electrolytes, self-healing anti-corrosion coating, emitter in OLED and so forth.

In the chapter 2, a novel σ -p conjugated copolymer of phenylsilane and mesitylborane was synthesized by the dehydrocoupling polymerization using rhodium catalyst. Change in electronic states due to the incorporation of boron moiety was determined both by DFT calculations and experiments. The obtained colorless polymers were characterized by ^1H -NMR and ^{11}B -NMR spectra. Incorporation of boron was confirmed by ^{11}B -NMR, while the Si/B ratio was calculated by ^1H -NMR integration ratios. GPC analysis showed the M_n of the polymer as 1200-2900 g/mol. Copolymers showed high sensitivity towards fluoride ions both optically and electrochemically exhibiting “turn on” type of sensing mechanism.

In chapter 3, synthesis of highly alternating poly(borosiloxane) by dehydrocoupling polymerization was successfully carried out. The polymer sequence structure was understood by various model reactions. This particular polymer was examined for various applications and found to be a *multipurpose* material.

A solid state sensing experiment was designed to examine the affinity of the polymer towards fluoride ions and it was found to be highly sensitive (10^{-10} M of fluoride anion). Detection of such low concentration was possible by the synergistic contributions of both, the solid state electrochemical sensing measurements and the Si-O back-bonding in the polymer chain exposing

boron atom in a suitable conformation for reaction with fluoride. The kind of sensing behavior being presented here, is unprecedented under these conditions to the best of our knowledge which will open a new window for the development of fluoride anion sensing methods and materials.

Secondly, the self-healing behavior of poly(borosiloxane) under damage induced condition was achieved by heating to 45 °C. A reptile motion of the polymer was believed to be the mechanism for self-healing and thus was confirmed by SEM micrographs. The polymer coat behaved as a remarkable corrosion protectant to the metal surface. The self-healing property was also observed by monitoring electrochemical impedance measurements and depolarization studies. Good protection was observed after self-healing in samples which were subjected to scratch-heal test. This proved that the healing process was complete in all the facets.

Also, novel ion-gel electrolytes were prepared by doping the synthesized poly(borosiloxane) with low viscous ionic liquid and lithium salts. The ionic conductivity of the prepared samples was in the range of 10^{-5} - 10^{-3} Scm^{-1} . Also, the lithium transference number was found to be in range of 0.23-0.40. The samples prepared by doping with LiFSI showed relatively enhanced ionic conductivity as well as lithium ion transference number than samples with LiTFSi because of better interaction of borane with FSI anions.

In chapter 4, poly(silylene/phenylene/borane) ultraviolet emitter via thermally activated delayed fluorescence was successfully synthesized. The largely separated HOMO and LUMO were observed in DFT calculations with smaller ΔE_{ST} . The molecule was successfully designed to have large band gap to get emission in ultraviolet range. The quenching of PL was observed with dissolved oxygen, which confirmed the involvement of triplet excitons in PL. Prediction of triplet and singlet energies at room temperature provided a strong evidence of RISC by thermal activation. Thus prepared material is first example of solution processable ultraviolet emitter via TADF and can provide valuable dimension to the design of OLED emitters.